



YHELIG

This is to certify that the

dissertation entitled

Vibrational, Electronic and Structural Properties of High Valent Catalytic Intermediates of Horseradish Peroxidase

presented by

W. Anthony Oertling

has been accepted towards fulfillment of the requirements for

Ph. D. degree in Chemistry

Major professo

Date Guil 29, 1987.



RETURNING MATERIALS:
Place in book drop to remove this checkout from your record. FINES will be charged if book is returned after the date stamped below.

VIBRATIONAL, ELECTRONIC AND STRUCTURAL PROPERTIES OF HIGH VALENT CATALYTIC INTERMEDIATES OF HORSERADISH PEROXIDASE

By

W. Anthony Oertling

A DISSERTATION

Submitted to

Michigan State University in partial fulfillment of the requirements for the degree of

DOCTOR OF PHILOSOPHY

Department of Chemistry

1987

		1
		1
		ı
		1
		'

ABSTRACT

VIBRATIONAL, ELECTRONIC AND STRUCTURAL PROPERTIES OF HIGH VALENT CATALYTIC INTERMEDIATES OF HORSERADISH PEROXIDASE

By

W. Anthony Oertling

The active site of the two-electron oxidized compound I intermediate of horseradish peroxidase (HRP-I) is usually described as an oxoferryl porphyrin π cation radical. In order to assess separately the effects of each oxidation equivalent on the structural, electronic and vibrational properties of this heme complex we present a resonance Raman (RR) characterization of a series of model compounds. From comparison of the FeO stretching frequency, v(FeO), of synthetic oxoferryl hemes and oxoferryl heme proteins the predominant determinant of the v(FeO) is identified as a trans-ligand effect, with a lesser effect coming from H-bonding of the oxo ligand. Through a separate RR study of metalloporphyrin m cation radicals (MP+*) the vibrations of the oxidized porphyrin macrocycle are analyzed and compared to those of the parent metalloporphyrin (MP). The frequency of the vibrational modes in the 1450-1700 cm⁻¹ range of the MP⁺ are found to be an inverse linear function of porphyrin center-to-pyrrole nitrogen distance, similar to that which describes the vibrational frequencies of the parent compound. Thus, as is the case for the MP, the high frequency vibrations of the MP+ reflect porphyrin core geometry.

W. Anthony Oertling

In the enzymatic cycle, HRP-I is reduced by substrate to the more stable HRP-II. These two intermediates are thought to contain similar oxoferryl structures. Based on RR measurements of the $\nu(\text{FeO})$ by others, the oxo ligand of HRP-II is thought to be H-bonded at pH 7 but not as pH 11. We present RR scattering from a flowing HRP-I sample prepared by rapid mixing. The $\nu(\text{FeO})$ is very similar to that of HRP-II at high pH. This is taken to suggest that, unlike HRP-II, there is no H-bond to the oxo ligand of HRP-I at pH 7. A mechanism, consistent with these RR observations and past kinetic studies, is proposed for the reduction of HRP-I by p-cresol. The frequencies we measure for the in-plane vibrations of HRP-I, however, are not characteristic of a MP^{+*}. Possible explanations for this result are discussed.

선O, 약 물, 그리고 로콘

ACKNOWLEDGMENTS

For their various contributions to this work, my thanks is given to: the members of my family for support and encouragement; G.T. Babcock, G.E. Leroi and C.K. Chang for critical reading and guidance; Jerry Babcock, Pat Callahan and John McMahon for instruction in the measurement of Raman scattering; the entire supporting staff of the Chemistry Department, in particular Ron Haas and Deak Watters, for technical services; Dwight Lillie, Bob Kean, Harold Fonda and Ralph Thiim for computer programming. Special thanks is extended to my "partner", Asaad Salehi, for his sincerity, enthusiasm and perserverance. Thanks also goes to Carol Smith, Sharon Corner, Margy Lynch and Bill Draper for their efforts in the preparation of this manuscript. Kris Babcock and María Centeno are acknowledged for their fine cooking and Anheuser-Busch and Miller Breweries for their fine products, without which this work would have been much more difficult.

TABLE OF CONTENTS

	Page
LIST OF TABLES	v i
LIST OF FIGURES	viii
Chapter 1 - GENERAL INTRODUCTION	1
Significance of the Oxoferryl and Porphyrin π Cation Radical Structures Aim and Strategy of the Thesis Metalloporphyrin π Cation Radicals and Compound I References	3 5 5 14
CHAPTER 2 - CHARACTERIZATION OF SIX-COORDINATE OXOFERRYL PROTOHEME BY RESONANCE RAMAN AND OPTICAL ABSORPTION SPECTROSCOPY	
Summary Acknowledgments References & Notes	16 21 22
CHAPTER 3 - RESONANCE RAMAN SPECTROSCOPIC DETECTION OF DEMETALLATION OF METALLOPORPHYRIN π CATION RADICALS	
Summary	31
CHAPTER 4 VIBRATIONAL, ELECTRONIC AND STRUCTURAL PROPERTIES OF COBALT, COPPER AND ZINC OCTAETHYLPORPHYRIN # CATION RADICALS	
Summary Introduction Experimental Results	35
Effects of oxidation on the high frequency porphyrin core vibrations	39 40

	rage
Porphyrin diacid impurities	46
One- and two-electron oxidation of CoOEP	52
Near uv RR spectra	58
Visible RR spectra	64
Low temperature effects	70
Discussion	74
Structural correlations	75
Porphyrin core geometry	80
Ring buckling effects	84
Cobaltic octaethylporphyrin w cation radicals	85
Effects of one-electron, metal centered oxidation	
and axial ligation	86
Co ^{III} OEP+2ClO ₄	89
Co ¹¹¹ OEP '2Br	90
Conclusions	
Acknowledgments	94
References and Notes	95
CHAPTER 5 - DETAILS OF PEROXIDASE CATALYSIS SUGGESTED	
BY RESONANCE RAMAN MEASUREMENTS OF IRON-OXY	'GEN
STRETCHING FREQUENCIES OF HORSERADISH PEROXII INTERMEDIATES	
IntroductionExperimental	101
Materials	104
HRP-I	104
HRP-II	106
Model compounds	106
Instrumentation	106
Results	
High frequency RR scattering from HRP intermediates	110
Model compounds	
Frequency shifts	115
Low frequency RR scattering from HRP intermediates	116
Excitation profiles	120
Discussion	
Prediction of HRP-I vibrations from structural	
correlations	130
HRP-II	131
Photochemistry	131
Spin delocalization	
HRP-I*	
Kinetics and mechanism of HRP-I reduction	135
Conclusions	136
Future Work	137
Acknowledgments	138
References	139

LIST OF TABLES

		Page
2-1	Comparison of v (FeO) for Various Oxoferryl Species	20
4-1	Resonance Raman Frequencies (cm $^{-1}$), Depolarization Ratios and Optical Absorption Maxima (nm) for Parent MOEP Compounds and their Corresponding π Cation	
	Radicals, MOEP+*ClO ₄	. 77
4-2	Core Size Parameters from Crystal Structures of Metallo-	
	porphyrin 7 Cation Radicals and Related Compounds	83
4-3	Resonance Raman Frequencies and Optical Absorption Maxima for Axially Ligated Cu ^{II} , Ni ^{II} and Co ^{III} OEP	. 88
	Complexes	. 00
4-4	Comparison of Resonance Raman Frequencies (cm ⁻¹) and of Depolarization Ratios for Cobaltic OEP ⁺ Complexes	91
	of Depotalization hadros for Conditic Off Complexes	91

LIST OF FIGURES

	P	age
1-1	(a) Ferriprotoporphyrin IX. (b) Metallooctaethylporphyrin. Carbons a (or α) are bonded to the nitrogen atoms. Carbons b (or β) are bonded to the peripheral substituents. The methine, CH, positions are meso. The metal center, M, may be further ligated in the axial positions normal to the macrocycle plane	2
1-2	Optical absorption spectra of native HRP (N), HRP-I (I) and HRP-II (II). Reference 31.	4
1-3	The atomic orbital (AO) structure of two HOMOs of porphine. The AO coefficients are proportional to the size of the circles; solid lines indicate positive values, dashed lines negative. The view is from the positive z axis. The straight dashed lines indicate the nodes of the a_{1u} (π) orbital. Reference 14.	6
1-4	Optical absorption spectra of (a) cobaltic octaethylporphyrin π cation radicals, (b) compound I enzyme transients. $^2A_{2u}$ type spectra (——). $^2A_{1u}$ type spectra (). Reference 16.	8
1-5	Optical absorption spectra of compound I intermediates $(^2A_{1u}$ type). (a) native horse erythrocyte catalase (CAT) and CAT-I. Reference 26.	10
	(b) native chloroperoxidase (CPO) and CPO-I. Reference 24	10
1-6	Optical absorption spectra of compound I intermediates. $({}^{2}A_{2u}$ type).	
	(a) native ferric bromoperoxidase (BPO) and BPO-I. Reference 27	11
	(b) native lignin peroxidase (LiP) and LiP-I. Reference 29	11
	(c) Rapid scan spectrophotometric measurements for the reactions of intestinal peroxidase (IPO) and lactoperoxidase (LPO) with hydrogen peroxide at pH 7.1. Dashed lines represent native enzyme. the numbers show time in ms from the stop flow to the end of the wavelength scan. Thus, early times represent compound I spectra, and late times compound II. At intermediate times, mixtures were obtained. Reference 28	12

		rage
1-7	Absorption spectra of native cytochrome c peroxidase (CcP) and CcP-I. Reference 30. CcP-I contains an amino acid radical rather than a porphyrin radical.	13
2-1	Resonance Raman spectra of $^{18}\text{O}=\text{Fe}^{\text{IV}}(\text{Im})\text{PPDME}$ (upper trace), and $^{16}\text{O}=\text{Fe}^{\text{IV}}(\text{Im})\text{PPDME}$ (lower trace). Vertical line denotes ν (FeO); * denotes solvent peak. Spectra were obtained in toluene-d ₈ at -130 C with 15 mW (406.7 nm) incident on the sample. Inset: optical absorption spectrum of O=Fe ^{IV} (Im)PPDME in toluene at -90 C. The shoulder at 619 nm is due primarily to μ -oxo dimer contamination.	18
3-1	Resonance Raman spectra excited at 406.7 nm.	
	(a) Co ^{II} OEP+*ClO ₄ - prepared with AgClO ₄ ;	
	(b) Co ^{III} OEP+'2ClO ₄ - prepared with Fe(ClO ₄) ₃ ;	
	(c) Co ^{III} OEP ⁺ ·2ClO ₄ ⁻ , prepared with Fe(ClO ₄) ₃ and a trace amount of HClO ₄ ;	
	(d) $H_4OEP^{2+}2ClO_4^-$, prepared from $H_2OEP + HClO_4$. All	
	samples were dissolved in CH ₂ Cl ₂ . A spinning quartz cell	
	and ~20 mW laser power were used. Solvent bands are labelled with an *	27
	labelled with an	21
3-2	RR spectra of ZnOEP ⁺ ·ClO ₄ . (a) $\lambda_{\rm ex}$ = 390 nm; (b) - (d) show a time course at $\lambda_{\rm ex}$ = 406.7 nm for \sim 1 ml of sample in a quartz spinning cell with a laser power of 16 mW. The time values indicate total irradiation time at the end of the	
	scan	30
4-1	Electronic absorption spectra of (a) CuOEP+*ClO4- and	
	(b) ZnOEP+*ClO ₄ - (0.2 mM) in dry CH ₂ Cl ₂ . Extinction	
	coefficients were taken from references 29 and 4, respectively	42
4-2	RR spectra of Cu and ZnOEP and their corresponding cation radicals. (a) CuOEP; (b) CuOEP+*ClO ₄ -; (c) ZnOEP;	
	(d) ZnOEP ⁺ *ClO ₄ ⁻ , excitation at 390 nm (1.5 mJ/pulse,	
	$[ZnOEP^{+*}] \simeq 0.2 \text{ mM})$ reflects vibrations of the monomer.	
	CH ₂ Cl ₂ bands are marked with an *. CW laser power 20-35 mW, at 363.8 nm for (a)-(c).	45
	mw, at 363.8 nm for (a)–(c).	40
4-3	Resonance Raman spectra excited at 406.7 nm.	
	(a) Co ^{II} OEP ⁺ ·ClO ₄ ⁻ ;	
	(b) Co ^{III} OEP ⁺ ·2ClO ₄ ⁻ containing small amounts of porphyrin diacid impurity;	
	(c) H ₄ OEP ²⁺ 2ClO ₄ ⁻ ;	
	(d) a mixture of H ₃ OEP ⁺ ClO ₄ ⁻ and H ₄ OEP ²⁺ 2ClO ₄ ⁻ resulting from treatment of OEPH ₂ with AgClO ₄ ;	

		Page
	(e) H ₄ OEP ²⁺ 2Br ⁻ . RR bands of the solvent, dry CH ₂ Cl ₂ , are marked with an*. Vertical dashed lines mark the vibrations of the diacid, H ₄ OEP ²⁺ 2Br ⁻ . Laser power, 20 mW.	48
4-4	Electronic absorption spectra of porphyrin free base acids. (a) H ₄ OEP ²⁺ 2ClO ₄ ⁻ ; (b) a mixture of H ₃ OEP ⁺ ClO ₄ ⁻ and H ₄ OEP ²⁺ 2ClO ₄ ⁻ corresponding to Fig. 4-3d. Solvent, dry CH ₂ Cl ₂ .	51
4-5	Electronic absorption spectra of CoOEP and its oxidation products. (a) CoOEP(-); (b) Co ^{II} OEP ⁺ ·ClO ₄ ⁻ (); (c) Co ^{III} OEP ⁺ ·2ClO ₄ ⁻ (···). Solvent, dry CH ₂ Cl ₂ .	54
4-6	Electronic absorption spectra of oxidation products of CoOEP. (a) $Co^{III}(MeOH)_2OEPBr^-(-)$; (b) $Co^{III}OEPBr^-()$; (c) $Co^{III}OEP^+ 2Br (\cdots)$, the small feature at 401 nm is due to 1% $H_4OEP^{2+}2Br^-$ contamination as discussed in the text. Solvent, dry CH_2Cl_2 , except for (a) which contains $\sim 5\%$ methanol (MeOH).	57
4-7	RR spectra excited at 363.8 nm (~35 mW) of CoOEP and its oxidation products. (a) CoOEP; (b) Co ^{III} (MeOH) ₂ OEPClO ₄ ⁻ ; (c) Co ^{II} OEP ⁺ ·ClO ₄ ⁻ ; (d) Co ^{III} OEP ⁺ ·2ClO ₄ ⁻ ; (e) Co ^{III} (MeOH) ₂ OEPBr ⁻ ; (f) Co ^{III} OEPBr ⁻ ; (g) Co ^{III} OEP ⁺ ·2Br ⁻ . Solvent, dry CH ₂ Cl ₂ except (b) and (e) which contain ~5% methanol. Solvent bands are marked with an *.	60
4-8	RR spectra excited at 514.5 nm (100 mW). (a) CoOEP; (b) Co ^{III} (MeOH) ₂ OEPBr ⁻ ; (c) Co ^{III} OEPBr ⁻ . CH ₂ Cl ₂ bands marked *.	. 66

		Page
4-9	RR spectra of Co ^{III} OEP ⁺ ·2Br ⁻ . $\lambda_{ex} = (a) 620 \text{ nm}, 300 \text{ mW};$ (b) 647.1 nm, 250 mW; (c)-(d) 676.4 nm, 100 mW. CH ₂ Cl ₂	
	bands marked *. Spike (**) in (b) is Rayleigh scattering at 676.4 nm.	69
4-10	Electronic absorption spectra showing the conversion of $Co^{II}OEP^+:ClO_4^-$ to $Co^{III}(H_2O)_2OEPClO_4^-$ as the temperature is lowered. Solvent, "dry" CH_2Cl_2 ; path length $\simeq 2mm$ (EPR tube).	73
4-11	Porphyrin core vibrational mode frequencies (for Raman allowed bands, $1450-1700 \text{ cm}^{-1}$) vs. porphyrin core size for the indicated MOEP complexes and their corresponding cation radicals, MOEP^{+} · ClO_4 . Mode assignments are according to reference 33a. Open symbols correspond to parent MOEP frequencies; filled symbols correspond to MOEP^{+} · ClO_4 -frequencies. The regression analysis does not include the Ni (D _{2d}) points. Ct-N distances are from reference 45	78
4-12	Electronic transition energies vs. porphyrin core size for the indicated MOEP and MOEP*ClO ₄ - complexes. Open and filled symbols correspond to absorption band maxima of MOEP and MOEP*ClO ₄ -, respectively.	81
5-1	End view (a), longitudal section (b) and cross-section (c) of the eight-jet, tangential mixers. Ref. 48.	107
5-2	Instrumental configuration used for pulsed resonance Raman measurements of flowing HRP-I samples prepared by rapid mixing. Laser irradiation at 390 nm (5 ns pulses, 1 mJ/pulse, 10 Hz) was provided by pumping Exciton LD390 laser dye in the Quanta Ray Pulsed Dye Laser (PDL-1) with the third harmonic (355 nm) from the Nd:Yag DCR-1A laser. Raman scattering from the sample (at position X) was collected with a Spex 1459 Illuminator, dispersed in a triple monochromator, and detected and analyzed by using the EG&G PAR 1420 diode array detector and associated OMA II electronics. RR scattering excited at 390-435 nm from HRP-II samples in a cooled (2-5 C) cylindrical quartz spinning cell was also measured using this instrumentation. The 10 Hz rep rate was employed on all occasions.	109
5-3	High frequency RR spectra of HRP samples at 2-10 C, 1 mJ/pulse. Sample conditions and total accumulation times: (a) spinning cell, 20 min; (b) flowing in the capillary of the rapid mixer at 0.65-0.85 ml/min, 40 min; (c) spinning cell, 22 min.	112
5-4	RR spectra of model compounds in CH ₂ Cl ₂ . Conditions: 40-50 mW incident on sample in spinning cell at 25 C. Accumulation times: (a) 5.3 min: (b) 10 min	114

		Page
5-5	Low frequency RR spectra of HRP samples obtained under 390 nm excitation. Total accumulation times: (a) 85 min; (b) 16 O sample: 144 min, 18 O sample: 78 min; (c) 52 min; (d) 16 O sample: 48 min, 18 O sample: 48 min. The feature at 981 cm $^{-1}$ in (b) is due to sulfate ion in the 18 O ₂ preparation.	118
5-6	High frequency RR scattering from HRP-II, pH 10.8. Accumulation time for each spectrum was 10 min using 1 mJ/pulse. Excitation wavelengths were as indicated. The $1049~\rm cm^{-1}$ peak is from $0.2~\rm M~NO_3^-$ used as an internal standard to measure relative intensities. The $984~\rm cm^{-1}$ feature is from SO_4^- .	122
5-7	High frequency RR scattering from HRP-I, pH 7. (a) 1.9 mJ/pulse, 4 min; (b) 15 mW, 0.5 s/cm ⁻¹ ; sample flow rate, 0.22 ml/min; similar results were obtained flowing at 0.7 ml/min; (c) 1 mJ/pulse, 40 min.	125
5-8	Low frequency RR scattering from HRP-II, pH 10.8. Accumulation time was 10 min for (a)-(d), 20 min for (e)-(f), using 1 mJ pulses. The 983 cm ⁻¹ peak is from 0.2 M SO ₄ ⁻ used as an internal intensity standard. The 1049 cm ⁻¹ feature is from NO ₃ ⁻ .	127
5-9	Excitation profiles of $v_7 = 680 \text{ cm}^{-1}$, $v(\text{FeO}) = 787 \text{ cm}^{-1}$ and $v_4 = 1379 \text{ cm}^{-1}$.	129
5-10	Schematic diagram of the active site of HRP catalytic intermediates, showing HRP-I, the postulated photoproduct HRP-I*, the reaction of HRP-I with a phenolic substrate, and HRP-II.	134

CHAPTER I

GENERAL INTRODUCTION

Aerobic organisms reduce molecular oxygen (O_2) to water (H_2O) . Partial reduction of dioxygen can result in the formation of hydrogen peroxide (H_2O_2) and superoxide (O_2^-) . These compounds are potentially dangerous to the organism and are removed from the cell by enzyme catalases, peroxidases, and superoxide dismutases. While catalase enzymes convert hydrogen peroxide directly to water and dioxygen, peroxidases utilize hydrogen peroxide to oxidize various organic and inorganic compounds. 1

The active site of native peroxidases and catalyses most often contain a five-coordinate ferriprotoporphyrin IX prosthetic group as shown in Figure 1-1a. The proximal ligand to the iron may vary and is typically a histidine nitrogen (e.g. horseradish peroxidase, HRP),²⁻⁴ cysteine sulfur (e.g. chloroperoxidase, CPO),^{4,5} or tyrosine oxygen (e.g. bovine catalase, CAT).⁶

Horseradish peroxidase isolated from plants is the best characterized and most readily available of the peroxidase enzymes. The general catalytic mechanism of plant peroxidases is depicted by the following scheme proposed originally for HRP:7

Figure 1-1. (a) Ferriprotoporphyrin IX. (b) Metallooctaethylporphyrin. Carbons a (or α) are bonded to the nitrogen atoms. Carbons b (or β) are bonded to the peripheral substituents. The methine, CH, positions are meso. The metal center, M, may be further ligated in the axial positions normal to the macrocycle plane.

Native (Fe^{III}) + H₂O
$$\rightarrow$$
 compound I (Fe^{IV}) + H₂O compound I (Fe^{IV}) + AH \rightarrow compound II (Fe^{IV}) + A· compound II (Fe^{IV}) + AH \rightarrow native (Fe^{III}) + A· + H₂O 2A· \rightarrow products

In the first step of this sequence, the heme reacts with hydrogen peroxide to form compound I (green), which is two oxidation equivalents above the native ferric state. Compound I rapidly oxidizes the substrate in the second step, forming the more stable, second intermediate, compound II (red). In the final step of the reaction, compound II relaxes to regenerate the native ferric state of the enzyme (brown).

The structural, electronic and magnetic properties of peroxidase compounds I and II have been investigated for a number of years. Most studies have used HRP owing to the ease of isolation and purification as well as the stability of its compound I (HRP-I) relative to other peroxidases. The absorption spectra of native HRP, HRP-I and HRP-II appear in Figure 1-2. HRP-I is currently described as a spin-coupled oxoferryl porphyrin π cation radical complex. In this structure one electron has been removed from the ferric center to yield Fe^{IV} and the other electron has been removed from the porphyrin ring to yield a delocalized porphyrin π cation radical. The Fe^{IV} center is six-coordinate, being bound on the proximal side by histidine nitrogen and on the distal side by an oxime group, yielding a $O=Fe^{IV}-N(His)$ configuration axial to the heme ring, reducing the π cation radical but leaving the oxoferryl nitrogen ligation unchanged. e^{IV}

Significance of the Oxoferryl and Porphrin T Cation Radical Structures

The oxoferryl m cation radical structure is considered common to catalytic

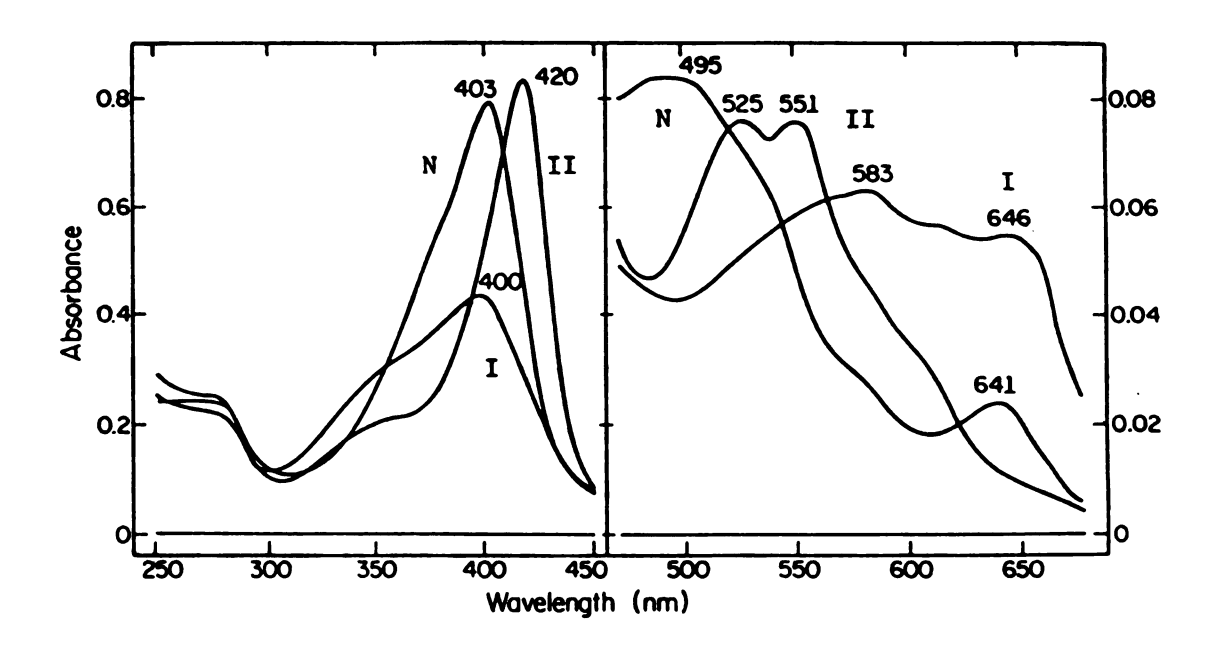


Figure 1-2. Optical absorption spectra of native HRP (N), HRP-I (I) and HRP-II (II). Reference 31.

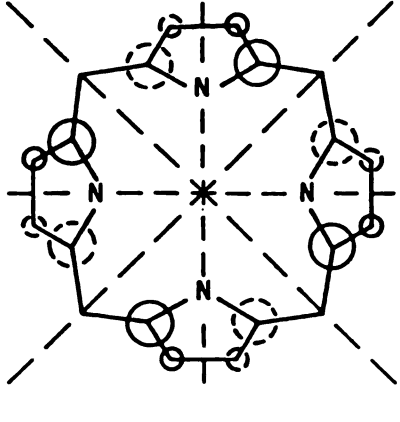
intermediates of a range of heme peroxidase and catalase enzymes $^{1-4}$ and possibly to cytochrome $P_{450}.^{10}$ The π cation radical structure has also been implicated in the photosynthetic process of both higher plants and bacteria 11 and in the catalytic cycles of nitrite and sulfite reductases. 12 The oxoferryl structure has also been proposed for an intermediate in the reaction of cytochrome oxidase with dioxygen. 13 Thus the significance of both the oxoferryl and the porphyrin π cation radical structures to the redox and electron transport functions of metalloporphyrins in nature is clear.

Aim and Strategy of the Thesis

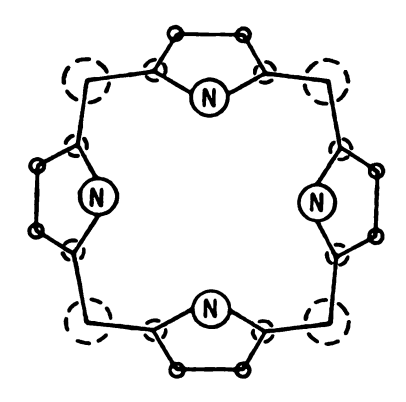
The aim of this work is to characterize the vibrational, electronic and structural properties of the first intermediate of the catalytic cycle of HRP, HRP-I, by using resonance Raman spectroscopy in conjunction with rapid mixing techniques applied to the enzyme in vitro. The difficulties associated with this measurement, the means adopted to circumvent them, and the results obtained by the technique are discussed in Chapter 5. In addition to the work with the enzyme, we utilize systematic spectroscopic studies of various model compounds to explore separately the properties of the oxoferryl-nitrogen linkage and the porphyrin π cation radical. This work is described in Chapters 2-4.

Metalloporphyrin T Cation Radicals and Compound I

Chapters 2 and 3 describe a spectroscopic study of highly symmetric (D_{4h}) metallooctaethylporphyrin π cation radicals (see Figure 1-1b). Oxidation of the porphyrin ring occurs by the removal of an electron from either of the nearly degenerate highest filled π molecular orbitals (HOMOs). In D_{4h} symmetry these oribtals are designated $a_{1u}(\pi)$ and $a_{2u}(\pi)$. Their structure is shown in Figure 1-3.14 As representative examples for discussion we choose two cobaltic



HOMO "a_{lu} (π)"



HOMO-1 "a_{2u} (π)"

Figure 1-3. The atomic orbital (AO) structure of two HOMOs of porphine. The AO coefficients are proportional to the size of the circles; solid lines indicate positive values, dashed lines negative. The view is from the positive z axis. The straight dashed lines indicate the nodes of the a_{1u} (π) orbital. Reference 14.

octaethylporphyrin T cation radicals, CoIIIOEP+2Br- and CoIIIOEP+2ClO₄-. These two compounds are thought to occupy the $^2\mathrm{A}_{1u}$ and $^2\mathrm{A}_{2u}$ electronic ground states, respectively. Much emphasis has been given to characterization of the spectroscopy of these (and other) metalloporphyrin \(\pi \) cation radicals (MP+*) in terms of these two electronic configurations. While this approach has been successful in the first approximation, especially for interpreting the EPR and ENDOR spectra of these compounds, 15,16 some controversy has emerged based on NMR results. 17 The original extension of the model compound studies to the enzyme intermediates is presented in Figure 1-4. Based on the similarity of the optical absorption spectra of HRP-I and CAT-I to that of Co^{III}OEP+*2ClO₄and Co^{III}OEP+·2Br-, respectively, Dolphin et al. 16 proposed porphyrin π cation structures for the enzyme intermediates. It is further suggested that both electronic states are represented by HRP-I (2A211) and CAT-I (2A111). EPR and ENDOR measurements have confirmed the " cation radical formulation for HRP-I.18,19 However, the question of electronic ground state for these and other compound I structures is unclear. The results for EPR and Mossbauer studies²¹⁻²³ often seem to contradict classifications suggested by optical absorption spectra. 20,24 More specifically, the EPR and Mössbauer measurements of compound I type intermediates often give evidence of magnetic coupling between the S=1 oxoferryl and the S=1/2 porphyrin π cation radical spin systems. Such interaction is not expected if the porphyrin radical resides in the $a_{li}(\pi)$ orbital owing to the lack of spin density on the nitrogen atoms (see Figure 1-3). However, chloroperoxidase compound I (CPO-I) and certain reconstituted HPR-I species exhibit both ²A_{lu} type absorption spectra and magnetic coupling. Thus a contradiction arises. Furthermore, the magnetic coupling between paramagnetic metal centers, such as the oxoferryl structure and porphyrin π cation radicals, is not well understood. 22,25 Part of this confusion is caused

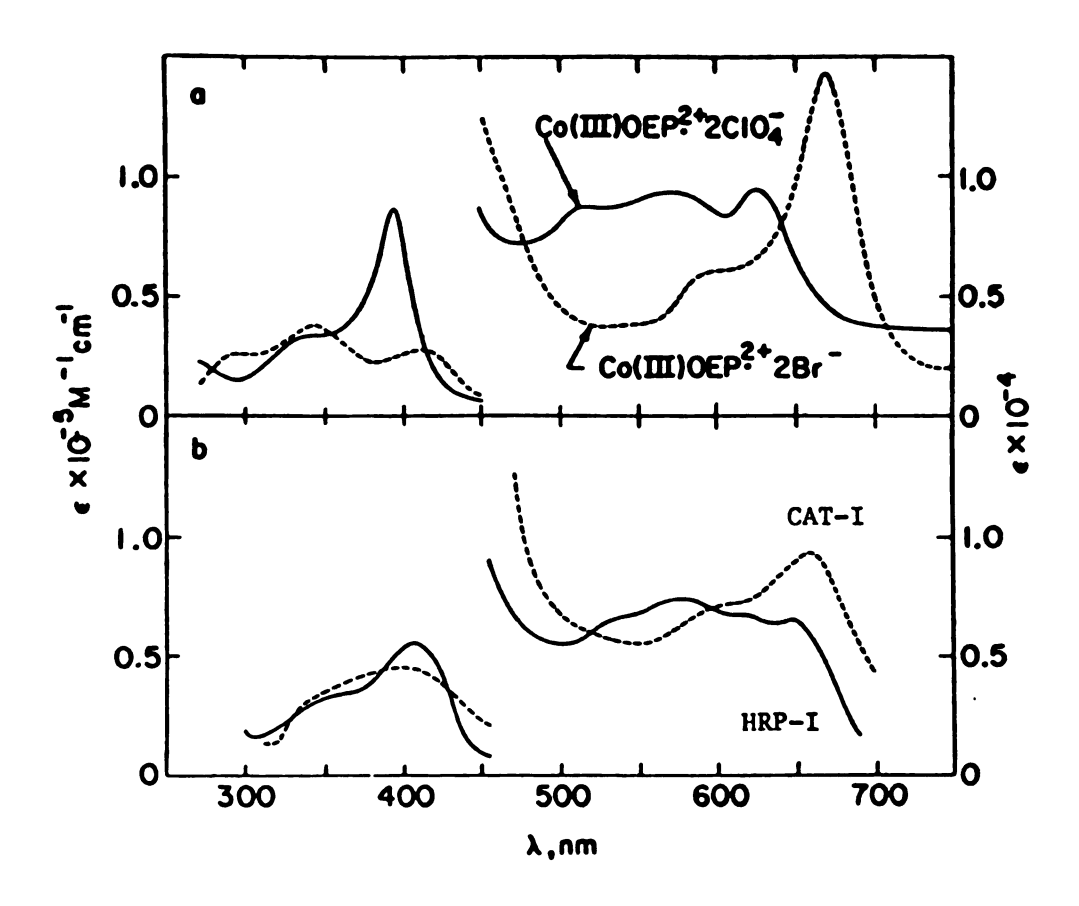


Figure 1-4. Optical absorption spectra of (a) cobaltic octaethylporphyrin π cation radicals, (b) compound I enzyme transients. $^2A_{2u}$ type spectra (--). Reference 16.

by the lack of knowledge of the effects of symmetry lowering on the spectral properties of metalloporphyrin π cation radicals.²² In the natural compound I systems the molecular symmetry is lowered (from D_{4h}) by asymmetric peripheral substitution of the ring, mixed axial ligation and possibly further by porphyrin core distortions. Neglecting core distortions (i.e. doming or buckling of the porphyrin ring system) the symmetry of compound I is $\boldsymbol{C}_{\boldsymbol{S}}$ or lower. An understanding of the relationship between the different mechanisms of symmetry lowering and the electronic ground state as well as an understanding of how each influence of spectroscopy of the MP+ are necessary to resolve these questions. It has been suggested that S₄ type ruffling of the porphyrin ring may provide an overlap pathway for antiferromagnetic coupling in ferric porphyrin π cation radicals.²⁵ Thus, with our MP⁺⁺ model work we take a structural approach which focuses on understanding the effects of the porphyrin core geometry on the vibrational and electronic properties of the MP+. It is anticipated that the resulting correlations can be used to suggest core geometries for unknown structures. Below, in Figures 1-5, 1-6 and 1-7 optical absorption spectra of various catalase and peroxidase compound I intermediates are collected.

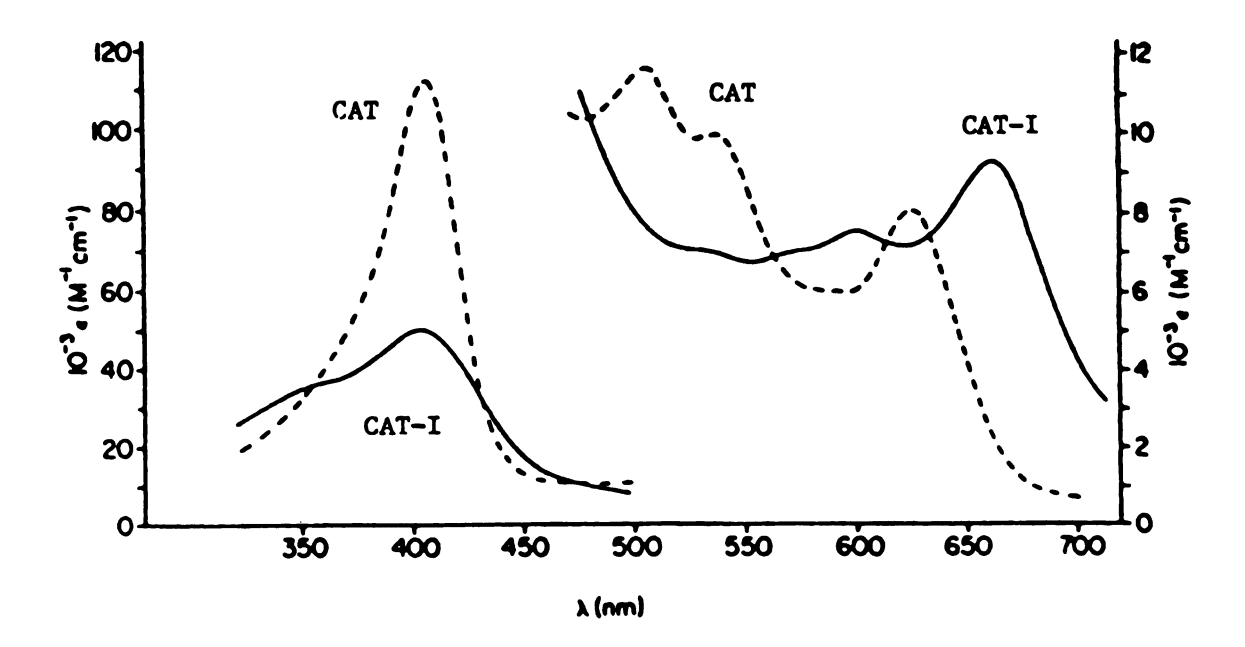
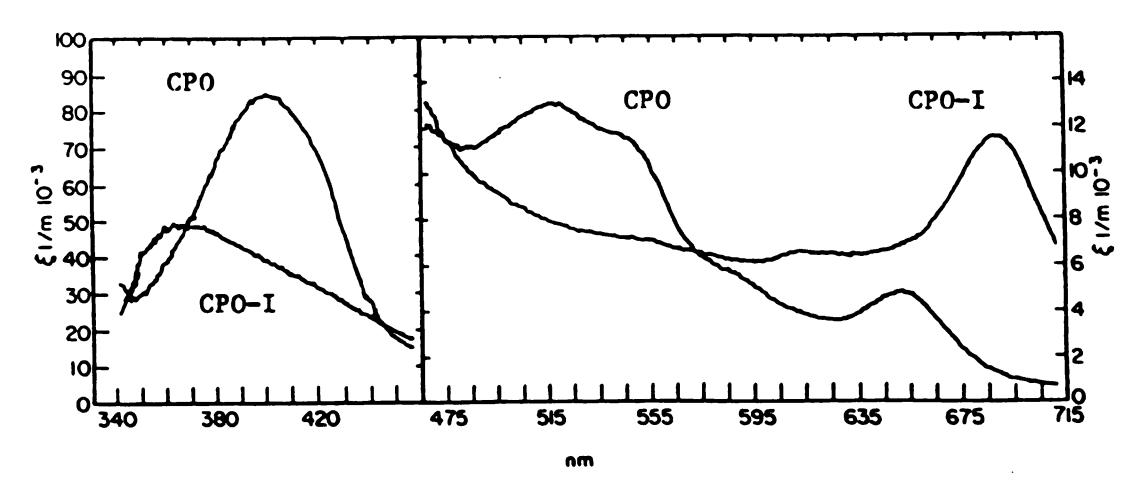


Figure 1-5. Optical absorption spectra of compound I intermediates $(^2A_{1u}$ type). (a) native horse erythrocyte catalase (CAT) and CAT-I. Reference 26.



(b) native chloroperoxidase (CPO) and CPO-I. Reference 24.

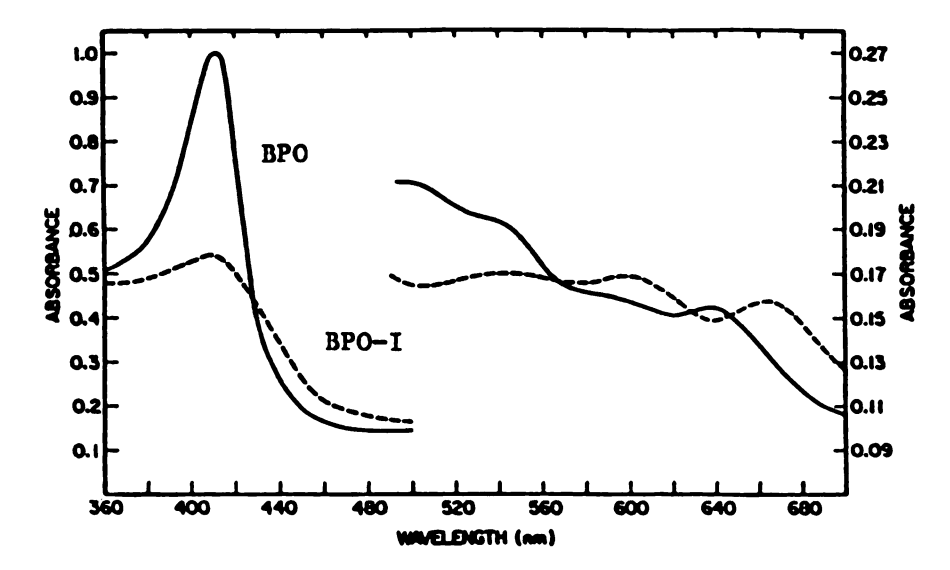
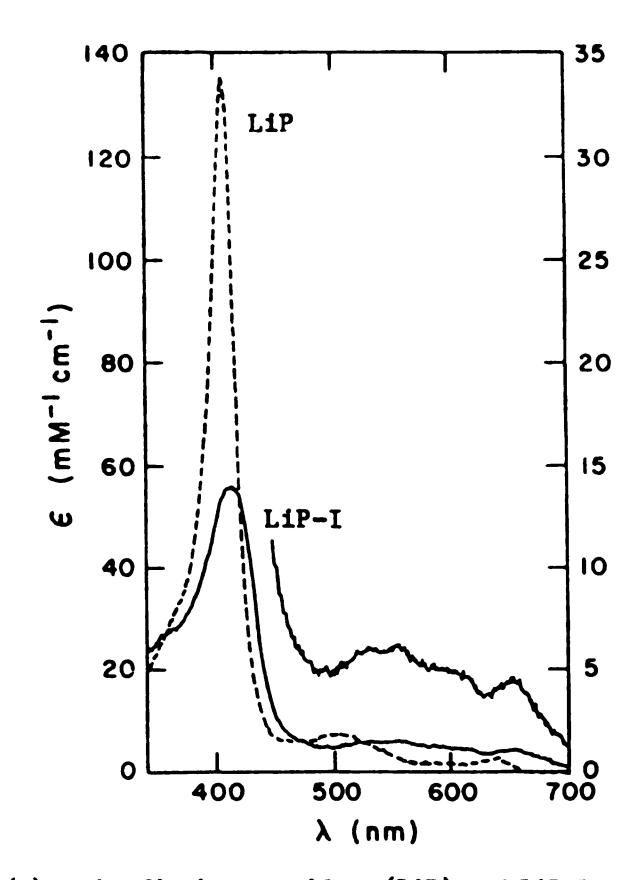
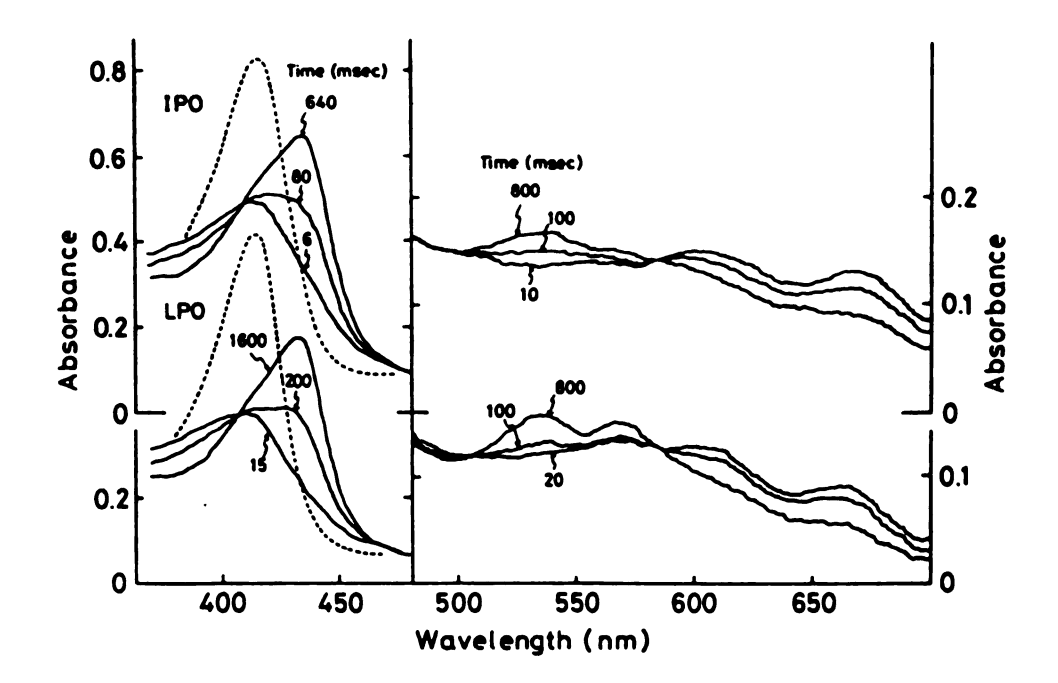


Figure 1-6. Optical absorption spectra of compound I intermediates. $(^2A_{2u}$ type). (a) native ferric bromoperoxidase (BPO) and BPO-I.

Reference 27.



(b) native lignin peroxidase (LiP) and LiP-I. Reference 29.



(c) Rapid scan spectrophotometric measurements for the reactions of intestinal peroxidase (IPO) and lactoperoxidase (LPO) with hydrogen peroxide at pH 7.1. Dashed lines represent native enzyme. the numbers show time in ms from the stop flow to the end of the wavelength scan. Thus, early times represent compound I spectra, and late times compound II. At intermediate times, mixtures were obtained. Reference 28.

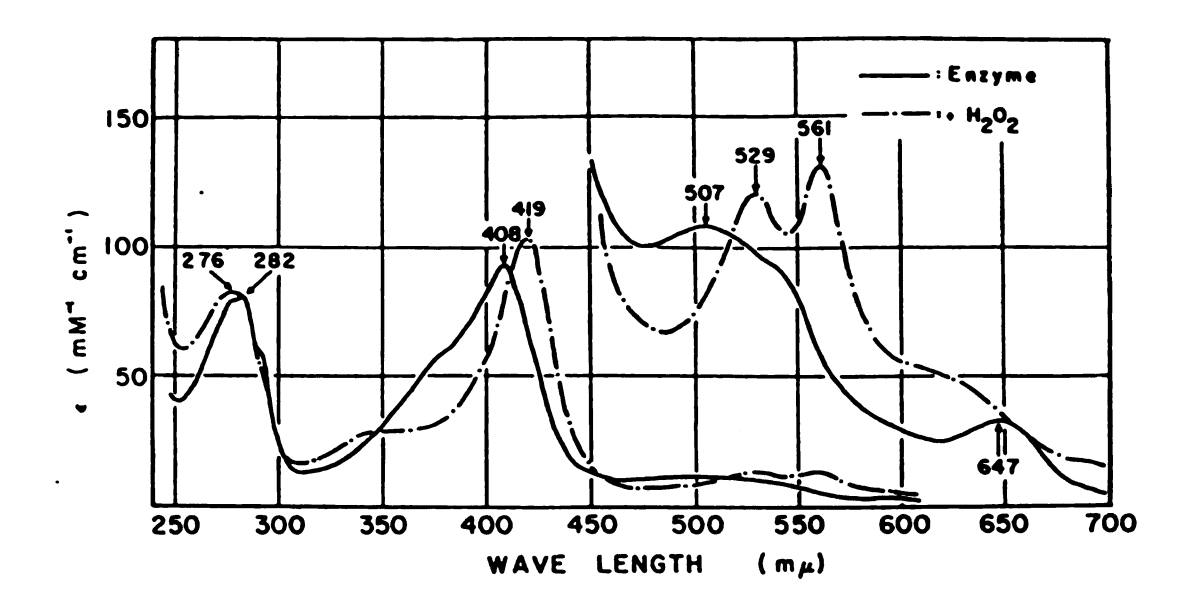


Figure 1-7. Absorption spectra of native cytochrome c peroxidase (CcP) and CcP-I. Reference 30. CcP-I contains an amino acid radical rather than a porphyrin radical.

REFERENCES

- 1. Bolscher, B. Ph.D. Thesis.
- 2. Dunford, H.B.; Stillman, J.S., Coord. Chem. Rev. 1976, 19, 187-251.
- 3. Frew, J.E.; Jones, P., Adv. Inorg. Bioinorg. Mech. 1984, 3, 175-213.
- 4. Hewson, W.D.; Hager, L.P. in "The Porphyrins"; Dolphin, D., Ed.; Academic Press: New York, 1979; Vol. VII, pp. 295-332.
- 5. Cramer, S.P.; Dawson, J.H.; Hodgson, K.O.; Hager, L.P., J. Am. Chem. Soc. 1978, 100, 7282-7290.
- 6. Murthy, M.R.N.; Reid, R.J.; Sicignano, A.; Tanaka, N.; Rossmann, M.G., J. Mol. Biol. 1981, 152, 465-499.
- 7. (a) Chance, B., Arch. Biochem. Biophys. 1952, 41, 416-424; (b) George, P., Nature 1952, 169, 612-613.
- (a) Theorell, H.; Ehrenberg, A., Arch. Biochem. Biophys. 1952, 41, 442-461;
 (b) Brill, A.S.; Williams, R.J.P., Biochem. J. 1961, 78, 253-263;
 (c) Blumberg, W.E.; Peisach, J.; Wittenberg, B.A.; Wittenberg, J.B., J. Biol. Chem. 1968, 243, 1854-1862; (d) Wittenberg, B.A.; Kampa, L.; Wittenberg, J.B.; Blumberg, W.E.; Peisach, J., J. Biol. Chem. 1968, 243 1863-1870; (e) Peisach, J.; Blumberg, W.E.; Wittenberg, B.A.; Wittenberg, J.B., J. Biol. Chem. 1968, 243, 1871-1880.
- 9. (a) Keilin, D.; Hartree, E.F., Biochem. J. 1951, 49, 88-109; (b) Shannon, L.M.; Kay, E.; Lew, J.Y., J. Biol. Chem. 1966, 241, 2166-2172.
- 10. Groves, J.T.; Haushalter, R.C.; Nakamura, M.; Nemo, T.E.; Evans, B.J., J. Am. Chem. Soc. 1981, 103, 2884-2886.
- 11. Parson, W.W.; Ke, R. in "Photosynthesis: Energy Conversion by Plants and Bacteria"; Govindjee, Ed.; Academic: New York, 1983.
- 12. Chang, C.K.; Hanson, L.K.; Richardson, P.F.; Young, R.; Fajer, J., Proc. Natl. Acad. Sci. USA 1981, 78, 2652-2656.

- 13. Blair, D.F.; Witt, S.N.; Chan, S.I., J. Am. Chem. Soc. 1985, 107, 7389-7399.
- 14. Maggiora, G.M., J. Am. Chem. Soc. 1973, 95, 6555-6559.
- 15. Fajer, J.; Davis, M.S. in "The Porphyrins", Dolphin, D., Ed.; Academic Press: New York, 1979; Vol. IV, pp. 197-256.
- Dolphin, D.; Forman, A.; Borg, D.C.; Fajer, J.; Felton, R.H., Proc. Natl. Acad. Sci. USA 1971, 68, 614-618.
- 17. Morishima, I.; Takamaki, Y.; Shiro, Y., J. Am. Chem. Soc. 1984, 106, 7666-7672.
- 18. Schulz, C.E.; Devaney, P.W.; Winkler, H.; Debrunner, P.G.; Doan, N.; Chiang, R.; Rutter, R.; Hager, L.P., FEBS Lett. 1979, 103, 102-105.
- 19. Roberts, J.E.; Hoffman, B.M.; Rutter, R.; Hager, L.P., J. Biol. Chem. 1981, 256, 2118-2121.
- 20. DiNello, R.K.; Dolphin, D., J. Biol. Chem. 1981, 256, 6903-6912.
- 21. Rutter, R.; Valentine, M.; Henrich, M.P.; Hager, L.P.; Debrunner, P.G., Biochemistry 1983, 22, 4769-4774.
- 22. Schultz, C.E.; Rutter, R.; Sage, J.T.; Debrunner, P.G.; Hager, L.P., Biochemistry 1984, 23, 4743-4754.
- 23. Rutter, R.; Hager, L.P., J. Biol. Chem. 1982, 257, 7958-7961.
- 24. Palcic, M.M.; Rutter, R.; Araiso, T.; Hager, L.P.; Dunford, B.H., Biochem. Biophys. Res. Comm. 1980, 94, 1123-1127.
- 25. Gans, P., Buisson, G.; Duée, E.; Marchon, J.-C.; Erler, B.S.; Scholz, W.F.; Reed, C.A., J. Am. Chem. Soc. 1986, 108, 1223-1234.
- 26. Schonbaum, G.R.; Chance, B. in the "The Enzymes"; Boyer, P.D., Ed.; Academic Press: New York, 1976, Vol. 13, pp. 363-408.
- 27. Manthey, J.A.; Hager, L.P., J. Biol. Chem. 1985, 260, 9654-9659.
- 28. Kimura, S., Yamazaki, I., Arch. Biochem. Biophys. 1979, 198, 580-588.
- 29. Renganathan, V.; Gold, N.H., Biochemistry 1986, 25, 1626-1631.
- 30. Yonetoni, T., J. Biol. Chem. 1965, 240, 4509-4514.
- 31. Hewson, W.D.; Hager, L.P., J. Biol. Chem. 1979, 254, 3182-3186.

CHAPTER 2

CHARACTERIZATION OF SIX-COORDINATE OXOFERRYL PROTOHEME BY RESONANCE RAMAN AND OPTICAL ABSORPTION SPECTROSCOPY*

SUMMARY

As a model for oxoferryl intermediates of heme enzymes, we have synthesized (1-methylimidazole) oxoferryl protoporphyrin IX dimethyl ester, O=Fe^{IV}(Im)PPDME, and characterized it by using optical absorption and resonance Raman spectroscopy. We observe an FeO stretching frequency, ν (FeO), of 820 cm⁻¹ for O=Fe^{IV}(Im)PPDME, which is assigned by its shift to 784 cm⁻¹ upon substitution of ¹⁶O with ¹⁸O. While the optical absorption spectrum of the six-coordinate protoheme model is very similar to that of oxoferryl myoglobin, its ν (FeO) is 23 cm⁻¹ higher. Based on results from five- and six-coordinate oxoferryl porphyrin models, we attribute this higher frequency to weaker imidazole ligation and an absence of protic environmental effects.

*Robert T. Kean, W. Anthony Oertling, and Gerald T. Babcock, <u>J. Am. Chem. Soc.</u>, 1987, in press.

Oxoferryl species, O=Fe^{IV}, have been postulated in the catalytic cycle of cytochrome c oxidase. 1 as the oxygen donating species in cyctochrome P-450.2 and as intermediates in the reactions of catalases and peroxidases.³ Given the diverse chemistry catalyzed by these various enzymes, heme pocket modulation of the chemical reactivity of the O=Fe^{IV} unit seems likely. Resonance Raman detection of the v (FeO) in various protein species and model compounds supports this notion. In a comparison of oxoferryl peroxidase species. 4 oxoferryl myoglobin,⁵ and five- and six-coordinate heme model compounds,^{6,7} the frequency of v(FeO) varies by $\sim 85 \text{ cm}^{-1}$ (see Table 2-1). This is in strong contrast to v(Fe-O₂) which varies by only ~10 cm⁻¹ in protein species and heme model compounds.⁸ In addition, there are distinct differences in the optical spectra of the various oxoferryl protein species. 9-11 Previously reported oxoferryl model compounds have given insight into the factors affecting the v (FeO) frequency, but since they were made on non-physiologically active hemes, they do not give specific information about the optical spectra or the other Raman active vibrations of the protoheme-containing oxoferryl protein species. To address these points, we present here optical and Raman data for a six-coordinate, imidazole-ligated, oxoferryl protoheme model compound.

The (1-methylimidazole) oxoferryl protoporphyrin IX dimethyl ester, O=Fe^{IV} (Im)PPDME, was prepared according to reference 12. The optical absorption spectrum^{13a} is inset in Figure 2-1. The shoulder at 619 nm is due primarily to μ -oxo dimer contamination. The peak positions compare favorably with those of oxoferryl hemoglobin, 9 and oxoferryl leghemoglobin, 10 (\sim 418, 545, and 575 nm) but are most similar in both wavelengths and relative intensities to oxoferryl myoglobin (\sim 420, 550, and 580 nm at pH 6.8). 11 The spectrum of O=Fe^{IV} (Im)PPDME, like the oxoferryl globin species, is distinct from that of horseradish peroxidase compound II (HRP-II; \sim 418, 527, and 555 nm). 14 In Figure 2-1 we

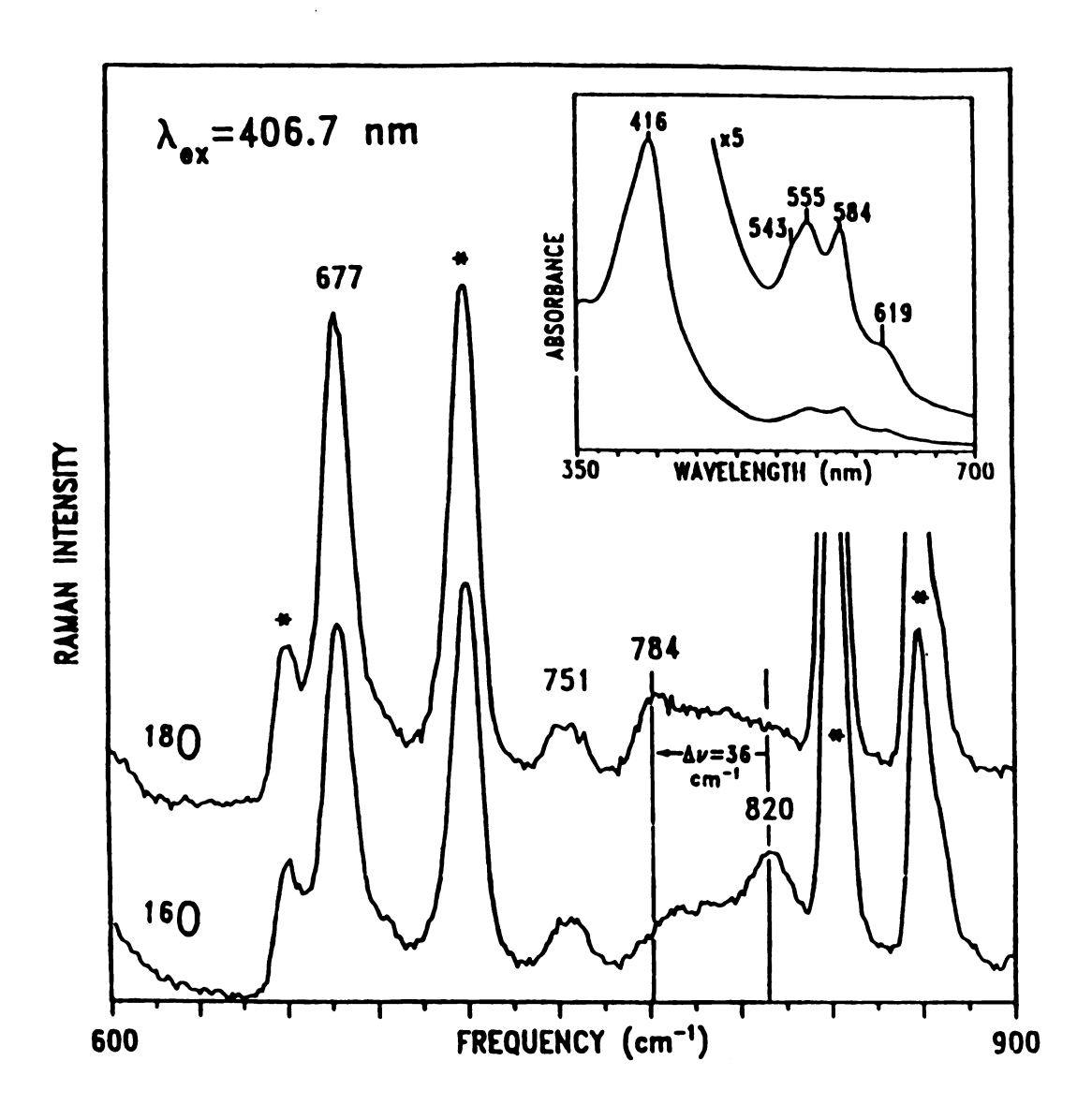


Figure 2-1. Resonance Raman spectra of $^{18}\text{O=Fe}^{IV}(Im)\text{PPDME}$ (upper trace), and $^{16}\text{O=Fe}^{IV}(Im)\text{PPDME}$ (lower trace). Vertical line denotes ν (FeO); * denotes solvent peak. Spectra were obtained in toluene-dg at -130 C with 15 mW (406.7 nm) incident on the sample. Inset: optical absorption spectrum of O=Fe $^{IV}(Im)\text{PPDME}$ in toluene at -90 C. The shoulder at 619 nm is due primarily to μ -oxo dimer contamination.

present the intermediate frequency region of the Raman spectrum 13b of O=Fe^{IV} (Im)PPDME. The peak at 820 cm⁻¹ shifts to 784 cm⁻¹ upon substitution of ¹⁶O by ¹⁸O, and is assigned to FeO stretching vibration. The 36 cm⁻¹ shift is expected for an exoferral structure. The ν (FeO) frequency observed for O=Fe^{IV} (Im)PPDME does not vary with temperature over the range -90 C to -190 C or with porphyrin ring substituents (TPP or OEP).15 This frequency is compared with the v (FeO) frequencies of other oxoferryl species in Table 2-1. The high frequency region of the O=Fe^{IV}(Im)PPDME spectrum (not shown) contains features of both HRP-II¹⁶ and oxoferryl myoblobin⁵ vet it is not identical to either.¹⁵ The similarity of the optical spectrum of oxoferryl myoglobin with that of O=Fe^{IV} (Im)PPDME indicates that the two are electronically very similar. The difference in the v (FeO) frequencies suggests environmental perturbations. Differences in the v(FeO) frequency between the peroxidase species and oxoferryl myoglobin have been discussed in terms of hydrogen bonding effects^{4c,e} and out-of-plane iron effects.⁵ It has been suggested that π charge donation from the protein into the porphyrin may be important in the mechanism of horseradish peroxidase. 17 but it is not known whether this has any affect on the v(FeO) frequency. Comparison of these systems with the model compounds gives further insights into the variables which affect the v(FeO) frequency.

A trans ligand effect is seen very clearly in the model compounds (see Table 2-1). The five-coordinate models display the highest ν (FeO) frequency, while the strong ligand (Im), six-coordinate samples display the lowest frequency. Electron density from the sixth ligand, along the z axis (normal to the heme plane), may compete with the ferryl oxygen for σ -bonding 18 and weaken the FeO bond. Alternately, if the iron is initially displaced toward the oxygen in the five-coordinate species, the presence of a strong sixth ligand may pull the

Species ^a	ν (FeO) ^b	Ref.
HRP-II pH 6.0	776	4c,e
HRP-II pH 11.0	787	4b,c
CcP-I	767	4 d
oxoferryl Mb	797	5
$O=Fe^{IV}TMP$	843	21
O=Fe ^{IV} TPP	852	6
O=Fe ^{IV} OEP	852	6
O=Fe ^{IV} (THF)TpivPP	829	7
O=Fe ^{IV} (Im)TpivPP	807	7
O=Fe ^{IV} (Im)PPDME	820 ^c	
O=Fe ^{IV} (Im)TPP	820	
O=Fe ^{IV} (Im)OEP	820	

Abbreviations: HRP-II, horseradish peroxidase compound II; CcP-I, cytochrome c peroxidase compound I; Mb, myoglobin; TMP, tetramesitylporphyrin; TPP, tetraphenylporphyrin; OEP, octaethylporphyrin; THF, tetrahydrofuran; Im, 1-methylimidazole; TpivPP, "picket fence" porphyrin, tetra(o-pivaloylphenyl)-porphyrin; PPDME, protoporphyrin IX dimethyl ester. b Frequency in c m⁻¹.

^c This work and reference 15.

iron into plane causing greater π interaction between iron and porphyrin orbitals, and a weakening of the FeO π -bond.⁵ The difference in the ν (FeO) frequency of our models (in toluene) versus the (TpivPP)⁷ species (in THF) appears to results from solvent effects since temperature and ring substituent effects were ruled out above. This may reflect stronger imidazole binding in the more polar and non-aromatic THF. Although hydrogen bonding of the oxo ligand to the distal histidine could be involved, the lower v (FeO) frequency of oxoferryl myoglobin may indicate stronger proximal imidazole ligation in myoglobin than in the model compounds. This seems reasonable since the imidazole is protein bound in myoglobin and may not easily move or rotate to less strongly ligating configurations available to the free solution models. Similar trans ligand effects may contribute to the difference in v(FeO) frequencies observed for HRP-II and oxoferryl myoglobin. For the respective five-coordinate ferrous enzymes, the higher $\nu(Fe^{II}\text{-imidazole})$ frequency for HRP indicates stronger imidazole ligation. 19,20 For the oxy complexes, v (FeII-imidazole) is also higher for HRP than for myoglobin but its $v(Fe-O_2)^{8c}$ is lower. A similar inverse relationship (Fe^{II}_CO) and trans ligand strength has been reported for monomeric between insect hemoglobins 18a and heme model compounds. 18b

ACKNOWLEDGMENTS

We thank Dwight Lillie for data handling and graphics software. This research was supported by NIH grant GM 25480.

REFERENCES AND NOTES

- 1. (a) Wikstrom, M., Proc. Natl. Acad. Sci. USA 1981, 78, 4051-4054; (b) Blair, D.F.; Witt, S.N.; Chan, S.I., J. Am. Chem. Soc. 1985, 107, 7389-7399.
- 2. Groves, J.T. in "Cytochrome P-450: Structure, Mechanism and Biochemistry"; Ortiz de Montellano, P. Ed; Plenum Press: New York, 1985; Chapter I.
- 3. Hewson, W.D.; Hager, L.P. in "The Porphyrins", Vol. VII; Dolphin, D. Ed.; Academic Press: New York, 1979, pp 295-332.
- 4. (a) Terner, J.; Sitter, A.J.; Reczek, C.M., Biochim. Biophys. Acta 1985, 828, 73-80; (b) Hashimoto, S.; Tatsuno, Y.; Kitagawa, T., Proc. Japan Acad. 1984, 60(B), 345-348; (c) Sitter, A.J.; Reczek, C.M.; Terner, J., J. Biol. Chem. 1985, 260, 7515-7522; (d) Hashimoto, S.; Teraoko, J.; Inubushi, T.; Yonetani, T.; Kitagawa, T., J. Biol. Chem. 1986, 261, 11110-11118; (e) Aν(FeO) value of 775 cm⁻¹ (HRP-II, pH 7, H₂O buffer) is reported which shifts to 777 cm⁻¹ in D₂O buffer. Hashimoto, S.; Tatsuno, Y.; Kitagawa, T., Proc. Natl. Acad. Sci. USA 1986, 83, 2417-2421.
- 5. Sitter, A.J.; Reczek, C.M.; Terner, J., Biochim. Biophys. Acta 1985, 828, 229-235.
- 6. (a) Bajdor, K.; Nakamoto, K., J. Am. Chem. Soc. 1984, 106, 3045-3046;
 (b) Proniewicz, J.M.; Bajdor, K.; Nakamoto, K., J. Phys. Chem. 1986, 90, 1760-1766.
- 7. Schappacher, M.; Chottard, G.; Weiss, R., J. Chem. Soc., Chem. Commun. 1986, 2, 93-94.
- 8. (a) Spiro, T.G. in "Iron Porphyrins", Part II; Lever, A.B.P.; Gray, H.B. Ed.; Addison Wesley: Reading, Mass, 1983; pp. 107-133; (b) Kean, R.T., unpublished results; (c) Van Wart, H.E.; Zimmer, J., J. Biol. Chem. 1985, 206, 8372-8377.
- 9. Dalziel, K.; O'Brien, J.R.P., Biochem. J. 1954, 56, 648-659.
- 10. Aviram, I.; Wittenberg, B.A.; Wittenberg, J.B.; J. Biol. Chem. 1978, 253, 5685-5689.

- 11. George, P.; Irvine, D.H., Biochem. J. 1952, 52, 511-517.
- 12. LaMar, G.N.; de Ropp, J.S.; Latos-Grazynski, L.; Balch, A.L.; Johnson, R.B.; Parish, D.W.; Cheng, R., J. Am. Chem. Soc. 1983, 105, 782-787.
- 13. (a) Optical absorption spectra were obtained by using a house build optical dewar mounted in a Perkin-Elmer Lambda 5. The sample was contained in an EPR tube which was cooled to -90°C by flowing cold nitrogen gas; (b) Raman spectra were obtained with a Spex 1401 scanning monochromator (with PMT detection) by using 15 mW incident power at 406.7 nm (Spectra-Physics model 164 Kr ion) in a backscattering geometry. The samples, contained in EPR tubes, were spun continuously in a dewar while the desired temperature was maintained by flowing cold nitrogen gas.
- 14. Blumberg, W.E.; Peisach, J.; Wittenberg, B.A.; Wittenberg, J.B., J. Biol. Chem. 1968, 243, 1854-1862.
- 15. Kean, R.T.; Babcock, G.T., manuscript in preparation.
- 16. Terner, J.; Reed, D.E., Biochim Biophys. Acta 1984, 789, 80-86.
- 17. Shelnutt, J.A.; Alden, R.G.; Ondrias, M.R., J. Biol. Chem. 1986, 261, 1720-1723.
- 18. (a) Gersonde, K.; Kerr, E.A.; Yu, N-T.; Parish, D.W.; Smith, K.M., J. Biol. Chem. 1986, 261, 8678-8685; (b) Kerr, E.A.; Mackin, H.C.; Yu, N-T., Biochemistry 1983, 22, 4373-4379.
- 19. Teraoko, J.; Kitagawa, T., Biochem. Biophys. Res. Comm. 1980, 93, 694-700.
- 20. Teraoka, J.; Kitagawa, T., J. Biol. Chem. 1981, 256, 3969-3977.
- 21. Hashimoto, S.; Tatsuno, Y.; Kitagawa, T. In "Proceedings of the Tenth International Conference on Raman Spectroscopy; Petiolas, W.L.; Hudson, B. Ed.; Univ. of Oregon: Eugene, 1986, pp. 1-28, 1-29.

CHAPTER 3

RESONANCE RAMAN SPECTROSCOPIC DETECTION OF DEMETALLATION OF METALLOPORPHYRIN T CATION RADICALS*

SUMMARY

Soret resonance Raman (RR) spectrum of samples of several different metalloporphyrin π cation radicals (MP+*) prepared by both chemical and electrochemical oxidation in CH_2Cl_2 reveal the presence of free base diacid salts produced by demetallation of the complexes. The large extinction coefficient of the diacid salt allows its selective enhancement by the RR technique at concentration levels not always evident in absorption spectra but sufficient to cause serious artifacts in the RR spectra of these samples, making recognition and analysis of the scattering from the MP+* impossible. Proper control of experimental conditions, particularly choice of excitation frequency, can eliminate these complications and produce RR spectra of MP+* free of contributions from the diacid salt.

^{*} W. Anthony Oertling, Asaad Salehi, Chi K. Chang, and Gerald T. Babcock, J. Phys. Chem., 1987, in press.

Resonance Raman (RR) spectroscopy has been utilized to extract structural and electronic information from naturally occurring metalloporphyrin systems and their models, and has recently been applied to synthetic metalloporphyrin π cation radicals (MP+·).1-3 The preparative techniques for MP+· generation, however, rarely produce a homogeneous sample.4 Owing to the selective enhancement afforded by Soret excitation RR, it is possible to detect trace amounts (less than 3%) of porphyrin free base diacid salts in samples of MP+· prepared by chemical and electrochemical oxidation in CH₂Cl₂. If unrecognized, the presence of the diacid salt may cause serious artifacts in the RR spectra of these samples that prevent accurate analysis of scattering from the MP+·.1 Proper control of experimental conditions, particularly the choice of excitation frequency, can produce RR spectra of MP+· free of contributions from the diacid.3,5

One-electron oxidation of Co and Zn octaethylporphyrin (OEP) in dry CH₂Cl₂ leads to divalent metal porphyrin π cations.^{3,6} Laser excitation at 363.8 nm selects against resonance enhancement of possible residual starting materials and produces good quality RR spectra.³ RR spectra of these MP⁺ samples excited at 406.7 nm, however, are often dominated by bands not present in spectra of 363.8 nm and not assignable to parent MP modes.⁷ The frequencies of these bands (most noteworthy are those at 1394 and 1558 cm⁻¹) show no metal dependence. These facts suggest the presence of an impurity which absorbs strongly near 406.7 nm.

Figure 3-1a and 3-1b show RR scattering excited at 406.7 nm from samples of Co^{II}OEP⁺·ClO₄⁻ prepared with AgClO₄ and Co^{III}OEP⁺·2ClO₄⁻ prepared with Fe(ClO₄)₃, respectively.⁸ Although the RR spectra of these two species excited at 363.8 nm are very similar³, with excitation at 406.7 nm additional bands appear in the spectrum of the cobaltic OEP⁺· relative to the cobaltous sample.

Figure 3-1. Resonance Raman spectra excited at 406.7 nm.

- (a) Co^{II}OEP+·ClO₄- prepared with AgClO₄;
- (b) Co^{III}OEP+ 2ClO₄ prepared with Fe(ClO₄)₃;
- (c) Co^{III}OEP^{+*}2ClO₄⁻, prepared with Fe(ClO₄)₃ and a trace amount of HClO₄;
- (d) $H_4OEP^{2+}2ClO_4^-$, prepared from $H_2OEP + HClO_4$. All samples were dissolved in CH_2Cl_2 . A spinning quartz cell and ~ 20 mW laser power were used. Solvent bands are labelled with an *.

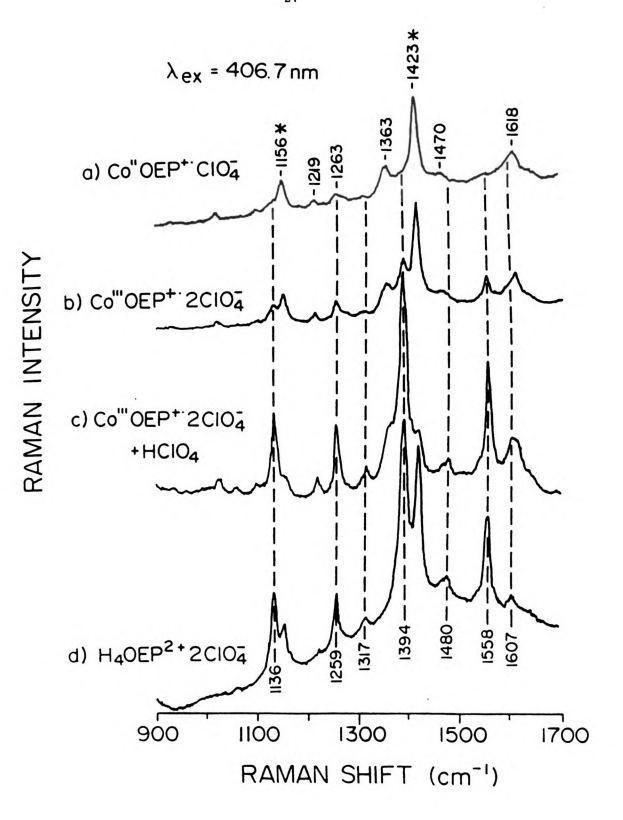
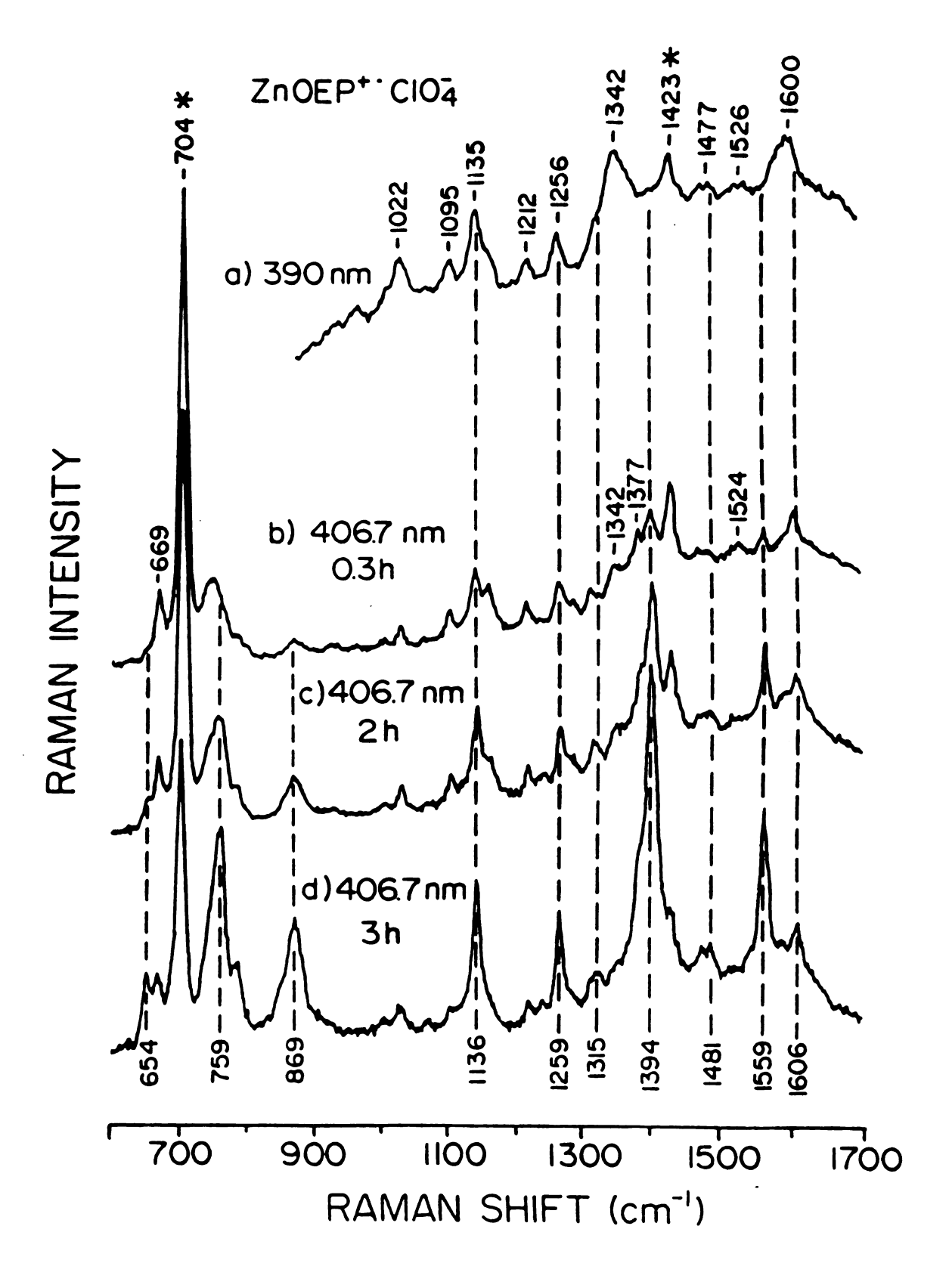


Figure 3-1c shows scattering from a sample of $Co^{III}OEP^{+}\cdot 2ClO_4^-$ prepared with $Fe(ClO_4)_3$ and a trace amount of $HClO_4$. The added intensity of the spurious bands in this spectrum suggests that the impurity is caused by acid promoted demetallation of the $MP^{+}\cdot$ and protonation of the resultant free base porphyrin. Figure 3-1d shows the RR spectrum of the diacid salt $H_4OEP^{2+}2ClO_4^-$, confirming this as the interfering species.

Thus, RR spectra of MP⁺⁺ samples exicted at 406.7 nm may contain artifacts due to free base diacid salts present at concentrations too low to be obvious in the optical absorption spectrum yet high enough to dominate the RR scattering at 406.7 nm. This is clear from the Soret optical properties of the impurity: the Soret band sharpens dramatically and red-shifts to 406 nm (ε = 430mM⁻¹cm⁻¹) upon formation of the diacid from OEPH₂.⁹ Thus, the narrowed bandwidth, the increased extinction coefficient ε and the coincidence of the Soret transition energy with the laser line at 406.7 nm, explain the selective scattering from the impurity.

Figure 3-2 shows scattering excited at 390 and 406.7 nm of ZnOEP+ClO₄-. The absence of bands at 1394 and 1558 cm⁻¹ indicates no contributions from the impurity with 390 nm excitation. Spectra excited at 406.7 nm show bands at 1394 and 1559 cm⁻¹ as depicted in Figure 3-2b. Unlike the Co^{III}OEP+2ClO₄-sample, which appears to be stable to prolonged laser irradiation, the contributions from the impurity (marked by the dashed lines) increase dramatically with repeated scanning of the ZnOEP+ClO₄-sample until they dominate the spectrum as shown in Figure 3-2c-d. The solvent bands at 704 and 1423 cm⁻¹ show the opposite trend and decrease in intensity, indicating stronger absorbance at 406 nm as the impurity concentration increases. Indeed, for this MP+ sample with the Soret band at 387 nm, the Soret absorbance at 406 nm of the protonated porphyrin was easily seen to increase in parallel with

Figure 3-2. RR spectra of ZnOEP⁺·ClO₄. (a) $\lambda_{\rm ex}$ = 390 nm; (b) - (d) show a time course at $\lambda_{\rm ex}$ = 406.7 nm for ~1 ml of sample in a quartz spinning cell with a laser power of 16 mW. The time values indicate total irradiation time at the end of the scan.



the changes in the RR spectrum. 11

These results suggest a number of conclusions: (i) oxidation of MP samples in CH2Cl2 often results in the formation of free base diacid impurities which can be detected by RR at 406.7 nm; (ii) owing to trace amounts of aqueous acid impurities in reagents, oxidation with Br₂ or Fe(ClO₄)₃ is more likely to cause demetallation and diacid formation than oxidation with AgClO4 or electrochemical techniques; (iii) MOEP+ complexes prepared by electrochemical or AgClO₄ oxidation show detectable diacid formation for M = Mg or Zn but not for Co^{II} or Ni, suggesting that the ease of demetallation is core size dependent for the MP+ as it is for the parent MP;12 (iv) demetallation of ZnOEP+*ClO₄- is enhanced by laser light in the Soret region of the spectrum; and (v) though diacid formation may be limited to chlorinated solvents and use of another solvent may minimize demetallation, the utility of CH2Cl2 for RR spectroscopy and porphyrin oxidations may not be easily replaced. Recognition and elimination of these artifacts is essential to characterizing the vibrational spectra of the MP+ species. Excitation at 363.8 nm produces RR spectra free of these artifacts and illustrates vibrational similarity of $^2A_{1\imath\imath}$ and $^2\mathrm{A}_{2\mathrm{u}}$ radical types. 5,13 This similarity was obscured by the occurrence of diacid impurities in RR samples of the presumed ²A_{1u} species of previous studies.1

ACKNOWLEDGMENTS

This research was supported by the NIH grants GM-25480 (G.T.B.) and GM-36520 (C.K.C.).

REFERENCES AND NOTES

- 1. Kim, D.; Miller, L.A.; Rakhit, G.; Spiro, T.G., J. Phys. Chem. 1986, 90, 3320-3325.
- 2. Yamaguchi, H.; Nakano, M.; Itoh, K., Chem. Lett. 1982, 1397-1400.
- 3. Salehi, A.; Oertling, W.A.; Babcock, G.T.; Chang, C.K., J. Am. Chem. Soc. 1986, 108, 5630-5631.
- 4. Huet, J.; Gaudemar, A.; Boucly-Goester, C.; Boucly, P., Inorg. Chem. 1982, 21, 3413-3419.
- 5. Oertling, W.A.; Salehi, A.; Chung, Y.C.; Leroi, G.E.; Chang, C.K.; Babcock, G.T. J. Am. Chem. Soc. 1987, submitted.
- 6. (a) Fuhrhop, J.H., Struct. Bonding 1974, 18, 1-67; (b) Dolphin, D.; Mulijiani, Z.; Rousseau, K.; Borg, D.C.; Fajer, J.; Felton, R.H., Ann. N.Y. Acad. Sci. 1973, 206, 177-200.
- 7. Our results show the phenomenon to be widespread. In addition to examples presented here, we have observed similar aritfacts when using Br_2 to oxidize CoOEP and MgOEP. Oxidation of NiTPP, CuOEP, and FeOEPCl by $\mathrm{Fe}(\mathrm{ClO}_4)_3$ in $\mathrm{CH}_2\mathrm{Cl}_2$ also produces significant amounts of analogous impurities.
- 8. OEPH₂ was prepared according to Wang, C.B.; Chang, C.K. Synthesis 1979, 548-549. Insertion of metals was carried out by standard methods: Falk, J.E. "Porphyrins and Metalloporphyrins"; Elsevier: New York, 1964, 798. The metalloporphyrins were purified by recrystallization and/or chromatography to eliminate traces of free base. CH₂Cl₂ freshly distilled from CaH₂ was used as a solvent for all preparations. Details of oxidations are presented in references 3 and 5. Raman measurements on spinning samples at 406.7 nm were made as described by Ondrias, M.R., Babcock, G.T., Biochim. Biophys. Res. Comm. 1980, 93, 29-35.
- (a) Corwin, A.H.; Chivvis, A.B.; Poor, B.W.; Whitten, D.G.; Baker, E.W.,
 J. Am. Chem. Soc. 1968, 90, 6577-6583; (b) Ogoshi, H.; Watanabe, E.;
 Yoshida, Z., Tetrahedron 1973, 29, 3241-3245.

- 10. Excitation at 390 nm was provided by a pulsed laser system described by Oertling, W.A.; Babcock, G.T., J. Am. Chem. Soc. 1985, 107, 6406-6407. The RR spectral contribution from the diacid impurities are less obvious with pulsed excitation than with CW excitation at similar wavelengths, most likely reflecting a long-lived Soret excited state of the diacid species not in resonance at 390 nm.
- 11. ZnOEP*ClO₄ was prepared by oxidation with AgClO₄. Use of Fe(ClO₄)₃ as an oxidant for ZnOEP is more difficult to control as an excess will rapidly oxidize the sample to the dication. Along with this a copious amount of the diacid impurity is produced as is evidenced by the rapid growth of a sharp absorption band at 405 nm. Three control RR experiments at 406.7 nm were performed: degassed ZnOEP in CH₂Cl₂ showed no sign of the impurity (ref. 1), whereas anaerobic samples of ZnOEP*ClO₄ exhibited behavior like that shown in Fig. 2, and OEPH₂ in CH₂Cl₂ rapidly became protonated during the same time period of laser irradiation. The band at 1377 cm⁻¹ in Figure 3-2b is from unoxidized starting material and indicates the presence of the diacid under conditions of incomplete oxidation. Samples containing no detectable trace of neutral ZnOEP showed the same behavior. Samples of ZnOEP*ClO₄ not exposed to laser light showed no sign of diacid formation detectable by optical absorption spectra.
- 12. (a) Buchler, J.W.; Puppe, L.; Rohbock, K.; Schneehage, H.H., Ann. N.Y. Acad. Sci. 1973, 206, 116; (b) Shelnutt, J.A., J. Am. Chem. Soc. 1983, 105, 774-778. Free base porphyrin diacid impurities (ca 1%) have been reported in preparation of Zn and Mg porphyrin dications by Fajer, J.; Borg, D.C.; Forman, A.; Dolphin, D.; Felton, R.H., J. Am. Chem. Soc. 1970, 92, 3451-3459. It is possible that under certain conditions demetallation might occur via the dication species (e.g. footnote 11), especially for the Mg complex. However, because the second oxidation potential of ZnOEP (1.02 V, ref. 6a) is beyond the oxidizing power of our AgClO₄/CH₂Cl₂ system (0.9 V, ref. 3), demetallation via a ZnOEP²⁺ species is unlikely in this case.
- 13. Shimomura, E.T.; Phillippi, M.A.; Goff, H.M., J. Am. Chem. Soc. 1981, 103, 6778-6780.

CHAPTER 4

VIBRATIONAL, ELECTRONIC AND STRUCTURAL PROPERTIES OF

COBALT, COPPER AND ZINC OCTAETHYLPORPHYRIN T CATION RADICALS*

SUMMARY

Optical and resonance Raman (RR) spectroscopic characterization of the oxidation products of several metallooctaethylporphyrins has been carried out. One-electron oxidation of the macrocyclic yields a series of divalent metal substituted octaethylporphyrin π cation radicals, $M^{II}OEP^{+}\cdot ClO_4^-$ (M = Ni, Co, Cu and Zn). The porphyrin core vibrational frequencies above 1400 cm⁻¹ of these complexes are described by a linear function of center-to-pyrrole nitrogen distances. A comparison of these structural correlations and of Raman depolarization ratios with those of the parent MOEP compounds is used to establish vibrational mode assignments for the cations. The agreement between the correlation parameters of the MOEP and MOEP+ClO₄- suggests similar potential energy distributions in the normal modes of both species. We find

*W. Anthong Oertling, Asaad Salehi, Young C. Chung, George E. Leroi, Chi K. Chang, and Gerald T. Babcock, J. Am. Chem. Soc., 1987, submitted.

that the frequencies of the stretching modes with predominantly CbCb character increase, whereas those with $C_{a}C_{m}$ and $C_{a}N$ character decrease in the cation radical relative to the neutral metalloporphyrin. Similar trends in Soret band maxima for the # cation radicals and their parent compounds reflect changes in the relative energy of the $a_{2u}(\pi)$ orbital. These structural correlations seem to be essentially insensitive to ${}^{2}A_{2u}$ vs. ${}^{2}A_{1u}$ radical designation. With the vibrational mode correlations as a guide to evaluation of porphyrin core geometry. we have carried out a detailed analysis of the oxidation products of Co^{II}OEP suggest structures for the two-electron oxidized Co^{III}OEP+2ClO₄ and Co^{III}OEP+2Br. Differences in the high frequency vibrations of these two compounds are interpreted in terms of expansion or possible ruffling of the porphyrin core in the latter relative to the former compound. RR excitation in the 600-680 nm region of the $Co^{\mbox{\footnotesize III}}\mbox{\footnotesize OEP}^{\mbox{\footnotesize +-}}\mbox{\tiny 2Br}^{\mbox{\footnotesize --}}$ absorptions shows a lack of anomalously polarized scattering and produces spectra similar to those obtained with near uv excitation. This suggests the absence of strong Herzberg-Teller (HT) coupling between the excited electronic states of the π cation radical.

INTRODUCTION

Oxidized states of metalloporphyrins (MP) participate in the redox chemistry of a vareity of biological structures including light-harvesting photosynthetic systems and heme proteins. Oxidation of the MP may occur at the central metal, at the porphyrin ligand, or at both locations. The Fe²⁺/Fe³⁺ redox chemistry characteristic of the electron transfer function of cytochromes is well known and metalloporphyrin structures oxidized at both the central metal and the porphyrin ligand have been implicated in the catalytic cycles of heme peroxidases, P450 monooxygenases, and catalases. Because of the extensive π system,

oxidation at the porphyrin yields a delocalized π cation radial; indeed, in the case of the special pair bacteriochlorophyll <u>a</u> dimer in the photosynthetic bacterial reaction center, radical character may be shared between two porphyrin rings.² Characterization of metalloporphyrin π cation radicals is thus of interest because of their widespread occurrence in nature and because of the often unusual chemistry in which they participate.

Both chemical and electrochemical preparations of a variety of metallooctaethylporphyrin (MOEP) and metallotetraphenylporphyrin (MTPP) π cation radicals have been reported. 3-6 These oxidized complexes have been characterized principally by optical absorption, 7 EPR, 8 MCD, 9 NMR^{10,11} and IR¹² spectroscopies, and X-ray crystallography.¹³ Systematic resonance Raman (RR) studies of synthetic metalloporphyrin π cation radicals (MP⁺) can identify structural and electronic factors which influence their redox properties and chemical reactivity. Although RR spectroscopy has been applied to a few MP++ systems, these studies are limited in scope for various reasons. Attempts to measure RR scattering from the oxoferryl porphyrin " cation radical of horseradish compound I (HRP-I) are complicated peroxidase by photochemistry, 14,15 and special precautions are required to obtain its spectrum. 16 Analysis of the RR scattering from the bacteriochlorophyll cation radical is obscured by the complexity of the parent system. 17 The work of Yamaguchi et al. 18 on MTPP+ complexes is not strictly relevant owing to the strong vibronic coupling and altered substituent pattern of the TPP which reduces its significances as a biological model for RR studies. 19 The MOEP+ system studied by Kim et al.²⁰ is an ideal choice for systematic RR investigation; however, recent work 21 has revealed that some of the spectra reported by these authors were contaminated by artifacts from porphyrin diacid salt impurities produced by demetallation of their MOEP+ samples. This led to incorrect assignments of the principal vibrational modes and to erroneous conclusions concerning the nature of metalloporphyrin π cation radical Raman scattering. This circumstance necessitates a re-examination of the RR spectra of these systems.

The high symmetry (D_{4h}) and saturated C_b substituents make OEP the most simple biologically relevant porphyrin ligand for RR study, and the oxidation products of cobaltous octaethylporphyrin (CoOEP) in particular are of interest. One-electron oxidation of CoOEP in CH₂Cl₂ may occur at either the metal or the porphyrin.²² Depending on the counterion present, the CoOEP two-electron oxidation product displays one of two distinct optical absorption spectra. These are proposed as typical of the two possible electronic ground states which result from loss of an electron from one or the other of the two nearly degenerate HOMOs, a_{1u} (π) or a_{2u} (π), of the porphyrin π system. 9,23,24 The similarity of the optical spectra of Co^{III}OEP+'2ClO₄- and Co^{III}OEP+'2Brto those of HRP-I and catalase compound I (CAT-I) led to the early assignment of the electronic states of these enzyme transients as ${}^{2}A_{2u}$ and ${}^{2}A_{1u}$, respectively.²⁴ The versatility of the CoOEP system thus allows us to compare metal vs. porphyrin centered oxidation products for the one-electron case, and $^2\mathrm{A}_{2\mathrm{U}}$ vs. $^2\mathrm{A}_{1\mathrm{U}}$ radicals for the two-electron case, all with the same MOEP species. Comparison of the cobaltous π cation radical, $Co^{II}OEP^{+}ClO_4^-$, with other $M^{II}OEP^{+}ClO_4^-$ species illustrates structural trends in both the RR frequencies and Soret absorption maxima which are consistent with recent calculations²³ and very similar to those of the parent MOEP species. Exclusion of the artifacts arising from the diacid salt impurities reveals a closer vibrational similarity of $^2\mathrm{A}_{2\mathrm{u}}$ and $^2\mathrm{A}_{1\mathrm{u}}$ radical types than was thought previously. 20 RR excitation in both the Soret and visible absorption bands of cobaltic OEP+* samples provide spectra which suggest the absence of strong Herzberg-Teller coupling of electronic states and a similar scattering mechanism in both spectral regions.

EXPERIMENTAL

Preparation of OEPH₂ was carried out according to the recent method of Wang and Chang²⁵ and metal insertion was achieved by standard methods.²⁶ The metalloporphyrins were purified by recrystallization and/or chromatography to eliminate traces of free base. CH_2Cl_2 freshly distilled from CaH_2 was used as a solvent for all preparations.

Oxidations were performed chemically at room temperature by using solid anhydrous $AgClO_4$, solid $Fe(ClO_4)_3$ or dilute Br_2 in CH_2Cl_2 . $Co^{II}OEP^+ClO_4^-$, $Zn^{II}OEP^+ClO_4^-$, and $Cu^{II}OEP^+ClO_4^-$ were prepared by stirring dry CH_2Cl_2 solutions of CoOEP, ZnOEP, and CuOEP, respectively, with a 3-fold excess of $AgClO_4$ for 1-3 hours. 22 $Co^{III}OEP^+ClO_4^-$, was prepared by stirring excess $Fe(ClO_4)_3$ in a solution of CoOEP for ~ 10 minutes. $Co^{III}OEPBr^-$ and $Co^{III}OEP^+CBr^-$ were prepared by dropwise addition of dilute Br_2 to CoOEP in CH_2Cl_2 . $Mg^{II}OEP^+ClO_4^-$ and $Mg^{II}OEP^+Br^-$ were prepared similarly from MgOEP.

Dropwise addition of methanol (MeOH) to CH₂Cl₂ solutions of Co^{III}OEP+·ClO₄- and Co^{III}OEPBr- resulted in the formation of species with similar absorption spectra, presumably Co^{III}(MeOH)₂OEPClO₄- and Co^{III}(MeOH)₂OEPBr-, respectively.²⁷ Identical samples were made by oxidation of CoOEP with HClO₄ and HBr, respectively, in 3:1 CH₂Cl₂:MeOH. All oxidations and ligand changes were monitored by optical absorption measurements with either a Cary 219 or a Perkin Elmer Lambda 5 spectrophotometer.

Raman spectra excited at 351.1, 363.8 and 390 nm were measured with a Spex 1877 triple monochromator and Spex 1459 collection optics in conjunction

with an EG&G PAR 1420 diode array detector and associated OMA II electronics. The 351.1 and 363.8 nm laser emissions were from a Coherent 90-05 Argon ion laser; the 390 nm line was the output of a Nd:YAG (Quanta Ray DCR-1A) pumped pulsed dye laser (PDL-1) in which LD390 (Exiton) laser dye was used. Instrumentation used to measure Raman scattering at 406.7, 514.5, 620, 647.1 and 676.4 nm included a Spex 1401 double monochromator with photon counting detection interfaced to a DEC LSI 11-2 computer. The lasers were powered by a Spectra Physics Model 265 Exciter; the lines at 406.7, 647.1 and 676.4 nm were from a Model 164 Krypton ion laser, the 514.5 nm line was from a Model 165 Argon ion laser, and the 620 nm line was the output of an Argon ion pumped Spectra Physics Model 375 dye laser in which Rhodamine 590 (Exciton) laser dye was used.

Samples were spun in a cylindrical quartz cell for Raman measurements, although static samples in cuvettes gave identical spectra. Absorption spectra were checked before and after each Raman measurement. Of the oxidized species examined, only ZnOEP+*ClO4- and MgOEP+*Br- showed any significant laser induced change. Samples of Co^{III}OEP+*2ClO4- and ZnOEP+*ClO4- prepared and studied under anaerobic conditions exhibited RR scattering identical to samples which were not deoxygenated, and for this reason samples were not routinely degassed. 28

RESULTS

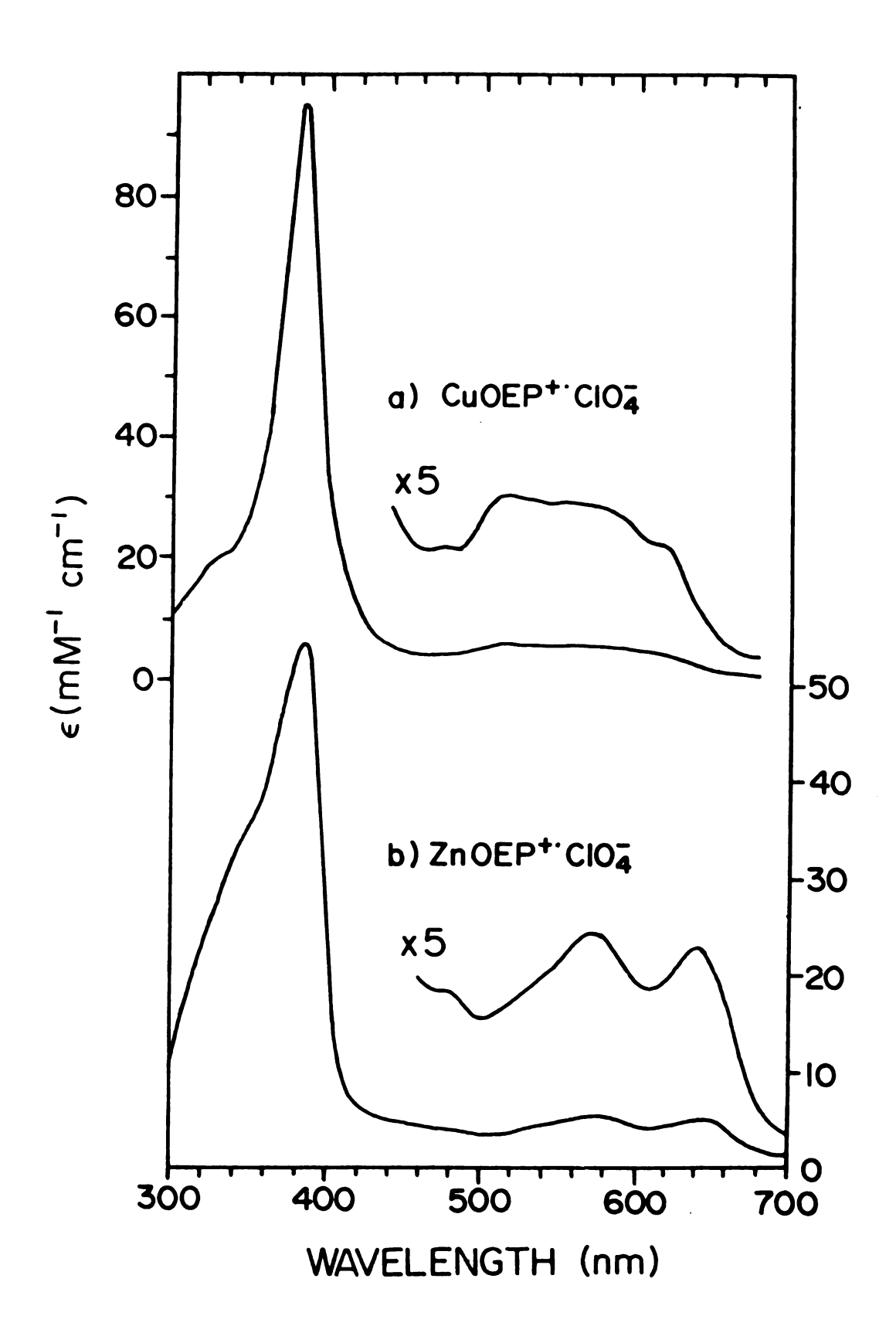
Effects of oxidation on the high frequency porphyrin core vibrations. Although the cobaltic OEP+* system is of principal interest owing to its relevance to the compound I type enzyme intermediates, results from the Cu and ZnOEP+* systems are presented first. The chemistry of the cobalt system is complicated by the two easily obtainable redox states of the metal center and by the diversity

of one- and two-electron oxidation products possible. The Cu^{II} and Zn^{II}OEP systems are simpler in that, under the conditions utilized here, oxidation occurs exclusively at the porphyrin ligand. Since the porphyrin dication is currently of little physiological interst, we consider only the singly oxidized state here. Thus, we can establish the effects of oxidation on the porphyrin core vibrational modes before addressing the more complex cobalt system.

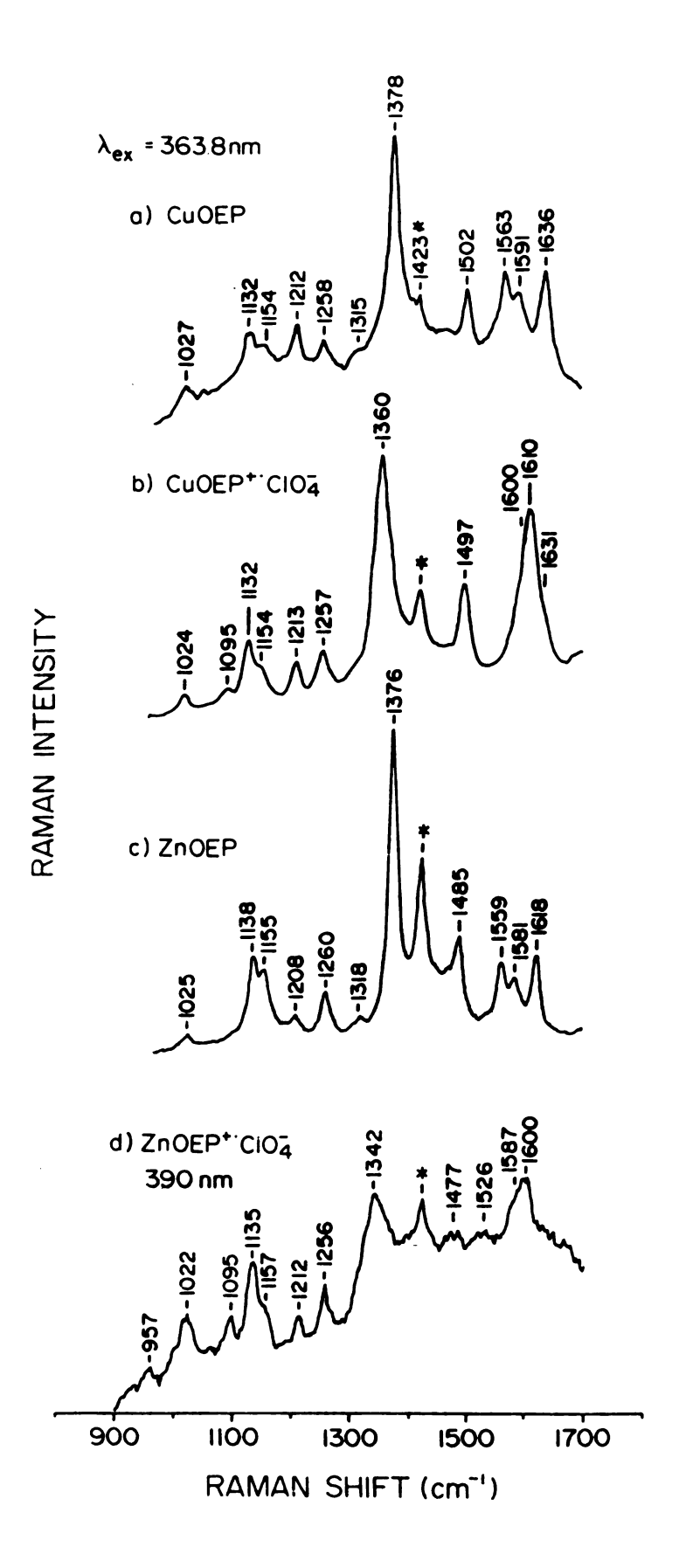
One-electron oxidation of CuOEP and ZnOEP. The optical absorption spectra of ClO₄ complexes of CuOEP+ and ZnOEP+ are shown in Figure 4-1. The absorption spectrum of CuOEP+*ClO₄- is like that reported earlier²⁹ and has features usually attributed to the ${}^{2}A_{2u}$ state. 9,23,24 The Soret band is blue-shifted and diminished in intensity with respect to that of the parent compound and is without noticeable structure. The absorption in the visible region is broad and diffuse, extending through the range 500-640 nm. The actual electronic ground state of CuOEP+*ClO₄- is difficult to establish, however, owing to the lack of an EPR signal from this compound under most conditions.³⁰ Indeed, recent NMR measurements suggest a ²A₁₁₁ state for CuOEP+*ClO₄-,¹⁰a seemingly in contradiction with the absorption spectrum. The ground electronic configuration of the ZnOEP+ species, however, is determined by EPR measurements to be ${}^2A_{1u}$. The absorption spectrum of $ZnOEP^{+}ClO_4^-$ presented in Figure 4-1b agrees well with earlier measurements.^{4,31} Although previous work indicates that ZnOEP+*ClO₄- in CH₂Cl₂ solutions is monomeric, Figure 4-1b shows that significant dimerization of this compound takes place at the concentrations used here (0.2 - 0.5 mM). The high-energy shoulder ~ 350 nm and the absorbance at 573 nm are attributed primarily to the dimer species.31 Dilution of ZnOEP+ ClO₄ samples results in reduced intensity of these features, consistent with decreased dimerization, as shown earlier.4

Figure 4-2 shows the RR spectra (1000-1700 cm⁻¹) obtained with near uv

Figure 4-1. Electronic absorption spectra of (a) CuOEP+*ClO₄- and (b) ZnOEP+*ClO₄- (0.2 mM) in dry CH₂Cl₂. Extinction coefficients were taken from references 29 and 4, respectively.



excitation of complexes of CuOEP+*ClO₄- and ZnOEP+*ClO₄- and their respective neutral parent compounds. RR enhancement of vibrations of ZnOEP+*ClO4dimers was avoided by using laser excitation at 390 nm, well to the red of the dimer absorption. Under these excitation conditions, most of the resonance enhanced vibrations shown in Figure 4-2 correspond to totally symmetric fundamentals. The bands above 1400 cm⁻¹ are known to reflect porphyrin core $geometry^{32}$ and are of principal interest to this work. From the mode designations established by Abe et al.,33a the v_3 , v_{11} , v_2 and v_{10} modes of CuOEP are identified at 1502, 1563, 1591 and 1636 cm⁻¹, respectively, in Figure 4-2a. The intense high frequency envelope from 1570-1650 cm⁻¹ is poorly resolved in the CuOEP+*ClO₄- spectrum in Figure 4-2b; however, three distinct bands with different depolarization ratios are evident from polarized scattering (spectra not shown). Thus, together with the feature at 1497 cm⁻¹, there are four bands present above 1400 cm⁻¹ and 1:1 correlation with the modes of the parent compound is possible. We recognize the v_3 , v_{11} , v_2 and v_{10} frequencies of $CuOEP^{+}ClO_4^-$ at 1497, 1600, 1610 and 1631 cm $^{-1}$, respectively. While caution should be exercised in the vibrational assignment of the MOEP+ based on analogy to the parent MOEP,34 our mode assignments are based on structural trends and depolarization ratio measurements discussed in detail below. The intense band at 1378 cm⁻¹ in the CuOEP spectrum in Figure 4-2a is v_4 , the "oxidation state marker" of heme proteins. 35 This band is identified in the corresponding [™] cation radical spectrum (Fig. 4-2b) at 1360 cm⁻¹. Thus, in the high frequency region, the modes involving primarily $C_a C_m$ stretching character (v_3 and v_{10})³³ decrease in frequency upon oxidation of the porphyrin ring, while modes involving primarily C_bC_b stretching character (v_{11} and v_2) increase in frequency. The frequency of v4, primarily a CaN stretch, decreases upon formation of the porphyrin π cation radical. These trends are common to all of the MOEP systems RR spectra of Cu and ZnOEP and their corresponding cation radicals. (a) CuOEP; (b) CuOEP⁺·ClO₄⁻; (c) ZnOEP; (d) ZnOEP⁺·ClO₄⁻, excitation at 390 nm (1.5 mJ/pulse, [ZnOEP⁺·]~0.2 mM) reflects vibrations of the monomer. CH₂Cl₂ bands are marked with an *. CW laser power 20-35 mW, at 363.8 nm for (a)–(c).



studied here.

The RR spectra of ZnOEP and ZnOEP+ClO₄- are shown in Figure 4-2c and d. The vibrational mode assignments for the parent compound are analogous to those of CuOEP. For example, the ν_4 , ν_3 , ν_{11} , ν_2 and ν_{10} modes of ZnOEP appear at 1376, 1485, 1559, 1581 and 1618 cm⁻¹, respectively, in Figure 4-2c. For the oxidized species (see Fig. 4-2d), these vibrations occur at 1342, 1477, 1587, 1600 and 1617 cm⁻¹, respectively. The ν_{10} frequency of ZnOEP+ClO₄- is estimated to be 1617 cm⁻¹ from depolarization ratio measurements and spectra obtained under 363.8 nm excitation (not shown). Inspection of these vibrational frequencies reveals shifts in the Zn cation radical spectrum similar to those observed upon oxidation of CuOEP.

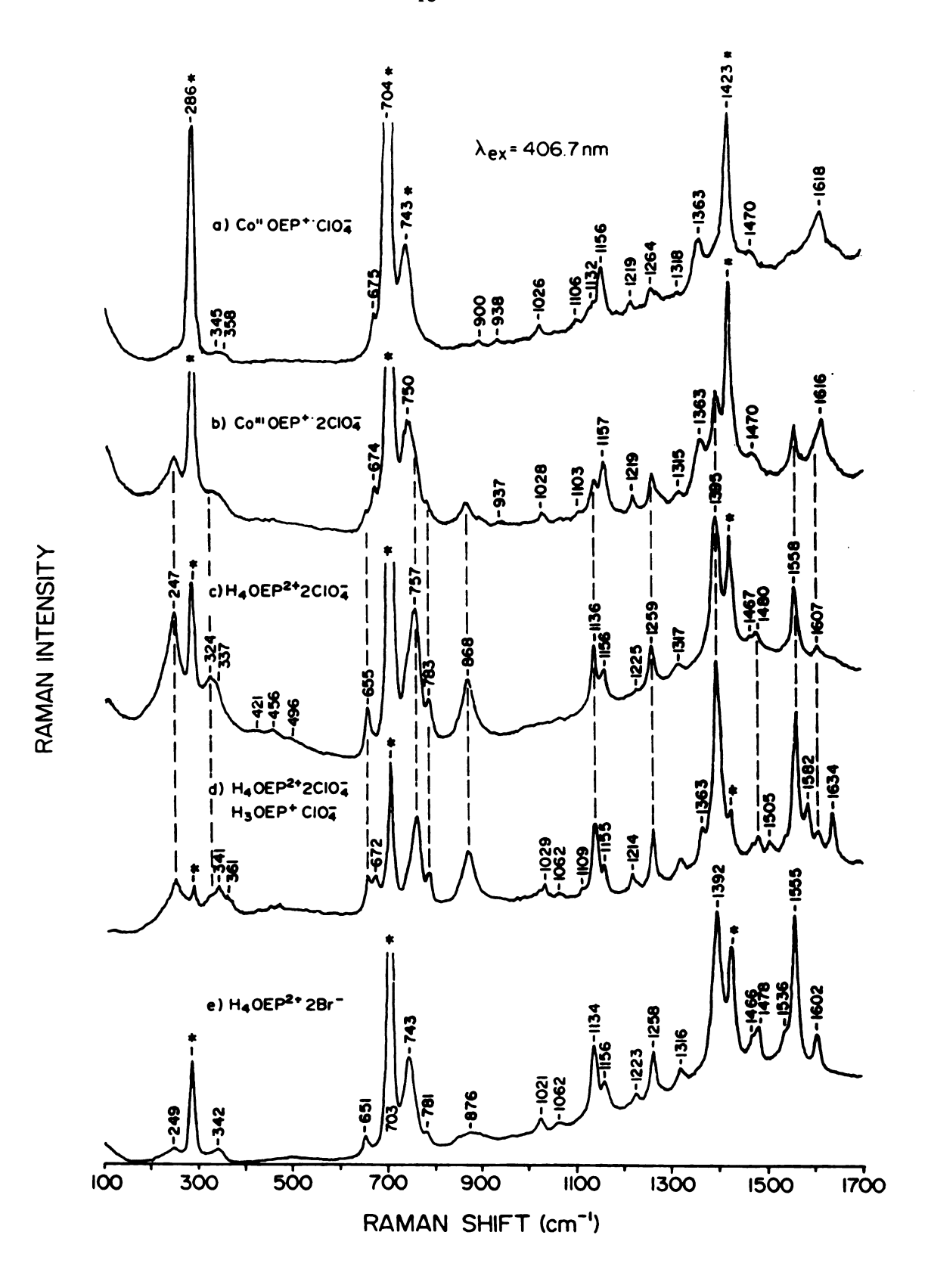
Porphyrin diacid impurities. Resonance Raman excitation of $ZnOEP^{+}ClO_4^-$ at 406.7 nm (spectrum not shown) reproduces the features present in the 390 nm spectrum (Fig. 4-2d). However, additional peaks are present with 406.7 nm excitation which cannot be correctly assigned to any $ZnOEP^{+}ClO_4^-$ species. As we established earlier, 21 these vibrations arise from porphyrin diacid salt impurities produced by demetallation of the $ZnOEP^{+}ClO_4^-$ complex. Because the intensity of the diacid vibrations may totally obscure those of the metalloporphyrin π cation radical under certain excitation conditions, it is essential that these artifacts be recognized and eliminated from RR spectra of these compounds. We present here additional information on this subject.

Figure 4-3a and b show RR scattering under 406.7 nm excitation from samples of Co^{II}OEP⁺·ClO₄⁻ prepared with AgClO₄ and of Co^{III}OEP⁺·ClO₄⁻ prepared with Fe(ClO₄)₃, respectively. Although the RR spectra of these two samples excited at 363.8 nm are similar²² (cf. Fig. 4-7c and d), excitation at 406.7 nm produces additional features in the spectrum of cobaltic OEP⁺· relative to the cobaltous sample (Fig. 4-3a and b). These added vibrational contributions

Figure 4-3. Resonance Raman spectra excited at 406.7 nm.

- (a) Co^{II}OEP+*ClO₄-;
- (b) Co^{III}OEP+ 2ClO₄ containing small amounts of porphyrin diacid impurity;
- (c) $H_4OEP^{2+}2ClO_4^-$;
- (d) a mixture of H₃OEP⁺ClO₄⁻ and H₄OEP²⁺2ClO₄⁻ resulting from treatment of OEPH₂ with AgClO₄;
- (e) $H_4OEP^{2+}2Br^{-}$.

RR bands of the solvent, dry CH_2Cl_2 , are marked with an*. Vertical dashed lines mark the vibrations of the diacid, $H_4OEP^{2+}2Br^-$. Laser power, 20 mW.



are from the diacid salt impurities. Figure 4-3c shows the RR spectrum of the interferring species, H₄OEP²⁺2ClO₄. Addition of AgClO₄ to a solution of H₂OEP in CH₂Cl₂ results in a mixture of mono- and diacid species which produces the RR spectrum shown in Figure 4-3d. Whereas the vertical lines identify the vibrations of the diacid, the additional peaks labelled in Figure 4-3d (e.g. those at 1505, 1582 and 1634 cm⁻¹) most likely arise from the monoacid species. This suggests that the mono- and diacid species have different vibrational properties, possibly owing to the lowered symmetry resulting from the inequivalence of the x and y axes in the monoacid structure. The formation of diacid in the sample of Co^{III}OEP+2ClO₄- prepared with Fe(ClO₄)₃ probably results from aqueous acid (i.e. HClO₄) present in the reagent. Thus, acid demetallation of the MP followed by protonation of the resultant free base could compete with the oxidation process. The lack of artifacts in the spectrum in Figure 4-3a illustrates that this process does not occur when anhydrous AgClO₄ is used to oxidize CoOEP. The spectrum in Figure 4-3d is of interest because it suggests the possibility of both monoacid and diacid contamination of MP+. samples. Furthermore, the absence of aqueous acid impurities in the AgClO₄ reagent suggests that porphyrin acid formation is a true by-product of the oxidation process in certain cases, and not merely the result of "wet" oxidant. Figure 4-3e illustrates that changing the counterion for the diacid from ClO₄to Br decreases the frequencies of the intense vibrational bands above 1300 cm⁻¹ by approximately 3 cm⁻¹. The above observations are all pertinent to the interpretation of the RR spectrum of Co^{III}OEP+2Br obtained with 406.7 nm excitation by Kim et al.,20 which we suggest results from H₄OEP²⁺2Br⁻ (possibly mixed with H₃OEP⁺Br⁻) impurities present in the sample.

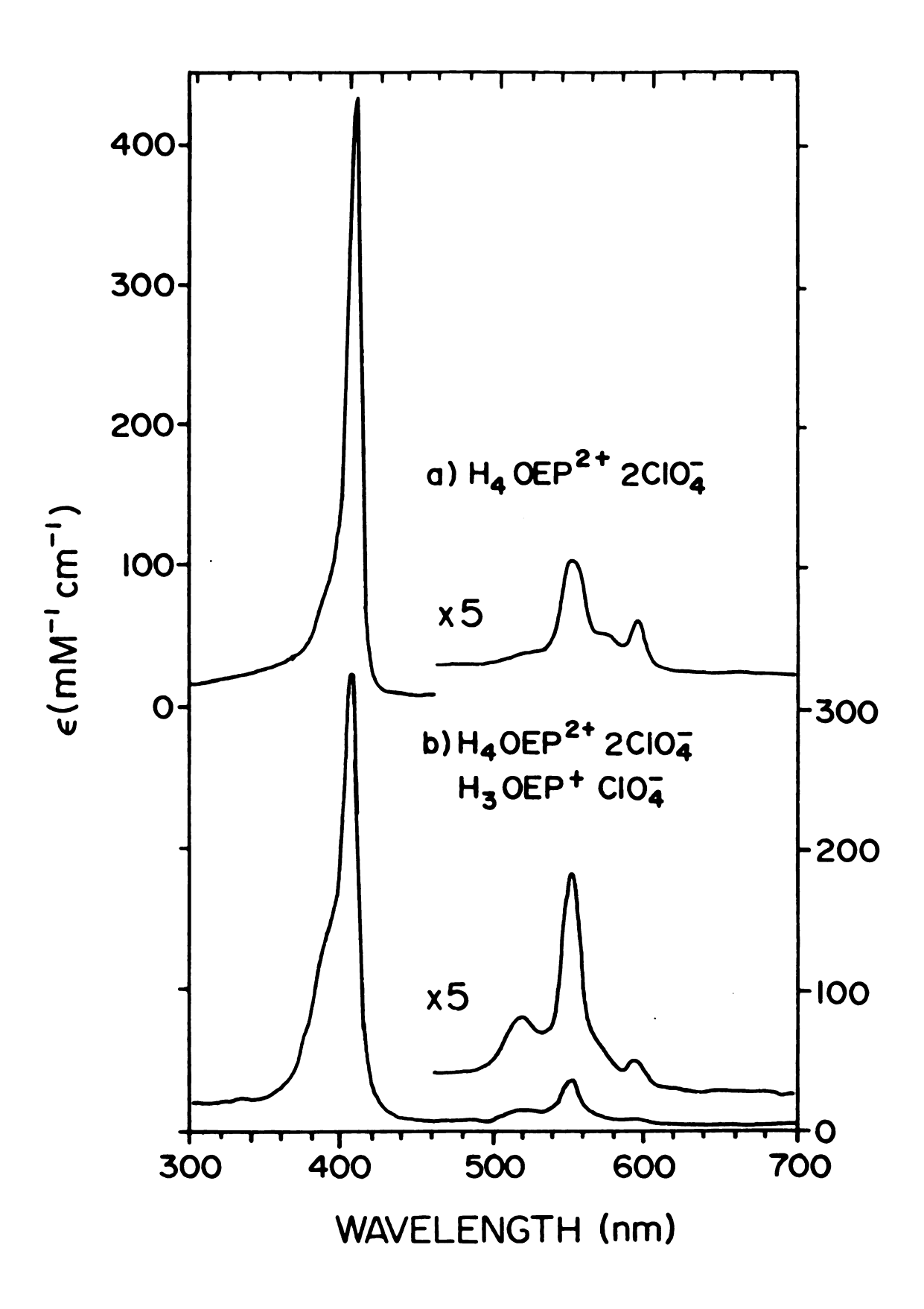
The strong enhancement of the diacid vibrational modes with 406.7 nm excitation, even when the species occurs as a minor impurity (less than 3%)

Figure 4-4. Electronic absorption spectra of porphyrin free base acids.

(a) H₄OEP²⁺2ClO₄⁻;

(b) a mixture of H₃OEP⁺ClO₄⁻ and H₄OEP²⁺2ClO₄⁻ corresponding to Fig. 4-3d.

Solvent, dry CH₂Cl₂.

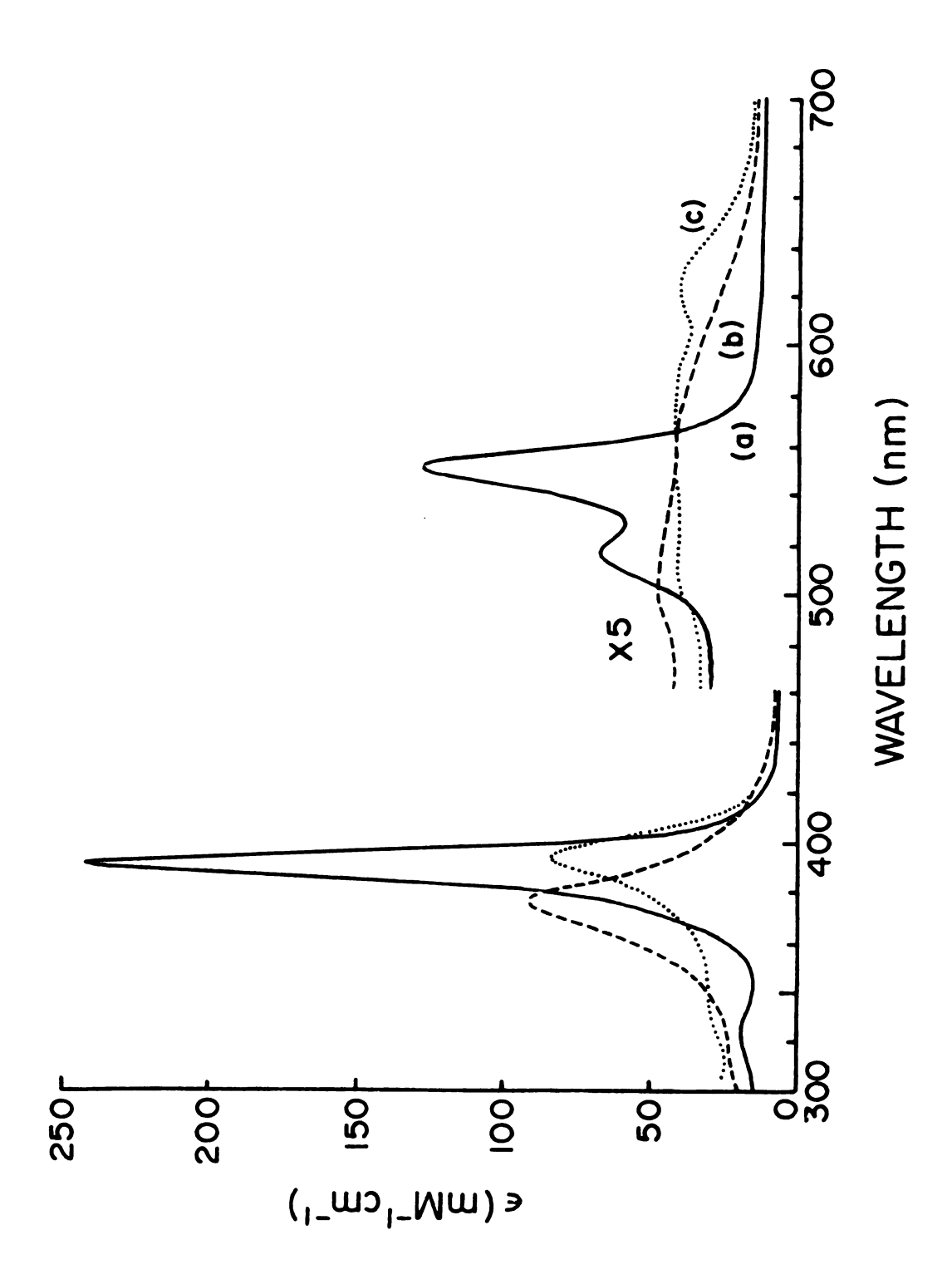


in MP+ samples, is rationalized by its optical properties. Figure 4-4a shows the optical absorption spectrum of the H₄OEP²⁺2ClO₄ sample used for the RR measurement shown in Figure 4-3c. Figure 4-4b shows the absorption spectrum of a mixture of mono- and diacids produced by the addition of AgClO₄ to OEPH2 in CH2Cl2 and corresponds to the sample used for the RR spectrum in Figure 4-3d. Contributions to the absorption spectrum from the monoacid are evidenced by the high energy shoulder (~390 nm) in the Soret and by the absorption maximum at 518 nm.³⁶ While this sample is predominantly (>80%) monoacid, the RR spectrum (Fig. 4-3d) is dominated by the diacid vibrations, owing to the large extinction coefficient (430 $mM^{-1}cm^{-1}$) and close correspondence of the Soret band (406 nm) of the latter species to the laser line (406.7 nm). The extent of demetallation and diacid formation in MOEP+* sample is dependent on a number of factors, including the oxidation method, solvent and core size of the MOEP+. In some cases it is enhanced by laser irradiation in the Soret band region.²¹ By exciting well to the blue of the absorption maxima of these potential contaminants, we avoid the complications imposed by these species upon RR measurements.

One— and two-electron oxidation of CoOEP. Figure 4-5 shows uv-visible absorption spectra of CoOEP and products of its oxidation in dry CH_2Cl_2 in the presence of ClO_4 . The spectrum of the starting material, CoOEP, and the product of ring centered, one-electron oxidation, $Co^{II}OEP^{+}ClO_4$, are shown in Figure 4-5a and b, respectively. Figure 4-5c shows the spectrum of the two-electron oxidation product, $Co^{III}OEP^{+}2ClO_4$. As we recently demonstrated, $Co^{III}OEP^{+}2ClO_4$ as we recently demonstrated, $Co^{III}OEP^{+}2ClO_4$ be a spectrum of the presence of axial ligands which coordinate more strongly than ClO_4 . Such coordination promotes electron transfer from Co^{II} to the electron-depleted porphyrin. Addition of methanol (MeOH) to CH_2Cl_2 solutions of $Co^{II}OEP^{+}ClO_4$ produces

Figure 4-5.

Electronic absorption spectra of CoOEP and its oxidation products. (a) CoOEP(-); (b) Co II OEP $^{+}$ ·CIO $_{4}^{-}$ (---); (c) Co III OEP $^{+}$ ·2CIO $_{4}^{-}$ (···). Solvent, dry CH $_{2}$ Cl $_{2}$.



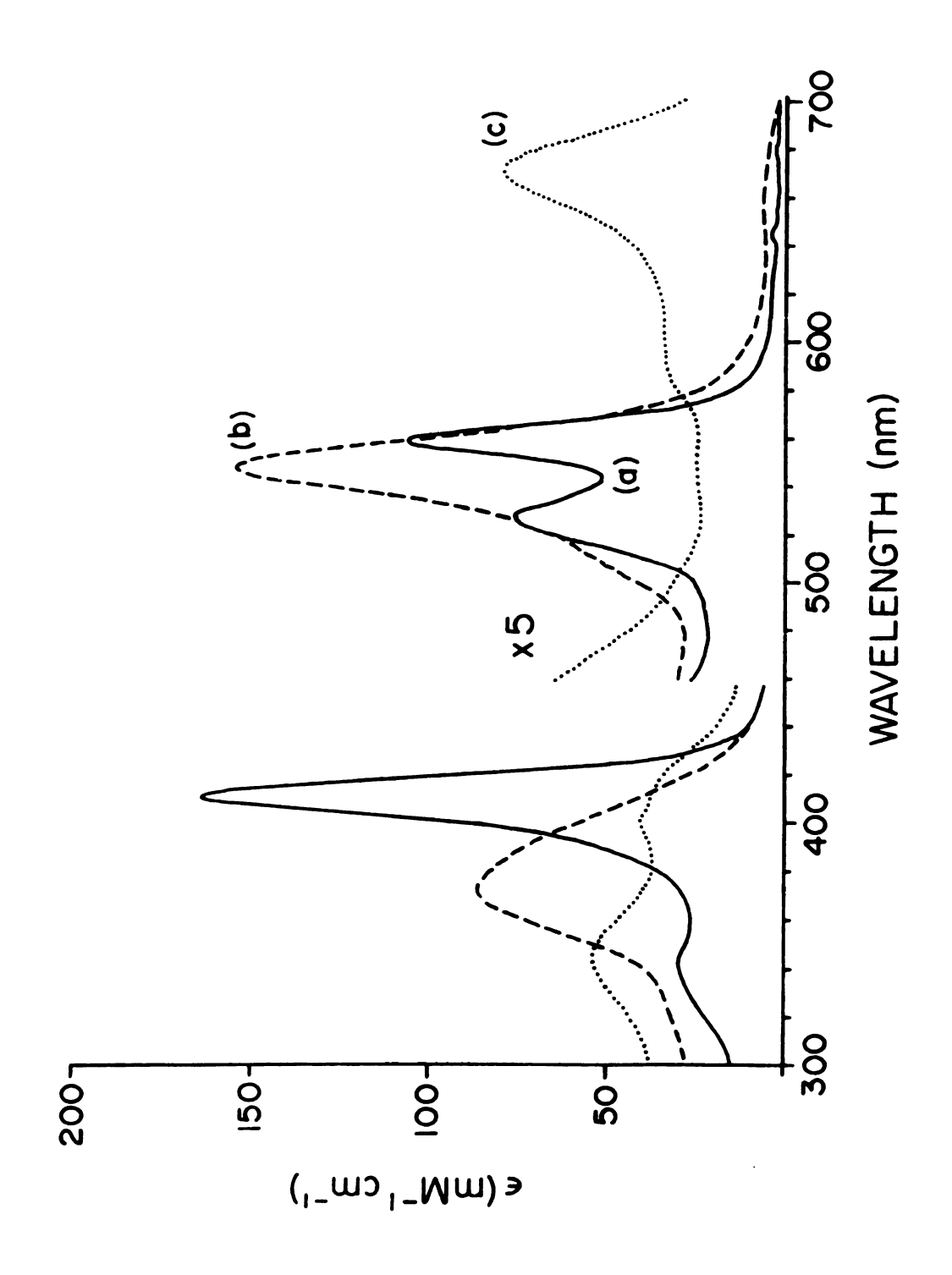
a cobaltic species, $Co^{III}(MeOH)_2OEPClO_4^-$, with an absorption spectrum similar to, but red-shifted with respect to that of the parent CoOEP species. Because water coordinates and produces a cobaltic species similar to the dimethanol adduct (see Fig. 4-10, below), rigorously anhydrous conditions are necessary to provide a homogeneous preparation of $Co^{II}OEP^{+}ClO_4^-$. The absorption spectrum of this species (Fig. 4-5b) closely resembles that of $NiOEP^{+}ClO_4^-$, 29 and has features usually attributed to the $^2A_{2u}$ state (as does $Co^{III}OEP^{+}2ClO_4^-$, Fig. 4-5c).

Figure 4-6 shows absorption spectra of three species obtained by Br₂ oxidation of CoOEP in CH₂Cl₂. One-electron oxidation in this case also produces two distinct species, but both exhibit metal centered oxidation. One-electron oxidation by Br₂ followed by dropwise addition of MeOH produces the six-coordinate Co^{III}(MeOH)₂OEPBr shown in Figure 4-6a. The absorption spectrum of this species is typical of six-coordinate cobaltic porphyrins 37 and similar, although slightly red-shifted, to that of the dimethanol adduct, Co^{II}(MeOH)₂OEPClO₄, described previously²² (see Table 4-1, below). One-electron oxidation of CoOEP by Br₂ in dry CH₂Cl₂ produces a presumably five-coordinate cobaltic porphyrin which displays the spectrum shown in Figure 4-6b. For this compound, Co^{III}OEPBr⁻, the Soret band (373 nm) blue-shifts with respect to that of CoOEP (391 nm), and the extinction coefficient ratio of the visible to the Soret band increases. The spectrum of the two-electron oxidized π cation radical, Co^{III}OEP+2Br-, is shown in Figure 4-6c. The near uv region contains three distinct bands, at 290 (not shown), 345 and 410 nm, and there are at least two bands in the visible region at ~600 and 670 nm. These features (split Soret with an intense red-shifted visible band) are considered typical of the $^2\mathrm{A}_{1\mathrm{u}}$ electronic state. 9,23,24 The feature at 401 nm in Figure 4-6c is attributed to the diacid salt (H₄OEP²⁺2Br⁻), the presence of which

Electronic absorption spectra of oxidation products of CoOEP. Figure 4-6.

(a) $Co^{III}(MeOH)_2OEPBr^-(-);$ (b) Co^{III}OEPBr⁻ (—);

(c) Co^{III}OEP⁺·2Br (···), the small feature at 401 nm is due to 1% H₄OEP²⁺2Br⁻ contamination as discussed in the text. Solvent, dry $\mathrm{CH}_2\mathrm{Cl}_2$, except for (a) which contains $^{\circ}$ 5% methanol (MeOH).

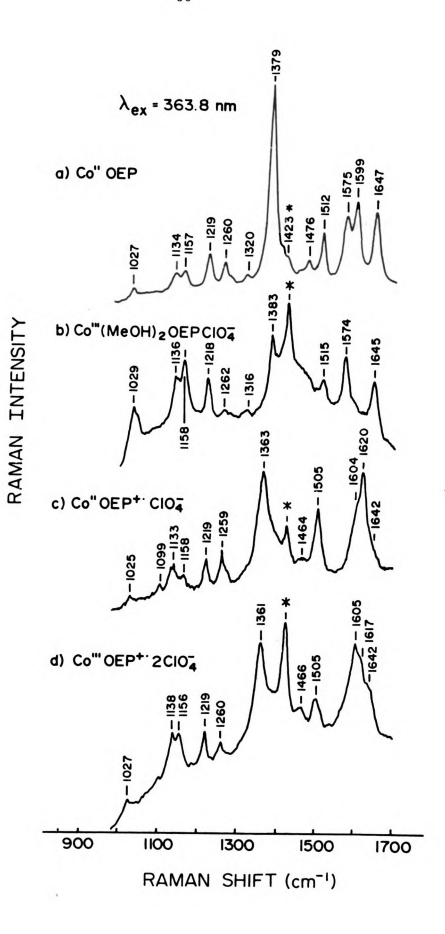


explains the subtle variations in band shape and maximum of the 410 nm transition evident in different preparations of this compound. 9,24 We estimate the diacid salt contamination in the preparation represented by Figure 4-6c to be $\sim 1\%$. 38

Near uv RR spectra of one- and two-electron oxidation products of CoOEP. Figure 4-7 collects RR spectra produced by 363.8 nm excitation of various products of CoOEP oxidation. The effects of metal centered, one-electron oxidation accompanied by axial metal ligation are demonstrated by comparing the spectra of CoOEP and Co^{III}(MeOH)₂OEPClO₄ depicted in Figure 4-7a and b. The oxidation state marker, v₄, increases from 1379 to 1383 cm⁻¹, reflecting depopulation of the porphyrin π^* orbitals caused by metal oxidation.³⁹ There is little systematic change in frequency of the modes above 1400 cm⁻¹, indicating that the core size of the porphyrin ring does not change significantly upon metal oxidation and addition of axial MeOH ligands. 32,40 The v_2 mode, which occurs at 1599 cm⁻¹ in CoOEP, is very weak in this spectrum of Co^{III}(MeOH)₂OEPClO₄-, but it is seen at 1596 cm^{-1} in spectra excited at 406.7 nm (not shown). The remaining high frequency bands of CoOEP (Fig. 4-7a) at 1512, 1575 and 1647 cm⁻¹ are assigned to v_3 , v_{11} and v_{10} , respectively. The weak mode at 1476 cm⁻¹ may correspond to v_{28} . Although this mode is not observed in Soret excited spectra of other MOEP complexes, it is reported for NiPP (PP=protoprophyrin IX) at 1482 cm⁻¹.40 These frequencies are consistent with CaCm stretching character of this mode. **Assignments** Co^{III}(MeOH)₂OEPClO₄ are similar. Figure 4-7c and d show the spectra of the cobaltous and cobaltic OEP++ complexes. Neglecting differences in relative intensity produced by the differences in Soret absorption, the RR spectra of ${\rm Co^{II}OEP^{+-}ClO_4^{-}}$ and ${\rm Co^{III}OEP^{+-}2ClO_4^{-}}$ are essentially identical and (above 1300 cm⁻¹) radically different from those of the neutral ring compounds in Figure 4-7a and b. These observations provide a strong fingerprint basis for

RR spectra excited at 363.8 nm (${\sim}35~\text{mW})$ of CoOEP and its oxidation products. Figure 4-7.

- (a) CoOEP;
- (a) Co^{III}(MeOH)₂OEPClO₄⁻; (c) Co^{II}OEP⁺·ClO₄⁻; (d) Co^{III}OEP⁺·2ClO₄⁻;

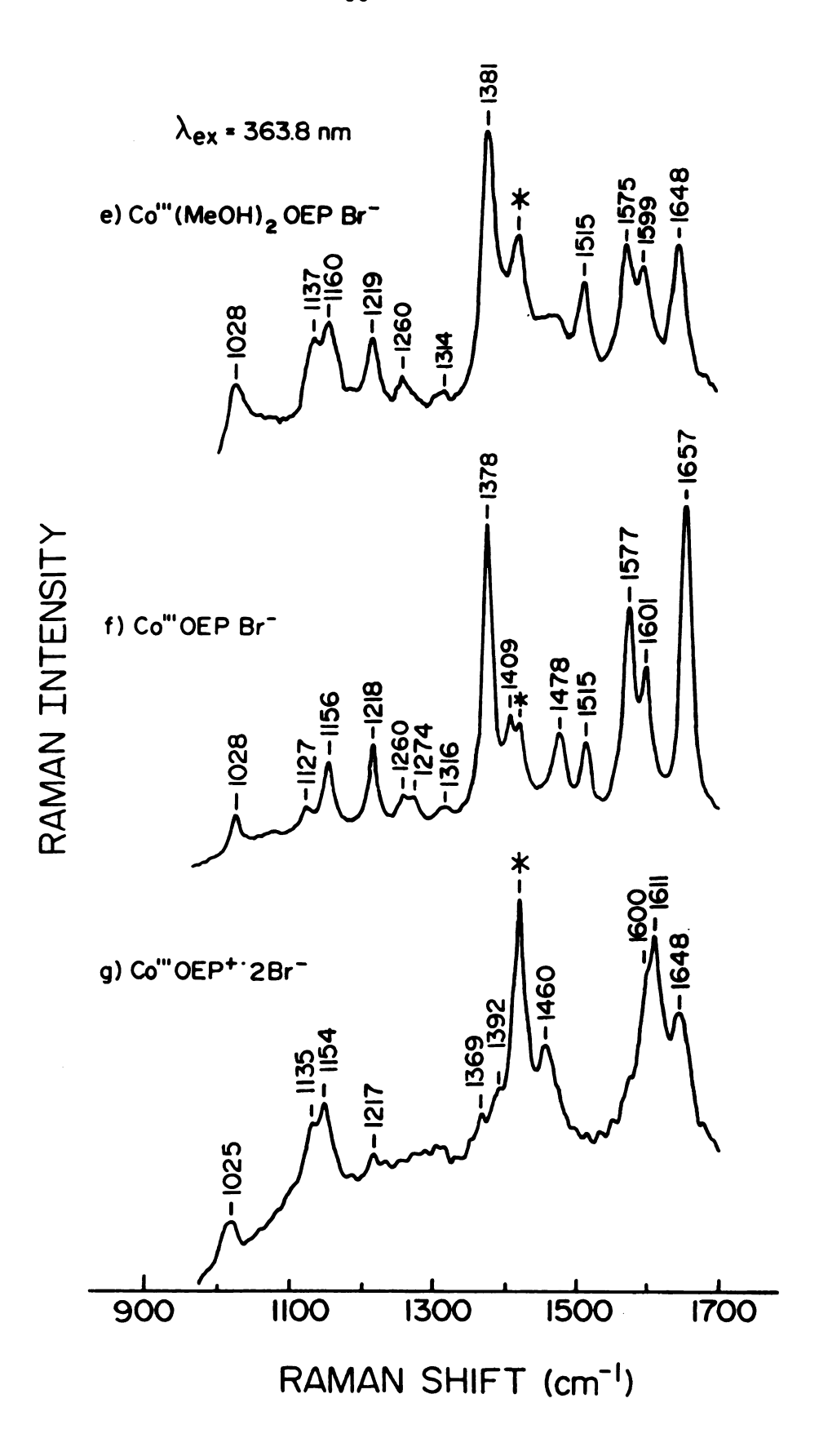


identifying the former species as an authentic π cation radical.²² Our assignments identify ν_4 , ν_{28} , ν_3 and ν_{10} at 1361, 1466, 1505, and 1642 cm⁻¹, respectively, for Co^{III}OEP+·2ClO₄- (Fig. 4-7d). Compared to the ring-neutral Co^{III} and Co^{III} species, all four of these modes have decreased in frequency, consistent with the generalizations made above. The C_bC_b stretching modes, ν_{11} and ν_2 , again show the opposite trend, as they are assigned to the intense features at 1605 and 1617 cm⁻¹. The assignments for Co^{II}OEP+·ClO₄- (Fig. 4-7c) are similar.

The RR spectra excited at 363.8 nm of the bromide adducts of oxidized CoOEP are shown in Figure 4-7e-g. The RR spectrum of Co^{III}(MeOH)₂OEPBr⁻. Figure 4-7e, is similar to that of CoOEP and CoIII(MeOH)2OEPClO₄ in Figure 4-7a and b. The RR spectrum of Co^{III}OEPBr⁻ is shown in Figure 4-7f. While v₄ (1378 cm⁻¹ is slightly lower than in the other Co^{III} compounds, the core sensitive bands v_{28} (1478 cm⁻¹), v_{3} (1515 cm⁻¹), v_{11} (1577 cm⁻¹), v_{2} (1601 ${\rm cm}^{-1}$) and particularly v_{10} (1657 ${\rm cm}^{-1}$) have increased in frequency, suggesting a slight core contraction in this species. 32,40 The spectrum of the π cationic radical species, Co^{III}OEP+·2Br- (Fig. 4-7g) is dominated by two bands around 1600 and 1611 cm $^{-1}$ (presumably v_{11} and v_{2} , respectively), similar to that of the other π cations discussed above. There is, however, no band easily assignable to v_4 . The features at 1460 and 1648 cm⁻¹ are assigned to v_{28} and v_{10} , respectively. The RR spectrum of this compound with laser excitation at 351.1 nm is essentially identical to the spectrum at 363.8 nm shown here. The v₃ vibration, which is enhanced in Soret RR spectra of neutral metalloporphyrins, does not appear in these spectra. We assign this mode to the polarized feature at 1497 cm⁻¹ present in the spectra obtained in resonance with the 670 nm transition of Co^{III}OEP+·2Br- (see below).

- (e) Co^{III}(MeOH)₂OEPBr⁻; (f) Co^{III}OEPBr⁻; (g) Co^{III}OEP⁺·2Br⁻.

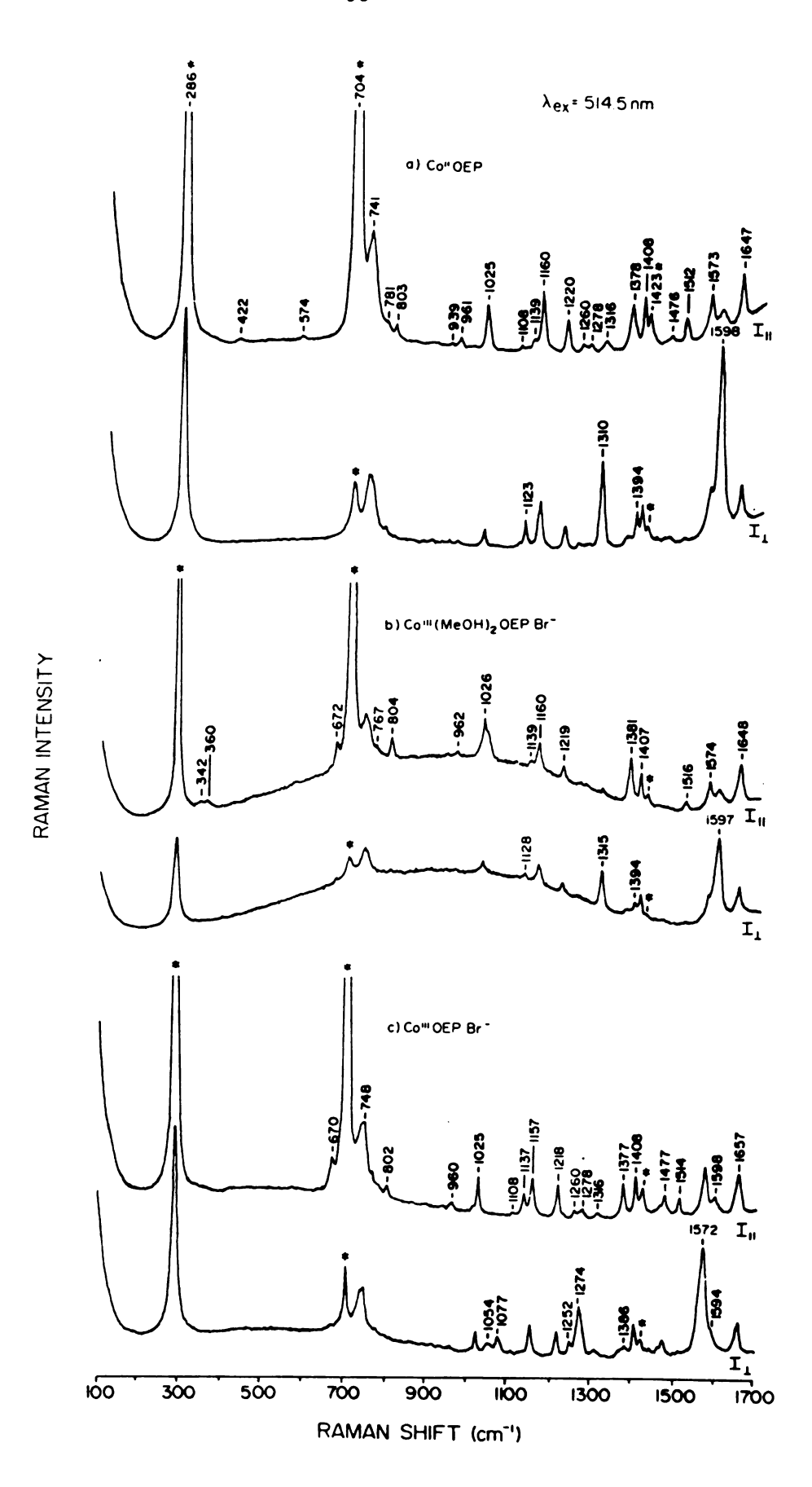
Solvent, dry CH₂Cl₂ except (b) and (e) which contain $\sim 5\%$ methanol. Solvent bands are marked with an *.



Visible RR spectra of one- and two-electron oxidation products of CoOEP. While Soret (or B band) resonance Raman excitation of neutral metalloporphyrins enhances totally symmetric modes (A_{1g} in D_{4h} symmetry) via a Franck-Condon (FC) scattering mechanism, excitation in the visible absorption (Q band) of these species enhances primarily nontotally symmetric modes ($\mathrm{B}_{1g},\ \mathrm{B}_{2g}$ and ${\rm A}_{2g}$) via a Herzberg-Teller (HT) mechanism. 41 In particular, excitation in the β or Q(0-1) band strongly enhances A_{2g} modes of the MP, 42 well known for their inverse polarization.⁴³ Figure 4-8a shows both polarization components of the spectrum of CoOEP obtained in Q(0-1) resonance under 514.5 nm excitation. The A_{2g} modes are easily identified in the I_{\perp} scan at 1123, 1310, 1394 and 1598 cm⁻¹ and are assigned as v_{22} , v_{21} , v_{20} and v_{19} , respectively. Although theory predicts that the value of the depolarization ratio, $\rho \equiv I_{\perp}/I_{\shortparallel}$, will be ∞ for these modes, the measured values are usually finite for various reasons. 43,44 The large ρ values obtained from Figure 4-8a indicate that in CH_2Cl_2 solutions CoOEP assumes a planar configuration and D_{4h} symmetry as does NiOEP in solution.45 In agreement with Soret RR data for these ring-neutral species, Figure 4-8b shows that little change occurs in the spectrum as the metal center is oxidized and ligated axially by MeOH; the ${\rm A}_{2g}$ modes of Co^{III}(MeOH)₂OEPBr⁻ are apparent at 1128, 1315, 1394 and 1597 cm⁻¹. The RR spectrum of Co^{III}OEPBr⁻ (Fig. 4-8c), however, is different from that of other ring-neutral MOEP compounds excited at 514.5 nm, of which the previous two examples are typical. While the A_{2g} modes in the spectra of CoOEP and Co^{III}(MeOH)₂OEPBr⁻ are absent in the spectrum of Co^{III}OEPBr⁻, the appearance of ap modes at 1054, 1077, 1252, 1274 and 1572 cm^{-1} is clear from the I₁ scan in Figure 4-8c. The $1572~\text{cm}^{-1}$ band is reported in the early study by Spaulding \underline{et} $\underline{al.}$, $\underline{^{45}}$ and this frequency is noted as an exception to the trends presented in that work. This band may not be assignable to $\,\nu_{\,19}$ since it is 230 cm^{-1} too Figure 4-8. RR spectra excited at 514.5 nm (100 mW).

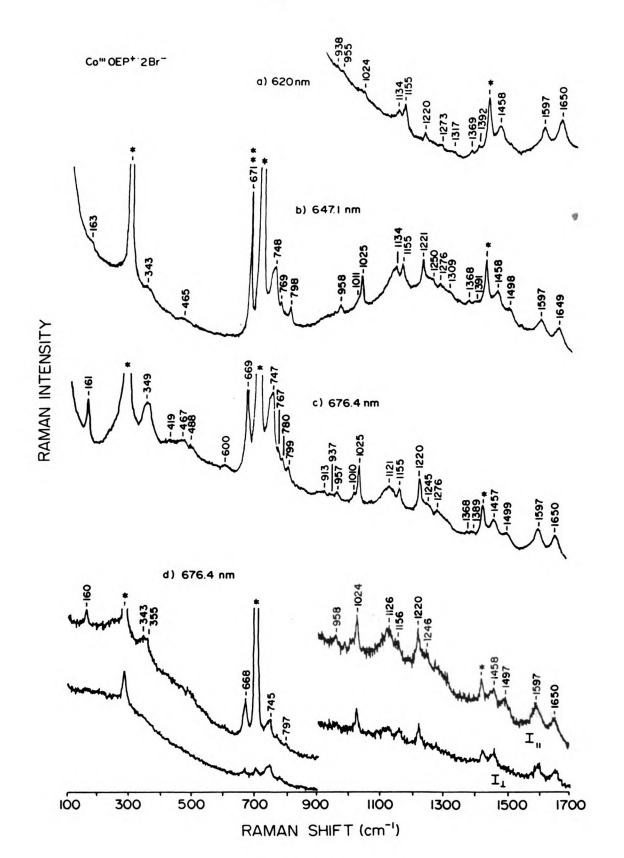
- (a) CoOEP; (b) Co^{III}(MeOH)₂OEPBr⁻; (c) Co^{III}OEPBr⁻.

 CH_2Cl_2 bands marked *.



low. It is possible that none of the ap modes appearing in the spectrum of this compound is assignable to an A_{2g} fundamental. E_g Raman active vibrations should also exhibit anamolous polarization in D_{4h} symmetry. However, owing to their relatively high frequencies it is improbable that these modes correspond to E_g vibrations. Furthermore, activation of E_g modes (out-of-plane) would presumably require electronic transition moments normal to the in-plane porphyrin transitions.⁴³ The appearance of these modes thus indicates a change in symmetry from D_{4h} , resulting in anamolous polarization of other vibrational species.^{41a}

In contrast to the cobaltic derivatives obtained by one-electron oxidation of CoOEP with Br₂, the two-electron oxidized cobaltic π cation radical, Co^{III}OEP+·2Br-, fails to exhibit ap modes when excited in the intense visible transition at 670 nm. Figure 4-9 shows RR spectra of $Co^{III}OEP^{+}2Br^{-}$ excited at 620, 647.1 and 676.4 nm. The high frequency spectrum from 1000-1700 cm⁻¹ produced with 620 nm excitation (Fig. 4-9a) is similar to the 363.8 nm spectrum (Fig. 7g), except that the 1611 cm⁻¹ (v_2) band observed with near uv excitation is absent from the 620 nm spectrum. The similarity of these spectra suggests that the same scattering mechanism(s) are effective in both Soret and visible RR spectra of this compound. As the excitation frequency is moved into 0-0 resonance with the 670 nm electronic transition, the enhancement of polarized modes at 160, 343, 355, 1126 and 1497 cm⁻¹ (tentatively assigned to v_3) is apparent in the spectra presented in Figure 4-9b-d. Figure 4-9d shows both parallel and perpendicular components to the scattering at 676.4 nm. The modes below 700 cm⁻¹ are clearly polarized, while the ρ values for those above 900 cm⁻¹ range from 0.4 - 0.75 with the exception of the mode at ~ 1497 cm⁻¹ (v_3) with $\rho = 0.3$. Clearly there are no ap modes present in these spectra. The ρ values obtained at 647.1 nm are the same as those measured from Figure 4-9. RR spectra of $Co^{III}OEP^{+}\cdot 2Br^{-}$. λ_{ex} = (a) 620 nm, 300 mW; (b) 647.1 nm, 250 mW; (c)-(d) 676.4 nm, 100 mW. CH_2Cl_2 bands marked *. Spike (**) in (b) is Rayleigh scattering at 676.4 nm.



scattering at 676.4 nm in Figure 4-9d. These observations suggest an absence of strong H-T coupling of the excited states of Co^{III}OEP+2Br-. We believe the band at 160 cm⁻¹ to be a mode involving the metal and the Br- ligand, although no experiments to confirm this suggestion have been attempted. This mode is also present in spectra excited at 406.7 nm (not shown).

For the ²A_{lu} radical, Co^{III}OEP+ 2Br-, RR excitation within the intense, strongly red-shifted electron transition at 670 nm produces RR spectra of reasonable quality which are free of contributions from other absorbing species. RR excitation within the much weaker, diffuse visible absorption bands of $^2A_{211}$ type radicals is much more difficult owing to the smaller RR scattering Room temperature scattering from Co^{II}OEP+*ClO₄- and cross-section. Co^{III}OEP+2ClO₄- with 514.5 nm excitation (not shown) is similar and consists of weak, poorly-resolved Raman bands on a high fluorescence background, and is obtained only at high laser power. Our data for Co^{II}OEP+*ClO₄- show anomalously polarized features at 1312 and 1597 cm⁻¹ and a polarized feature at 1383 cm⁻¹. However, these are all attributed to the ring-neutral cobaltic species, Co^{III}(H₂O)₂OEPClO₄-. Other weak features which we attribute to the cobaltous π cation radical seem to correspond to modes present in the spectrum of this sample excited at 363.8 nm (Fig. 4-7c). There is possibly an ap feature between 1560-1570 cm⁻¹ arising from the π cation radical; hower, further experiments are required to reach firm conclusions concerning the scattering mechanisms operative in visible region RR spectra of this and other $^{2}A_{211}$ type π cation radicals.

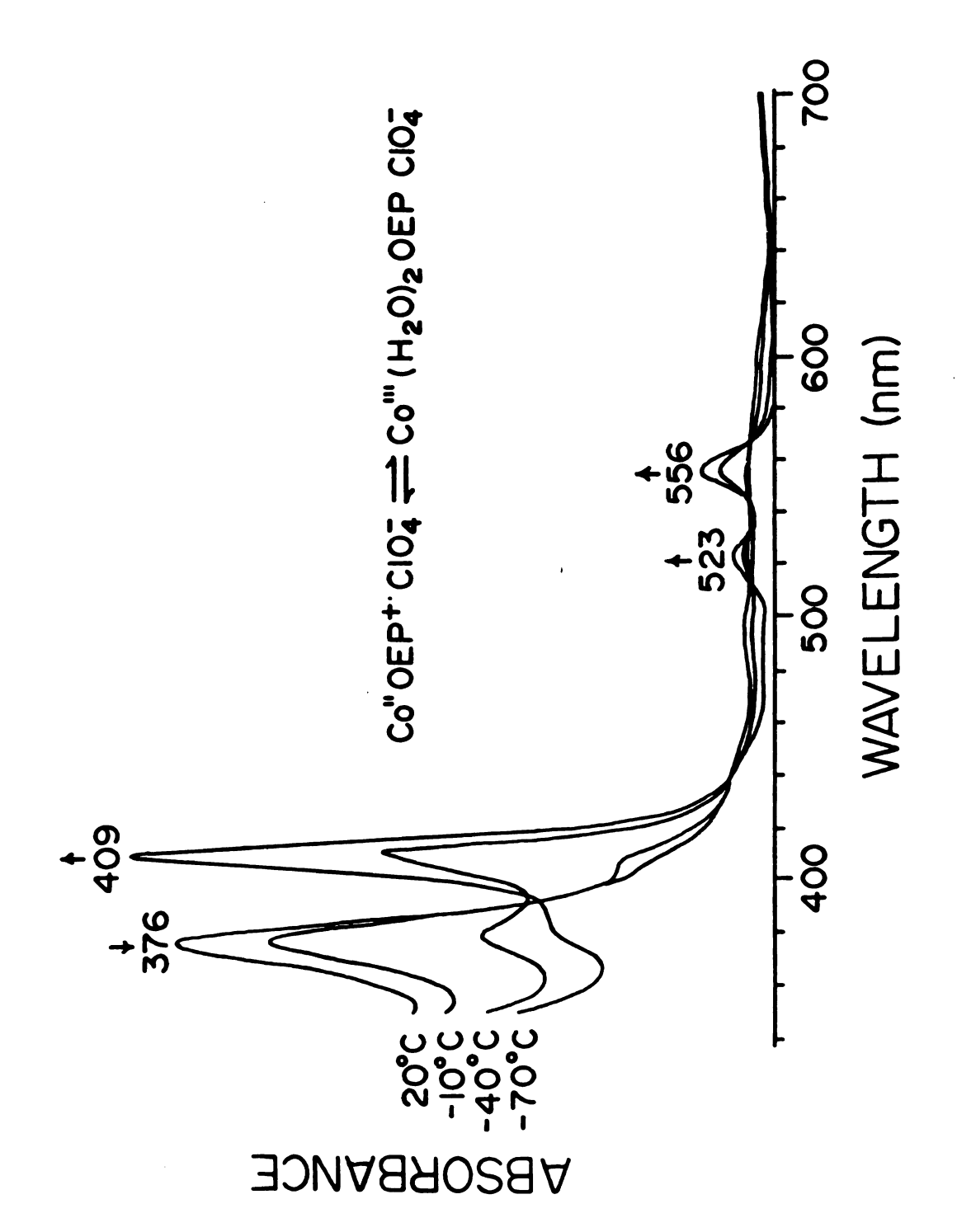
Low temperature effects. The results of our room temperature visible excitation RR work described above are in contrast to those obtained by Kim et al.²⁰ at low temperature (77K). While our work suggests a lack of anomalously polarized scattering from the π cations (at least for Co^{III}OEP+·2Br-), the earlier

study assigns $A_{\mbox{\footnotesize{2g}}}$ modes of the π cations only slightly changed in frequency from those of the parent compounds. We suggest that these features most likely arise from ring-neutral contaminants in the preparations. This is particularly feasible for visible Raman measurements on $^2\mathrm{A}_{211}$ type radicals, which must be excited in the diffuse 500-600 nm absorption, near the Q-bands of the ring-neutral compounds, in order to obtain resonance conditions. (Raman excitation in the 500-570 nm region of the ²A₁₁₁ radicals, e.g. Co^{III}OEP+·2Br-, will not achieve resonance conditions owing to the absence of absorption in this range by the π cation radical.) For example, RR scattering from ${\rm Co^{II}OEP^{+*}ClO_4^{-}}$ samples may contain contributions from the ring-neutral species, Co^{III}(H₂O)₂OEPClO₄-, owing to the difficulty in obtaining completely anhydrous conditions and the coincidence of common laser lines (e.g. 406.7 and 514.5 nm) with its absorption bands (409 and 523 nm). The technical difficulties in obtaining scattering from these $^2A_{211}$ type π cation radicals is magnified at low temperatures. Figure 4-10 shows optical spectra which document the formation of increased amounts of $Co^{III}(H_2O)_2OEPClO_4^-$ in a sample of $Co^{II}OEP^{+}ClO_4^$ as the temperature is lowered. As the 376 nm Soret band of the cobaltous π cation decreases in intensity, absorptions characteristic of the cobaltic complex at 409, 523, and 556 nm become apparent. Thus, simply lowering the temperature of this sample has much the same effect on the absorption spectrum as the addition of methanol,²² presumably due to increased diaxial ligation by H₂O with decreasing temperature. Freeze-pump-thawing to remove water vapor over the sample prior to cooling results in minimized conversion to Co^{III}(H₂O)₂OEPClO₄⁻, consistent with diaquo ligation.

Several other examples of the formation of ring-neutral species in preparations of metalloporphyrin π cation radicals have been observed. Addition of methanol at room temperature to CH₂Cl₂ solutions of the cobaltic π cation

Figure 4-10.

Electronic absorption spectra showing the conversion of $Co^{II}OEP^{+}$. ClO_4^- to $Co^{III}(H_2O)_2OEPClO_4^-$ as the temperature is lowered. Solvent, "dry" CH_2Cl_2 ; path length $\sim 2\,\mathrm{mm}$ (EPR tube).



Co^{III}OEP+.2ClO₄- will also produce Co^{III}(MeOH)₂OEPClO₄-, although much more methanol is required than in the previous case. The redox chemistry involved here is unknown, although it may be similar to the room temperature reduction of Fe^{III}(Cl⁻)TPP⁺·ClO₄ by imidazole (Im) which Fe^{III}(Im)₂TPPCl^{-.10b} Thus, strong axial ligation of the metal center may destabilze the porphyrin π cation radical. Similarly, Soret RR measurements at 406.7 nm on frozen samples of Co^{III}OEP+.2ClO₄- (not shown) show increased contributions from a Co^{III}(H₂O)₂OEPClO₄ type species with repeated scanning. Subsequent warming of these samples causes conversion back to cobaltic π cation radicals, as evidenced by the room temperature absorption spectrum, indicating reversible reduction in the low temperature case. Reversible conversion of Ni^{II}TPP+ to Ni^{III}TPP at low temperatures has also been reported; however, no axial ligation was implicated. 5,46 In general, low temperature RR studies are limited by elevated fluorescence levels and by the inability to measure depolarization ratios of frozen samples. Further complications are imposed by the increased aggregation of MOEP++ compounds which occurs upon cooling. 4,29,31,47 We note that under anhydrous conditions at room temperature both Co^{II}OEP+*ClO₄- and Co^{III}OEP+*2ClO₄- exhibit striking stability to relatively high power laser irradiation at 514.5 nm. Thus, in view of the above, attempts to utilize cryogenic RR techniques to stabilize these compounds is of questionable expediency and will not easily produce reliable spectra. Room temperature visible excitation RR studies of these ²A₂₁₁ type cation radicals will be limited, not by sample instability, but by the weak scattering cross-section offered by the samples.

DISCUSSION

In this section the four orbital model of the neutral metalloporphyrin

electronic states is introduced briefly in order to provide a framework for our analysis of the RR and uv-visible absorption spectra of the oxidized MP species. Next, spectra of the one-electron, ring-oxidized, MIIOEP+ClO₄- systems are shown to exhibit structural trends in both the vibrational frequencies and electronic transition energies which are similar to those of the parent MOEP systems. The one-electron, metal-oxidized cobaltic OEP system is then discussed in order to establish the electronic and structural effects of metal oxidation accompanied by axial ligation. Finally, the above correlations and analysis are used to examine structural and electronic properties of the two-electron oxidized Co^{III}OEP+2X-species.

In the four-orbital model of Gouterman⁴⁸ the optical absorption bands of the MP originate from transitions involving the nearly degenerate HOMOs (highest occupied molecular orbitals) of the porphyrin π system, $a_{1u}(\pi)$ and $a_{2u}(\pi)$, and the degenerate LUMOs (lowest unoccupied molecular orbitals), $e_g(\pi^*)$. Transitions to the CI (configuration interaction) mixed excited states, Q and B, produce the α and Soret bands, respectively. The red-shifts in the Soret and α band maxima produced by metal variation in the series Ni, Co, Cu, Zn, MgOEP are explained by variations in metal electronegativity producing a totally symmetric perturbation to the electronic states of the porphyrin. Red-shifts accompanying axial coordination are explained similarly, as an effective variation in electronegativity of the metal resulting in charge donation into the $a_{2u}(\pi)$ orbital of the ring system⁴⁸.

Structural correlations. The frequencies of many of the vibrations of the porphyrin macrocyclic are linear functions of the center-to-pyrrole nitrogen distance, d, or the core size. 32,45 This dependency is described by the expression $\nu = K(A-d)$ where K and A are parameters characteristic of the porphyrin macrocyclic. 49 For a given vibrational mode, the K value, i.e. the slope of

the line, is indicative of the P.E.D. (potential energy distribution), and increases with the percentage of C_aC_m stretching character. 32,50 Correlations of vibrational frequency to core size for a series of metal substituted porphyrins can be used to establish normal mode assignments. This approach has been used to assign vibrations of metallochlorophyll <u>a</u> complexes 51 and is particularly useful when combined with vibrational data from isotopically substituted porphyrins. 52 In the following, we use depolarization ratios and core size correlations from RR measurements to assign vibrational modes in MOEP^{+*} species. Similar analysis has been applied to establish RR band assignments of iron octaethylchlorin complexes. 53

Table 4-1 collects RR frequencies from 1300-1700 cm⁻¹ obtained with Soret excitation of divalent metal OEP+ complexes with ClO₄ counterions and juxtaposes them with known frequencies of the corresponding starting Depolarization ratios measured with 363.8 nm excitation and materials. wavelengths of the Soret band maxima are included. For MOEP+*ClO₄- complexes with core sizes of 2.00 Å or less (i.e., M = Ni, Co and Cu), our Soret RR results (λ_{ex} = 363.8 nm) agree well with those of Kim et al.²⁰ (λ_{ex} = 406.7 nm). This is because, for oxidation using AgClO₄ or electrochemical techniques, diacid impurities occur only for complexes with core sizes larger than 2.00 Å (i.e., M = Zn and Mg).²¹ Here we use RR frequencies for NiOEP+*ClO₄- taken from Kim et al. 20 ; however, we employ alternative vibrational mode assignments consistent with those we have made for other MOEP+* species. Figure 4-11 shows plots of these vibrational frequencies as a function of core size, assuming that there is no appreciable change in d upon oxidation of the porphyrin ring. The core size measurements are those used by Spaulding et al.⁴⁵ Given the assumptions inherent in the plot (see below), Figure 4-11 indicates that the high frequency RR bands of the MOEP+ in the 1400-1700 cm-1 range are metal

Table 4-1. Resonance Raman Frequencies (cm⁻¹), Depolarization Ratios and Optical Absorption Maxima (nm) for Parent MORP Compounds and their corresponding " Cation Radicals, MORP $^+$ Cl0 $_4^-$.

	Niorpa	NiOEP+·b	CoORP	COORP	CuORP	CuORP ++	ZnORP	ZnORP ⁺	Κ (cm ⁻¹ /A)	۷ (A)	1
Űa N	1383	1370	1379(0.2) ^c	1363(0.3)	1378(0.3)	1360(0.3)	1376(0.3)	1342(0.3)			!
, o e o	1519	1191	1512(0.3)	1505(0.4)	1502(0.3)	1497(0.4)	1485(0.4)	1477(0.4)	383(386) ^d 384	5.93 (5.89) 5.90	6
, 11, c,	1576	1605	1574(0.6)	1604(0.7)	1568(0.8)	1600(0.6)	1599(0.8)	1587(0.8)	197(227) 210	9.95 (8.90) 9.61	6
ر م م	1602	1623	1599(0.3)	1620(0.4)	1591(0.4)	1610(0.4)	1581(0.5)	1600(0.5)	243(266) 268	8.56 (7.98) 8.02	8
0,10°	1655	1651	1647(0.7)	1642(0.8)	1636(0.8)	1631(0.6)	1618(0.8)	1617(0.7)	415(403) 377	5.94 (6.06) 6.33	(9
Soret (III)	391	377	391	376	397	383	400	387			
, <u>(</u>	551		551		561		266				

Meference 33a. beference 20. Shewlarization ratios, given in parenthesis, were measu

The values of K and A in parenthesis were calculated from frequencies reported in reference 57a. Depolarization ratios, given in parenthesis, were measured with 363.8 nm excitation.

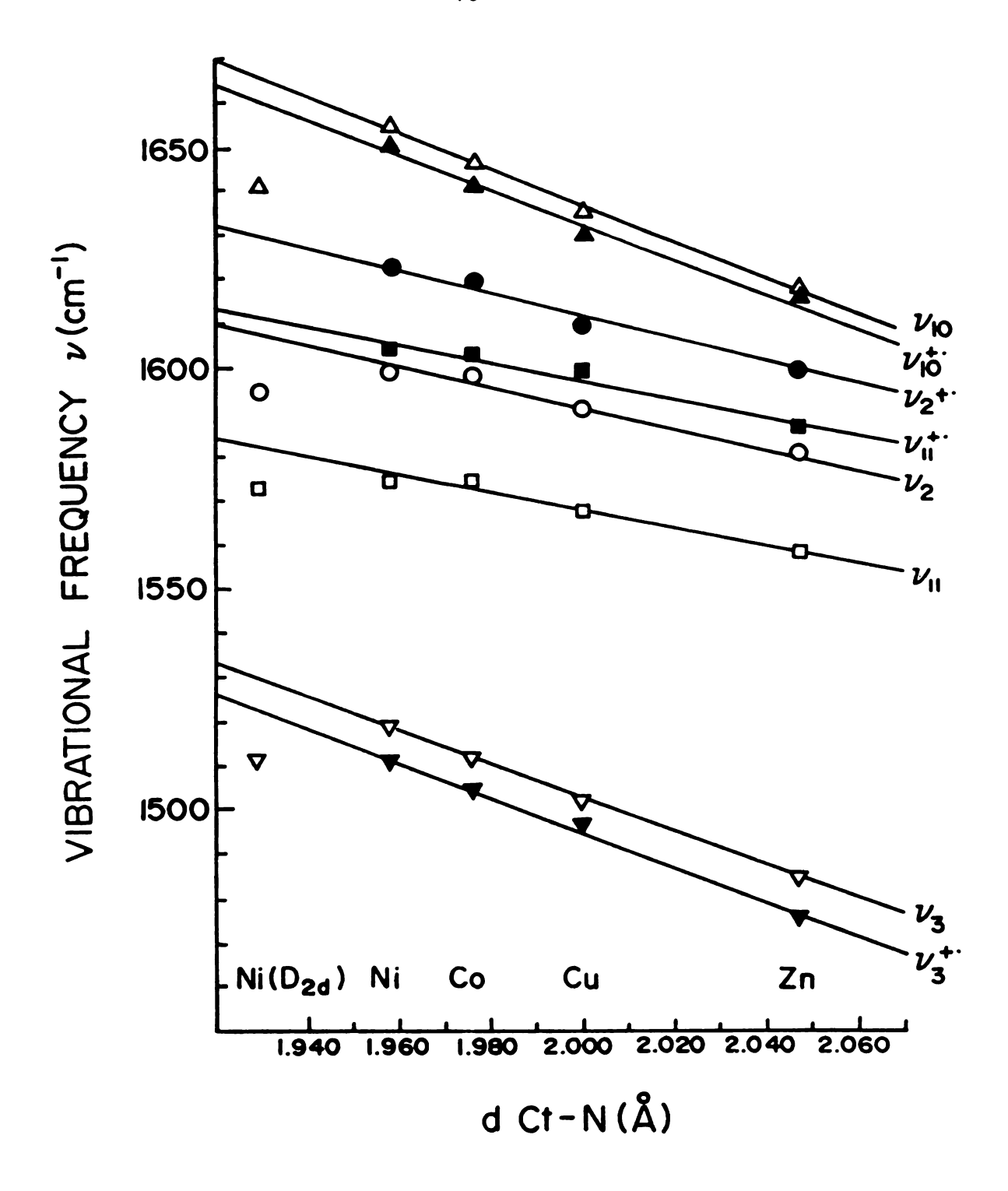


Figure 4-11. Porphyrin core vibrational mode frequencies (for Raman allowed bands, 1450-1700 cm⁻¹) vs. porphyrin core size for the indicated MOEP complexes and their corresponding cation radicals, MOEP⁺·ClO₄⁻. Mode assignments are according to reference 33a. Open symbols correspond to parent MOEP frequencies; filled symbols correspond to MOEP⁺·ClO₄⁻ frequencies. The regression analysis does not include the Ni (D_{2d}) points. Ct-N distances are from reference 45.

dependent and correlate to core size in the same manner as the analogous bands of the neutral parent species. The close agreement between the K values obtained for the neutral MOEP and the MOEP⁺⁺ for each mode suggests that little change occurs in the normal mode composition upon oxidation of the porphyrin ring.⁵⁴ Together with the relative agreement of the depolarization ratio measurements for modes of the MOEP and MOEP⁺⁺, these core size correlations provide support for our band assignments in the MOEP⁺⁺ spectra. Further confirmation will be provided by RR measurements on MOEP⁺⁺ incorporated with isotopic substitutions, which are in progress. Our results thus far suggest that, in general, normal mode calculations for the parent MP will remain useful for interpreting the vibrations of the MP⁺⁺ species.

Additional evidence of the correlation of vibrational frequencies of the porphyrin core stretching modes above 1400 cm⁻¹ to core size is provided by IR studies of MOEP+ compounds. 12 If we use complexes which presumably exhibit D_{4h} solution geometries, 55,56 i.e. Co^{III}OEP+2ClO₄-, Fe^{III}OEP+2ClO₄and Fe^{III}OEP+'2CF₃SO₃-, we can correlate their diagnostic IR band frequencies¹² to the core sizes provided by Spaulding et al.⁴⁵ Although the number of points is too few to establish a reliable correlation, we can estimate K and A from these data to be 420 cm⁻¹/ \mathring{A} and 5.67 \mathring{A} , respectively. They compare remarkably well to K and A values calculated for v_{38} from IR measurements of MOEP complexes obtained at 15K in argon matrices.⁵² While there is some controversy as to the normal mode composition of v_{38} , 32,33,52 these IR frequencies yield K and A values of 421.3 cm⁻¹/ \hat{A} and 5.69 \hat{A} , and imply predominantly C_aC_m stretching character for this mode. For CoOEP, ν_{38} is reported 52 at 1565 cm⁻¹, whereas the diagnostic IR band of Co^{III}OEP+'2ClO₄- is reported at 1554 cm $^{-1}$. The $^{\circ}10$ cm $^{-1}$ differences in these frequencies is in good agreement with the frequency decreases in $C_a C_m$ stretching modes resulting from porphyrin ring oxidation observed in our Raman work. This, and the agreement between K and A values, suggest that the diagnostic band of $MOEP^{+*}$ complexes corresponds to v_{38} of the parent MOEP.

In addition to RR frequencies, Table 4-1 also lists Soret maxima for MOEP and MOEP+ compounds. These values, along with a band energies for the parent MOEP, are plotted as a function of a core size in Figure 4-12. Absorption data for MgOEP (408 nm Soret, 580 nm a band) and MgOEP+*ClO₄- (392 nm Soret) in CH₂Cl₂ have been added. Our spectrum of the MgOEP⁺·ClO₄⁻ resembles the previous measurement by Dolphin et al.4 The Soret maximum for MgOEP+*ClO₄- used in Figure 4-12 represents the lowest energy transition in the near uv envelope of the absorption spectrum. The qualitative similarity of the trends for all transition energies is striking and can be explained by the dominance of the $a_{2u}(\pi) \rightarrow e_g(\pi^*)$ character of the transitions in determining the core size dependencies of these values. For the neutral MOEP the $a_{2u}(\pi)$ orbital energy may be considered to vary linearly with core size while the $e_g(\pi^*)$ and $a_{1u}(\pi)$ orbitals remain relatively constant. Thus, the $a_{2u}(\pi) \rightarrow e_g(\pi)$ character of the excited state determines the core size dependency of the and Soret band energies. Calculations by Edwards and Zerner²³ predict that, in the case of the $^2A_{2u}$ cobaltic porphin radical, the dominant transition in the Soret region has 30% $a_{2u}(\pi) \rightarrow e_g(\pi^*)$ character, while for the $^2A_{1u}$ cobaltic species the least energetic transition in the Soret envelope has 70% $a_{2u}(\pi) + e_g(\pi^*)$ character. Thus the correlations in Figure 4-12 suggests that the $a_{2u}(\pi) \rightarrow e_g(\pi^*)$ character of these transitions is responsible for the core size dependency of the Soret band energies in both the MOEP and MOEP+ compounds.

Porphyrin core geometry. The key assumption made in establishing the parameters K and A in the relation v = K(A-d) for the MOEP⁺ series is the

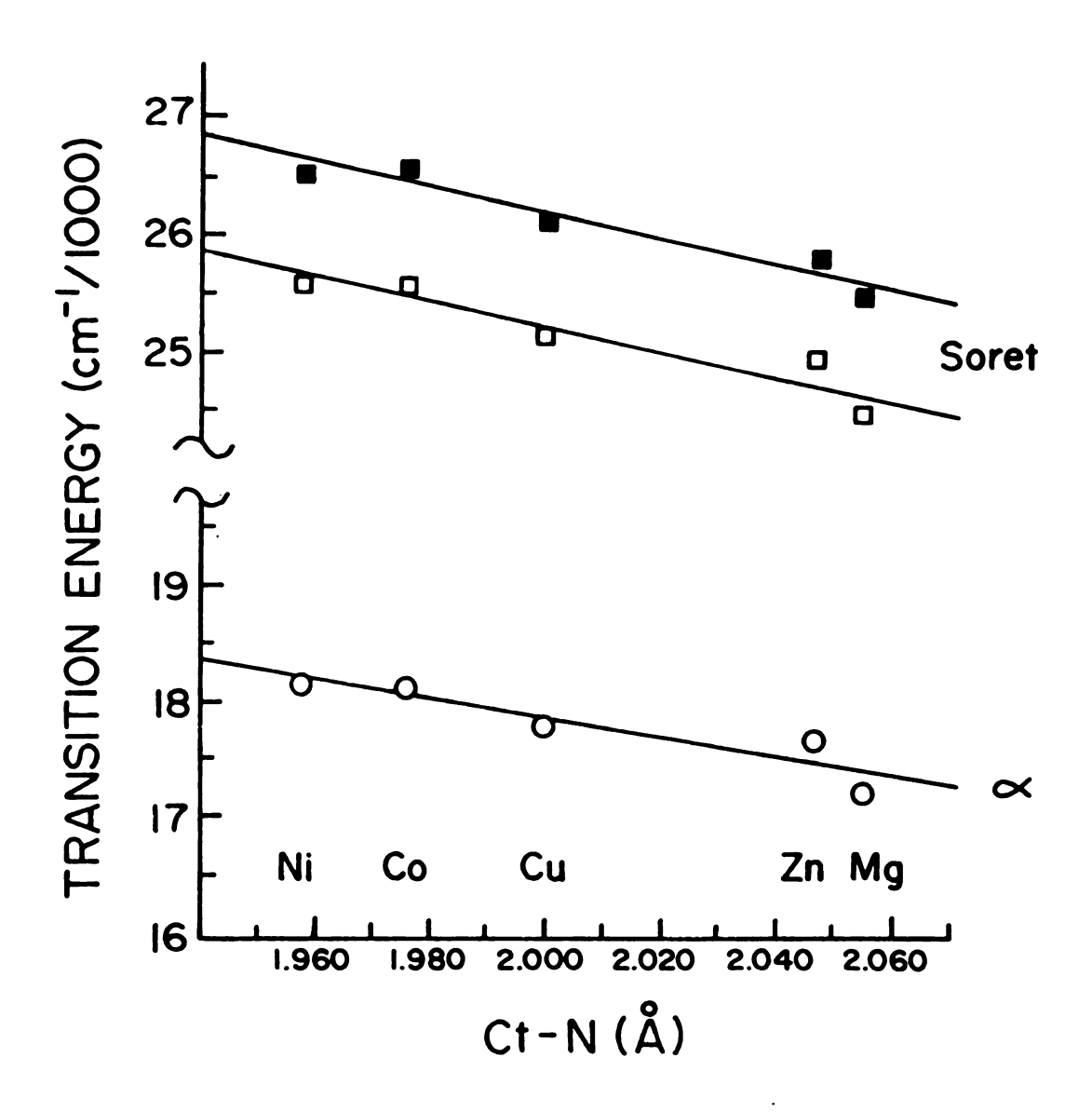


Figure 4-12. Electronic transition energies vs. porphyrin core size for the indicated MOEP and MOEP $^{+}$ ClO $_4$ - complexes. Open and filled symbols correspond to absorption band maxima of MOEP and MOEP $^{+}$ ClO $_4$ -, respectively.

invariability of the core size (d) upon oxidation of the parent MOEP. Table 4-2 summarizes the relevant parameters which describe the four X-ray crystal structures of metalloporphyrin m cation radicals determined to date, and compares them to the structures of the analogous parent compounds. The table also compares perchlorate ligated ferric TPP and OEP as a control to establish possible steric effects limited to TPP complexes. In each case the agreement between the structures of MP and MP+ is good in terms of the Ct-N distances and the metal displacements from the plane of the pyrrole nitrogens. However, the porphyrin core structures of MgTPP+ and ZnTPP+ display larger deviations from planarity than do the model parent structures. This is not considered to represent a significant general structural deviation between MP and MP+. and is explained rather as a result of steric interaction of the bulky ClO₄⁻ counter ions and the mesophenyl groups resulting from crystal packing forces. 13 Two other examples support this idea: 1) While crystalline CuTPP+*SbCl6- exhibits "unusually large ruffling of the porphyrin core", the CH₂Cl₂ solution structure is planar; 55 2) Crystalline Fe^{III}(ClO₄-)TPP exhibits core ruffling almost as large as the perchlorate ligated MTPP+ examples, whereas $Fe^{III}(ClO_4^-)OEP$ has a planar core (see Table 4-2). Thus, we conclude that CH₂Cl₂ solution structures of the type MOEP+*ClO₄- do not exhibit significant ruffling of the porphyrin core, and the lines described by Figure 4-11 and 4-12 are useful references, uncomplicated by the effects of macrocyclic distortions. The success of the correlation attests to this and suggests that in general we can assume that in solution the Ct-N distance of the MP+ and probably other aspects of core geometry are comparable to those of the parent MP. Thus, it is assumed that no significant changes in geometric structure of the porphyrin ring accompany the abstraction of an electron from the $a_{2u}(\pi)$ or $a_{1u}(\pi)$ orbital of the metalloporphyrin in solution.

Core Size Parameters from Crystal Structures of Metalloporphyrin * Cation Radicals and Related Compounds. Table 4-2.

•									
4Mb	Ref.	Ct-N (A)	Ct→M (A)	Core Ruffle (A)	- AP	Ref.	Ct-N (A)	Ct (F	Ruffle (A)
Mg(C104)TPP+	13	2.051	0.43	40.4	Mg(H ₂ 0)TPP	99	2.054	0.273	c.
Zn(C10_)TPP+'	13	2.047	0.347	₹0.4	Zn(Py)TPyP ^a	61	2.047	0.33	±0.17
Fe ^{III} (Cl ⁻)TPP ⁺ ·S _b Cl ⁻ ₆	55	2.01	0.5 ^b	"saddle shaped"	Fe ^{III} (x ⁻)TPP ^C	62	2.001	0.51	±0.14
Fe ^{III} (C10 ₄) ₂ TPP ⁺	55	2.045	0	"planar"	Fe ^{III} (H ₂ 0) ₂ TPP	63	2.045	0	±0.034
CuTPP * SbC1 =	22	1.988 ^d	٠.	"unusually	cutppe	2	1.981		
)					Fe ^{III} (ClO ₄)OEP	જ	1.977	0.26	±0.04
					Fe ^{III} (C10,)TPP	99	1.978	0.3	1 0.3

aTPyP= tetrapyridylporphyrin.

^bThis value is assumed in order to calculate Ct-N distance from Fe-N distances.

This represents an average from available X = halide structures.

du-N distance. If the Cu is displaced from the macrocycle plane the Ct-N distance will be less than this value.

*Copper porphyrins seem to exhibit two distinct crystal structures, one with a Ct-N distance of 2.00 A, another with d=1.98A (see ref. 45).

Ring buckling effects. Distortions of the porphyrin core are known to weaken the bonding in the macrocyclic, thus lowering the frequencies of stretching vibrations of the core and causing negative deviations from the relation $\nu=K(A-d).67$ The classic example is shown in Figure 4-11 by the vibrational frequencies of the D_{2d} form of NiOEP, 45 which displays deviations from planarity in the macrocyclic of \pm 0.5 Å. 68 Spiro et al. 67 conclude that the effects of core distortions on vibrational frequencies, although significant, are minor in comparison to changes in Ct-N distance, demonstrating that core size is the main determinant of the vibrational frequencies of the porphyrin macrocycle. Our results indicate that the relationship of core size to vibrational frequency is similar for the oxidized porphyrin ring. It is expected that the effects of core distortions, such as S_4 ruffling, will be manifest also in the vibrational frequencies of the MP+, producing negative deviations from the correlations of Figure 4-11.

This completes our structural analysis of the one-electron, ring-oxidized $M^{II}OEP^{+}ClO_4^{-}$ system. Before continuing, it is useful to summarize our conclusions thus far. If one assumes macrocyclic planarity of the CH_2Cl_2 solution structures of the MOEP series considered here, the close correspondence of the K values in the expression describing the porphyrin core vibrational frequencies $\nu = K(A-d)$ for both the MOEP and MOEP⁺⁺ implies: 1) the corrections of our mode assignments, 2) the essential invariance in the P.E.D. of the normal modes of the porphyrin ring upon oxidation, and 3) the absence of core ruffling in oxidized structures of type $M^{II}OEP^{++}ClO_4^{-}$ (for M=Ni, Co, Cu and Zn). The key assumption that the porphyrin core geometry (especially Ct-N distance) remains intact upon oxidation is based on comparison of crystal structures of $MP^{45,60-66}$ and $MP^{++13,55,56}$ species and has already been suggested. The success of the correlation of vibrational frequencies to

core size presented here suggests that the assumption is valid for the $MOEP^{+}\cdot ClO_4^-$ species. Since they seem independent of ${}^2A_{2u}$ vs. ${}^2A_{1u}$ electronic state character, these linear correlations establish a reference point useful to structurally based vibrational analysis of all $MP^{+}\cdot$ species. As an example, we predict structures for the two-electron oxidized cobaltic systems, $Co^{III}OEP^{+}\cdot 2X^-$. It is anticipated that a similar approach can be applied to both ferric and oxoferryl porphyrin π cation radical models and ultimately to compound I type intermediates of heme enzymes.

Cobaltic octaethylporphyrin ▼ cation radicals. The Co^{III}OEP+2X system is particularly interesting owing to the variety of spectrally distinct two-electron oxidation products possible as a function of counterions X⁻. Characterization of the effects of different counterions in terms of the extent of axial ligation and the relationship of axial ligation to the electronic ground and excited states is essential to understanding the rich variety of absorption spectra displayed by this system upon variation of X^{-.69} In order to compare the electronic spectra of Co^{III}OEP+2X- to the parent system, Co^{II}OEP, it is necessary to determine how oxidation of the metal and addition of axial ligands influence the electronic states of the OEP+ system. For example, the agreement between the Soret maxima of Co^{II}OEP (391 nm) and its two-electron oxidation product Co^{III}OEP+·2ClO₄- (393 nm), would be misleading without acknowledging the counterbalancing effects present. Recognition of the blue-shifted Soret maximum of the cobaltous species Co^{II}OEP+*ClO₄- (376 nm) isolates the effect of ring oxidation upon the Soret absorption maximum, and reveals a blue-shifted band of diminished intensity compared to the parent CoOEP. Axial ligation by the $\mathrm{ClO_4}^-$ ion is unlikely in the cobaltous OEP^{+*} because of the presence of an electron in the metal d_{χ^2} orbital. Thus, we consider this and the other MIIOEP+ ClO₄- complexes discussed here to contain four-coordinate metal centers, devoid of the effects of metal oxidation and axial ligation. Empirically we see that oxidation of the ring causes a 1000 cm⁻¹ blue shift in the Soret maximum with respect to the parent CoOEP. This is compensated for in Co^{III}OEP⁺⁻²ClO₄⁻ by a 1150 cm⁻¹ red-shift produced by oxidation at the metal center accompanied by weak axial ligation by the ClO₄⁻ ions. Compared to the cobaltous case noted above, weak ligation of the cobaltic center by both ClO₄⁻ ions in the latter complex is more likely because the d⁶ configuration of Co^{III} leaves the d₂2 orbital empty. Thus, we consider Co^{III}OEP⁺⁻²ClO₄⁻ to represent a six-coordinate complex, albeit with weak axial ligands. This example illustrates the importance of recognizing the combined effects of metal oxidation and axial ligation on the electronic states of the OEP⁺⁻ systems in order to interpret the absorption spectra correctly.

Effects of one-electron, metal centered oxidation and axial ligation. In order to assess these effects on the electronic transitions of the OEP+ system, a good starting point is to consider the effects of metal oxidation and ligation in the parent OEP system. For this analysis we utilize the ring-neutral Co^{III}(MeOH)₂OEPX⁻ as an example of a weakly ligated, six-coordinate cobaltic complex. Comparison of the spectra of this species to those of CoOEP will establish the effects of ligation and oxidation of the metal. These effects will be compared to the effects of axial ligation alone on Cu and NiOEP.

Shelnutt et al. 58 have shown that the red-shifts in the α and Soret bands of Cu and Ni porphyrins upon axial ligation are accompanied by expansion of the porphyrin ring as revealed by decreases in RR frequencies of the core size sensitive modes. The core expansion accompanying axial ligation in Ni porphyrins, confirmed by similar RR measurements by Kim et al. 69 , is much greater than in Cu porphyrins and involves a change in spin state and subsequent occupancy of the $d_{x^2-y^2}$ orbital of the Ni. 70 These spectroscopic results are explained

by a relative increase in the porphyrin $a_{211}(\pi)$ orbital energy level caused by the interaction of the metal atom with its axial ligands, and are thus in agreement with the model for axial ligation proposed by Gouterman.⁴⁸ Table 4-3 collects RR frequencies and absorption maxima for Cu, Ni and CoOEP and their axially ligated systems. We emphasize that with these examples we consider the effects of ligation alone for Cu and NiOEP, and ligation accompanied by metal oxidation for CoOEP. Inspection of Table 4-3 reveals that the red-shifts in the optical absorptions of Co^{III}(L)₂OEPX⁻ (where L = methanol or 1-methylimidazole) with respect to those of CoOEP are similar to those encountered upon ligation of CuOEP or NiOEP. Indeed, the magnitude of the Soret absorption red-shift for the cobalt system (1180 cm^{-1}) is between that of the copper (970 cm^{-1}) and nickel (1800 cm⁻¹) systems. However, the RR data clearly show that axial ligation and autoxidation of CoOEP is not accompanied by core expansion, as there is no decrease in the vibrational frequencies of Co^{III}(L)₂OEPX⁻ compared to CoOEP. The slight increases in v4 frequencies reflect a decrease in the $e_g(\ \pi^{\pmb{*}})$ orbital occupancy upon oxidation of Co^{II} to Co^{III} and are not related to core size. (The Cu and NiOEP systems show the opposite behavior and exhibit decreases in the v4 frequencies). RR wavenumbers reflect the structure of the ground state of the scattering species. Thus, red-shifts in the absorption spectra without concomitant decreases in RR frequencies suggest stabilization of the excited state, i.e. a decrease in the $e_{\sigma}(\pi^*)$ rather than an increase in the $a_{2u}(\pi)$ orbital energies upon axial ligation and metal oxidation of these species. These considerations indicate that the spectral red-shifts observed upon metal oxidation and ligation of CoOEP are not simply comparable to those caused by ligation alone of Cu and NiOEP. Whether these conclusions apply to ligation alone of cobaltous porphyrins under anaerobic conditions cannot be determined from this analysis.

Table 4-3

Resonance Raman Frequencies and Optical Absorption Maxima for Axially Ligated $\rm Cu^{II}$, Ni II and $\rm Co^{III}\rm OEP$ Complexes

			Frequency (cm^{-1})	cm ⁻¹)			u	Soret
	4	د م	٧11	٧19	20	٧10	(mu)	(mn)
CuOEP/hexane ^a	1378	1503	1568	1582		1637	562	398
Cu(pyr)OEPa	1376	1503°	1566	1580		1629	570	414
NiOEP/CH ₂ C1 ₂ b	1382	1519		1602	1601	1656	551	391
Ni(pip) ₂ OEP ^b	1370	1481		1559	1587	1615		421
Co ^{II} OEP	1379	1512	1575	1598	1598	1647	551	391
$Co^{III}(MeOH)_2OEPCIO_4^-$	1382	1515	1575	1597	1598	1647	556	409
Co ^{III} (MeOH) ₂ OEPBr-	1382	1515	1575	1596	1599	1648	558	411
Co ^{III} (Im) ₂ OEPX ⁻	1383	1514	1575		1598	1646	559	417

c v₃ frequency for Cu(pip)OEP (ref. 58a). b References 58b and 69. a Reference 58a.

pyr = pyrrolidine, pip = piperidine, and Im = 1-methylimidazole. Abbreviations used:

Co^{III}OEP+ 2ClO₄-. Having established the combined effects of metal oxidation and weak axial ligation on the electronic transitions and RR vibrations of Co^{II}OEP, we can consider like effects in the analogous π cation radical system, Co^{II}OEP+. Comparison of Soret maxima and RR frequencies (Fig. 4-7c and d) of Co^{II}OEP+*ClO₄- to those of Co^{III}OEP+*2ClO₄- reveals optical red-shifts without porphyrin cation radical core expansion in the latter compound. The spectral differences between these two species are analogous to those observed when comparing Co^{II}OEP to Co^{III}(MeOH)₂OEPClO₄-. In the former (π cation) case the Soret maximum shifts 1150 cm⁻¹, or from 376 to 393 nm; while in the latter (ring-neutral) case, the shift is from 391 to 409 nm or 1180 cm⁻¹. In both cases, RR results imply no change in the porphyrin core size. The similarity of these examples suggests that in both instances we are comparing a four-coordinate cobaltous species to a six-coordinate cobaltic one and that ring planarity and D_{4h} symmetry are maintained throughout. Furthermore, the absorption spectra imply that the behavior of the Soret absorption in these π cations is little changed from that of the ring-neutral analogues.

As discussed above, a key assumption in our analysis concerns the effects of ring oxidation per se on macrocycle geometry. Based on X-ray studies of crystaline compounds, ¹³ we assume that in general the core geometries of porphyrin π cations, MP+, are not significantly different from those of the parent compound MP. By "parent" we specifically refer to a complex as nearly identical as possible to the MP+ in all aspects other than macrocyclic oxidation state. That is, the oxidation state and coordination geometry of the central metal must be the same. For example, the "parent" compound for Co^{II}OEP+ ClO₄ is Co^{II}OEP, and the "parent" for Co^{III}(ClO₄-)₂OEP+ is Co^{III}(MeOH)₂OEPClO₄. (The cobaltic π cation radical complex is now written in a manner as to imply axial ligation by the perchlorate anions. Attempts

to exchange the perchlorate ligands for methanol result in reduction of the macrocycle and formation of the cobaltic dimethanol ring-neutral complex.)

Thus, our analysis suggests that the core sizes of all four of these complexes are the same, approximately 1.97 Å.

Co^{III}OEP⁺⁻2Br⁻. To date, EPR and ENDOR measurements are the most reliable criteria to establish the MP⁺⁻ electronic ground state (${}^{2}A_{2u}$ or ${}^{2}A_{1u}$).8 EPR measurements of Co^{III}OEP⁺⁻2ClO₄⁻ and Co^{III}OEP⁺⁻2Br⁻ are consistent with the ${}^{2}A_{2u}$ and ${}^{2}A_{1u}$ states, respectively.²⁴ Perhaps the most interesting aspect of the correlations presented in Figure 4-11 and 4-12 is the apparent insensitivity of the RR frequencies and Soret transition energies of the M^{II}OEP⁺⁻ClO₄⁻ complexes to radical electronic state. This implies that we can use these correlations for structural analysis of OEP⁺⁻ compounds of either radical type, and we can extend our discussion to include Co^{III}OEP⁺⁻2Br⁻.⁷¹

Aside from differences in relative intensities, the RR spectra of ${\rm Co^{III}OEP^{+}}{}^{\circ}{\rm 2ClO_4^{-}}$ and ${\rm Co^{III}OEP^{+}}{}^{\circ}{\rm 2Br^{-}}$ are similar (see Fig. 4-7d and g; Fig. 4-9). Table 4-4 compares the RR frequencies of these two complexes. The vibrational frequencies of the latter (presumably a ${}^2{\rm A_{1u}}$ complex), however, are 6-7 cm⁻¹ lower than those of the former (presumably a ${}^2{\rm A_{2u}}$ complex), with the as yet unexplained exception of ν_{10} . Because the core size correlations seem independent of radical electronic state, and because the frequency differences between these two complexes are small, we speculate that they can be attributed to differences in porphyrin core geometry caused by the different axial ligation of these two species. Decreases in frequency of the macrocyclic vibrations (above 1400 cm⁻¹) may result from either expansion or buckling of the porphrin core. It is reasonable to assume that ${\rm Co^{III}OEP^{+}}{}^{\circ}{\rm 2Br^{-}}$ is a six-coordinate complex with a planar porphyrin core. The ν_3 , ν_{11} , ν_2 and ν_{10} frequencies (Table 4-4) can then be used, along with R and A values

Table 4-4

Comparison of Resonance Raman Frequencies (cm⁻¹) and of Depolarization Ratios for Cobaltic OEP⁺⁻ Complexes

	Co ^{III} OEP+·2C1O ₄ -	Co ^{III} OEP+·2Br-
٧4	1361 (0.2)	?
ν 3	1505 (0.5)	1498 (0.3)
٧11.	1605 (0.7)	1598 (0.5)
v <u>2</u>	1617 (0.5)	1611 (0.4)
٧10	1642 (0.7)	1649 (0.7)

from Table 4-1, to predict a core size of 1.99 \pm 0.02 Å for this complex. This is to be compared to 1.974 \pm 0.008 Å predicted similarly for the core size $Co^{III}OEP^{+}\cdot 2ClO_4^{-}$. However, the possibility that the vibrational frequencies of $Co^{III}OEP^{+}\cdot 2Br^{-}$ are lowered from those of $Co^{III}OEP^{+}\cdot 2ClO_4^{-}$ as a result of porphyrin core distortions, rather than core expansion, cannot be ruled out by this analysis.⁷²

CONCLUSIONS

While the interpretation of the spectra described in this paper essentially ignores radical designation as $^2A_{211}$ or $^2A_{111}$, other researchers have emphasized the species symmetry of MP+ compounds. Characterization of the MP+ as $^{2}A_{2u}$ or $^{2}A_{1u}$, as revealed by spin density profiles, has been based primarily calculations, 47a, 73-75 as well **EPR ENDOR** on as and studies. 4,8,24,47a,73,75-77 These studies have established many useful generalizations concerning radical type. For instance, the porphyrin ring substituents have a profound influence, and structures of the type MTAP+* (where A is an alkyl or aryl group in the meso position) exhibit ²A₂₁₁ characteristics, ⁸ while MHP⁺ (where HP=hydroporphyrin) tend to be classified as $^2A_{111}$ radicals. 73,76,77 Structures of the type MOAP+* (octaalkylporphyrin where the Cb substituents are not necessarily identical) may exhibit either state depending primarily on the metal center and the axial ligands.8,24,73 Examples of the latter type include the high valent catalytic intermediates of heme peroxidases and catalases. The compound I structures of these enzymes are oxoferryl protoporphyrin IX cation radicals, usually decribed as O=Fe^{IV}(X⁻)PP⁺·.² The electronic state is considered to be mediated by the identity of the sixth ligand X-, and MO calculations predict that ligation by tyrosine or thiolates promotes the ${}^{2}A_{111}$ configuration (e.g. CAT-I and CPO-I, respectively)^{73,76} while imidazole ligation generally favors a predominantly $^2A_{2u}$ state (e.g. HRP-I). 73,74 EPR and ENDOR studies, however, are interpreted to suggest a $^2A_{2u}$ configuration for both HRP-I and CPO-I. 78 The EPR measurement of CPO-I (chloroperoxidase compound I) was judged inconsistent with a $^2A_{1u}$ configuration owing to the relatively strong antiferromagnetic coupling (between the S=1 oxoferryl structure and the S=1/2 π cation radical) suggested by the spectra. The authors reason that such coupling is more likely in the $^2A_{2u}$ configuration where relatively large spin densities are placed on the pyrrole nitrogens. 73

Distortions of the porphyrin ring may provide an orbital overlap pathway for the strong $|J| \approx 250~{\rm cm}^{-1}$, antiferromagnetic coupling displayed by ${\rm Fe^{III}(C1^-)TPP^{++}SbC1_6^{-}.55,56}$ While such magnetic coupling was previously thought to occur only in ${}^2{\rm A}_{2u}$ radicals,8 more recent interpretations⁷⁶ suggest magnetic coupling between the paramagnetic metal center and porphyrin π cation radical can occur in either radical type, with the radical type influencing the magnitude of the interaction. 55a While the weak coupling, $|J| \approx 2~{\rm cm}^{-1}$, displayed by HRP-I⁷⁸ has been attributed to possibly a planar configuration of the porphyrin ring, 56 the stronger, $|J| \approx 37~{\rm cm}^{-1}$, coupling for CPO-I⁷⁸ may reflect a more buckled configuration (other explanations are also possible 11,76,78,79). Recent work clearly indicates that evaluation of porphyrin core geometry must be addressed in order to interpret results from magnetic based techniques.

The similarity of the vibrational frequencies in the $1400-1700~cm^{-1}$ range of the proposed $^2A_{2u}$ and $^2A_{1u}$ π cation radicals $Co^{III}OEP^{+}\cdot 2C1O_4^{-}$ and $Co^{III}OEP^{+}\cdot 2Br^{-}$, respectively, suggest that these frequencies are insensitive to radical type. There are, however, small wavenumber differences which can be attributed to relatively minor differences in porphyrin core geometry of these two compounds. Because these geometric differences are as yet

speculative, other interpretations are plausible. Although these vibrations of the porphyrin macrocyclic may well be insensitive to radical electronic state, the abnormally high values of the ν (C_bC_b) modes provide a clear basis to identify ring centered oxidations, particularly in MOEP⁺⁺ species.²² Both the frequency and relative intensity of the ν_4 mode (1340-1370 cm⁻¹) may reflect $^2A_{2u}$ vs. $^2A_{1u}$ character. More information concerning electronic states will be provided by RR excitation profiles. Our intent in this work is to establish an approach to evaluate core geometry of oxoferryl porphyrin π cation radicals in enzymes in order to complement the NMR, EPR, and ENDOR results for these sytems.

ACKNOWLEDGMENTS

T.O. thanks Dwight Lillie and Bob Kean for their computer programming and Harold Fonda for discussion. This work was supported by NIH grants GM-25480 (G.T.B.) and GM-36520 (C.K.C.), and NSF grant CHE-86-10421 (G.E.L.).

REFERENCES AND NOTES

- (a) Frew, J.E., Jones, P. in "Advances in Inorganic and Bioinorganic Mechanism"; Academic Press: New York, 1984; Vol. 3, pp. 175-215;
 (b) Hewson, W.D.; Hager, L.P. in "The Porphyrins"; Dolphin D., Ed.; Academic Press: New York, 1979; Vol. 4, pp. 295-332.
- 2. (a) Norris, J.R., Sheer, R.; Katz, J.J. in "The Porphyrins"; Dolphin, D., Ed.; Academic Press; New York, 1979; Vol. 4, pp. 159-195; (b) Lubitz, W.; Lendziar, F.; Plota, M.; Möbins, K.; Tränkle, E., Springer Series in Chem. Phys. 1985, 42, 164-173.
- 3. Fuhrhop, J.H., Struct. Bonding 1974, 18, 1-67.
- 4. Dolphin, D.; Mulijinani, Z.; Rousseau, K.; Borg, D.C.; Fajer, J.; Felton, R.H., Ann. N.Y. Acad. Sci. 1973, 206, 177-200.
- 5. Wolberg, A.; Manassen, J., J. Am. Chem. Soc. 1970, 92, 2982-2991.
- 6. Phillippi, M.A.; Goff, H.M., J. Am. Chem. Soc. 1982, 104, 6026-6034.
- 7. Carnieri, N.; Harriman, A., Inorg. Chim. Acta 1982, 62, 103-107.
- 8. (a) Fajer, J.; Davis, M.S. in "The Porphyrins"; Dolphin D., Ed.; Academic Press: New York, 1979, Vol. 4, pp. 197-256, (b) Fajer, J.; Borg, D.C.; Forman, A.; Felton, R.H.; Vegh, L.; Dolphin, D., Ann. N.Y. Acad. Sci. 1973, 206, 349-364.
- 9. (a) Browett, W.R.; Stillman, M.J., Inorg. Chim. Acta 1981, 49, 69-77;
 (b) Browett, W.R.; Stillman, M.J., Biochim. Biophys. Acta 1981, 660, 1-7.
- 10. (a) Godziela, G.M.; Goff, H.M., J. Am. Chem. Soc. 1986, 108, 2237-2243;
 (b) Goff, H.M.; Phillippi, M.A., J. Am. Chem. Soc. 1983, 105, 7567-7571.
- 11. Morishima, I.; Takamuki, Y.; Shiro, Y., J. Am. Chem. Soc. 1984, 106, 7666-7672.
- 12. Shimomura, E.T.; Phillippi, M.A.; Goff, H.M., J. Am. Chem. Soc. 1983, 103, 6778-6780.

- (a) Barkigia, K.M.; Spaulding, L.D.; Fajer, J., Inorg. Chem. 1983, 22, 349-351; (b) Spaulding, L.D.; Eller, P.G.; Bertrand, J.A.; Felton, R.H., J. Am. Chem. Soc. 1974, 96, 982-987.
- 14. Nadezhdin, A.D.; Dunford, H.B., Photochem. Photobiol. 1979, 29, 899-903.
- (a) Teraoka, J.; Ogura, T.; Kitagawa, T., J. Am. Chem. Soc. 1982, 104, 7354-7356;
 (b) Van Wort, H.E.; Zimmer, J., J. Am. Chem. Soc. 1985, 107, 3379-3381.
- (a) Oertling, W.A.; Babcock, G.T., J. Am. Chem. Soc. 1985, 107, 6406-6407;
 (b) Ogura, T.; Kitagawa, T., submitted.
- 17. (a) Cotton, T.M.; Parks, K.D.; Van Duyne, R.P., J. Am. Chem. Soc. 1980, 102, 6399-6407; (b) Lutz, M. in "Advances in Infrared and Raman Spectroscopy"; Clark, R.J.H., Ed.; Wiley, New York 1984, Vol. XI, pp. 211-300.
- 18. Yamaguchi, H., Nakano, M.; Itoh, K., Chem. Lett. 1982, 1397-1400.
- 19. (a) Chottard, G.; Battioni, P.; Battioni, J.-P.; Lange, M.; Mansuy, D., Inorg. Chem. 1981, 20, 1718-1722; (b) Aramaki, S.; Hamaguchi, H.; Tasumi, M., Chem. Phys. Lett. 1983, 96, 555-559.
- 20. Kim, D.; Miller, L.A.; Rakhit, G.; Sprio, T.G., J. Phys. Chem. 1986, 90, 3320-3325.
- 21. Oertling, W.A.; Salehi, A.; Chang, C.K.; Babcock, G.T., J. Phys. Chem., submitted.
- 22. Salehi, A.; Oertling, W.A.; Babcock, G.T.; Chang, C.K., J. Am. Chem. Soc. 1986, 108, 5630-5631.
- 23. Edwards, W.D.; Zerner, M.C., Can. J. Chem. 1985, 63, 1763-1772.
- 24. Dolphin, D.; Forman, D.C.; Borg, J.; Felton, R.H., Proc. Natl. Acad. Sci. USA 1971, 68, 614-618.
- 25. Wang, C.B.; Chang, C.K., Synthesis 1979, 548-549.
- 26. Falk, J.E. in "Porphyrins and Metalloporphyrins"; Elsevier: New York, 1964, 798.
- 27. Alternative structural assignments for these compounds, particularly Co^{III}(MeOH)₂OEPBr⁻, are possible. A mixed diaxial species of the type (Br⁻)Co^{III}(MeOH)OEP was proposed by Johnson, A.W.; Kay, I.T., J. Chem. Soc. 1960, 2979-2983 and may better explain the similar, yet distinct absorption maxima of Co^{III}(MeOH)₂OEPClO₄⁻ and Co^{III}(MeOH)₂OEPBr⁻ (see Table 4-1 of the Discussion section). Further addition of MeOH to the latter compound produces a sample with identical absorption maxima to that of Co^{III}(MeOH)₂OEPClO₄⁻. For this work, however, a distinction between dimethanol ligation vs. mixed axial ligation of these complexes is not necessary. See also: Sugimoto, H.; Ueda, N.; Mori, M., Bull. Chem. Soc. Jpn. 1981, 54, 3425-3432.

- Under certain conditions, however, molecular oxygen (O2) was observed 28. to promote oxidation of metalloporphyrins. For instance, in the presence of excess (V0.1 mM) tertbutyl ammonium perchlorate, oxidation of CoOEP to Co^{III}OEP+ 2ClO₄ was observed, presumably via the formation of HClO₄ in CH2Cl2 solution, as discussed by Fukuzumi, S.; Ishikawa, K.; Tanaka, T., Chem. Lett. 1986, 1-4. Upon laser irradiation in Soret resonance at 406.7 nm or 390 nm, CH₂Cl₂ solutions of CuOEP, ZnOEP, CoOEP and Co^{II}OEP+ ClO₄ in the presence of O₂ were observed to undergo one-electron oxidation requiring various exposure times for each species. These effects were not observed with 363.8 nm excitation. Similar photochemical oxidation of CoTPP has been discussed by Gasyna, Z.; Browett, W.R.; Stillman, M.J., Inorg. Chem. 1984, 23, 382-384; and by Yamamoto, K.; Hoshino, M.; Kohno, M.; Ohya-Nishiguchi, H., Bull. Chem. Soc. Jpn. 1986, 59, 351-354. Both MgOEP and MgOEP*Br were difficult to work with for RR experiments; many spectra of these compounds were collected at the outset of our study, but they are not heavily relied on in this work.
- 29. Fuhrhop, J.H.; Mauzerall, D., J. Am. Chem. Soc. 1969, 91, 4174-4181.
- 30. Konishi, S.; Hoshino, M.; Imamura, M., J. Am. Chem. Soc. 1982, 104, 2057-2059.
- 31. Fuhrhop, J.H.; Wasser, P.; Riesner, D.; Mauzerall, D., J. Am. Chem. Soc. 1972, 94, 7996-8001.
- 32. Spiro, T.G. in "Iron Porphyrins" Lever, A.B.P.; Gray, H.B., Eds., Addison-Wesley: Reading, M.A. 1983; Part 2, pp. 89-159.
- 33. (a) Abe, M.; Kitagawa, T.; Kyogoku, Y., J. Chem. Phys. 1978, 69, 4526-4534;
 (b) Gladkov, L.L.; Solovyov, K.N., Spectrochim. Acta 1986, Vol. 42A, 1-10.
- 34. Boldt, N.J.; Donohoe, R.J.; Birge, R.R. and Bocian, D.F., J. Am. Chem. Soc. 1987, in press.
- 35. (a) Brunner, H.; Mayer, A.; Sussner, H., J. Mol. Biol. 1972, 70, 153;
 (b) Yamamoto, T.; Palmer, G.; Gill, D.; Salmeen, I.T.; Rimai, L., J. Biol. Chem. 1973, 248, 5211-5213.
- 36. Corwin, A.H.; Chivvis, A.B.; Poor, R.W.; Whitten, D.G.; Baker, W.E., J. Am. Chem. Soc. 1968, 90, 6577-6583.
- (a) Whitten, D.G.; Baker, E.W.; Corwin, A.H., J. Org. Chem. 1963, 28, 2363-2368; (b) Tsutsui, M.; Valapoldi, R.A.; Hoffman, L.; Suzuki, K.; Ferrari, A., J. Am. Chem. Soc. 1969, 91, 3337-3341.
- 38. We emphasize that the presence of trace amounts of diacid salts in preparations of MP⁺ in CH₂Cl₂ is not always evident from absorption spectra. For example, no diacid contributions to the absorption spectrum in Figure 4-5c of Co^{III}OEP⁺·2ClO₄⁻ are apparent, yet RR excitation at 406.7 nm reveals their presence as shown by Figure 4-3b. Likewise, RR measurements at 406.7 nm of Co^{III}OEP⁺·2Br⁻ preparations invariably reflect the presence of porphyrin acid impurities. Earlier, the blue-shifted

Soret absorption of metalloporphyrin dications allowed the detection of porphyrin diacid impurities from uv-visible absorption spectra of these samples (see ref. 47a). It was not until the application of the RR technique, however, that the presence of the diacid was recognized in metalloporphyrin π cation radicals (ref. 21).

- 39. Spiro, T.G.; Strekas, T.C., J. Am. Chem. Soc. 1974, 96, 338-345.
- 40. Choi, S.; Sprio, T.G.; Langry, K.C.; Smith, K.M.; Budd, D.L.; LeMar, G.N., J. Am. Chem. Soc. 1982, 104, 4345-4351.
- 41. (a) Stewart, B.; Clark, R.J.H., Struc. Bonding (Berlin) 1979, 36, 1-80;
 (b) Rousseau, D.L.; Friedman, J.M.; Williams, P.F., Topics Curr. Phys. 1978, 11, 202-252.
- 42. Shelnutt, J.A., J. Chem. Phys. 1981, 74, 6644-6657.
- 43. Spiro, T.G.; Strekas, T.C., Proc. Natl. Acad. Sci. USA 1972, 69, 2622-2626.
- 44. Verma, A.L.; Mendelsohn, R.; Bernstein, H.J., J. Chem. Phys. 1974, 61, 383-390.
- 45. Spaulding, L.D.; Chang, C.C.; Yu, N.-T.; Felton, R.H., J. Am. Chem. Soc. 1975, 97, 2517-2524.
- 46. Johnson, E.C.; Niem, T.; Dolphin, D., Can. J. Chem. 1978, 56, 1381-1388.
- 47. (a) Fajer, J.; Borg, D.C.; Forman, A.; Dolphin, D.; Felton, R.H., J. Am. Chem. Soc. 1970, 92, 3451-3459; (b) Mengersen, C.; Subrammanian, J.; Fuhrhop, J.H., Mol. Phys. 1976, 32, 893-897.
- 48. (a) Gouterman, M., J. Chem. Phys. 1959, 30, 1139-1161; (b) Gouterman, M., J. Mol. Spec. 1961, 6, 138-163.
- 49. Huong, P.V.; Pommier, J.C., C.R. Acad. Sci., Ser. C. 1977, 285, 519-522.
- 50. (a) Warshel, A., Rev. Biophys. Bioeng. 1977, 6, 273; (b) Callahan, P.M.; Babcock, G.T., Biochemistry 1981, 20, 952-958.
- 51. (a) Fujiwara, M.; Tasumi, M., J. Phys. Chem. 1986, 90, 5646-5650; (b) Fonda, H.N.; Babcock, G.T., Proc. 7th Intl. Cong. Photosyn. 1986, in press.
- 52. Kincaid, J.R.; Urban, M.W.; Watanabe, T.; Nakamoto, K., J. Phys. Chem. 1986, 90, 5646-5650.
- 53. Ozaki, Y.; Iriyama, K.; Ogoshi, H.; Ochiai, T.; Kitagawa, T., J. Phys. Chem. 1986, 90, 6105-6112.
- 54. The decrease in K value upon oxidation for v_{10} is not considered significant owing to the uncertainty in the v_{10} measurement of $ZnOEP^{+}ClO_4^{-}$ by Soret Excitation RR. Visible excitation of this compound at 647.1 nm, which should more clearly show the v_{10} band, was not possible owing to intense fluorescence emission centered around 675 nm. Thus it is possible that the relatively high v_{10} value measured for $ZnOEP^{+}ClO_4^{-}$ anomalously

- lowers the K value (for v_{10}) of the MOEP⁺ series.
- (a) Scholz, W.F.; Reed, C.A.; Lee, Y.J.; Scheidt, W.R.; Lang, G., J. Am. Chem. Soc. 1982, 104, 6791-6793; (b) Buisson, G.; Deronzier, A.; Duée, E.; Gans, P.; Marchon, J.-C.; Regnard, J.-R., J. Am. Chem. Soc. 1982, 104, 6793-6796.
- 56. Gans, P.; Buisson, G.; Duee, E.; Marchon, J.-C.; Erler, B.S.; Scholz, W.F.; Reed, C.A., J. Am. Chem. Soc. 1986, 108, 1223-1234.
- 57. (a) Kitagawa, T.; Ogoshi, H.; Watanabe, E. Yoshida, Z., J. Phys. Chem. 1975, 79, 2629-2635; (b) Shelnutt, J.A.; Ondrias, M.R., Inorg. Chem. 1984, 23, 1175-1177.
- 58. (a) Shelnutt, J.A.; Straub, K.D.; Rentzepis, P.M.; Gouterman, M.; Davidson, E.R., Biochemistry 1984, 23, 3946-3954; (b) Shelnutt, J.A.; Alston, K.; Ho, J.-Y.; Yu, N.-T.; Yamamoto, T.; Rifkind, J.M., Biochemistry 1986, 25, 620-628.
- the model presented here is an oversimplification. Similar trends in the $e_g(\pi^*)$ orbital energy levels (LUMO) are revealed by reduction potentials for MOEP complexes. Comparative measurements of the first oxidation potential reflect trends in the HOMO energies. The results show that both the HOMO and the LUMO rise in energy in the series Ni Cu, Zn, MgOEP; however, the HOMO levels increase more, thus producing the spectral red-shift. See ref. 29 and Fuhrhop, J.-H.; Kadish, K.M.; Davis, D.G, J. Am. Chem. Soc. 1973, 95, 5140-5147.
- 60. Timkovich, R.; Tulinsky, A., J. Am. Chem. Soc. 1969, 91, 4430-4432.
- 61. Collins, D.M.; Hoard, J.L., J. Am. Chem. Soc. 1968, 92, 3761-3771.
- 62. Mitra, S. in "Iron Porphyrins"; Lever, A.B.P.; Gray, H.B., Eds.; Addison-Wesley: Reading, Mass, 1982, Part II, pp. 3-42.
- 63. Scheidt, W.R.; Cohen, I.A.; Kastner, M.E., Biochemistry 1979, 18, 3546-3552.
- 64. Fleischer, E.B.; Miller, C.; Webb, L., J. Am. Chem. Soc. 1964, 86, 2342-2343.
- 65. Masuda, H.; Taga, T.; Osaki, K.; Sugimoto, H.; Yoshida, A.-I.; Ogoshi, H., Inorg. Chem. 1980, 950-955.
- 66. Reed, C.A.; Mashiko, T.; Bentley, S.P.; Kastner, M.E.; Sheidt, W.R.; Spartalian, K.; Lang, G., J. Am. Chem. Soc. 1979, 101, 2948-2958.
- 67. Spiro, T.G.; Strong, J.D.; Stein, P., J. Am. Chem. Soc. 1979, 101, 2648-2655.
- 68. Meyer, E.F., Acta Cryst. 1972, B28, 2162-2167.
- 69. Setsume, J.; Ikeda, M.; Kishimoto, Y.; Kitao, T., J. Am. Chem. Soc. 1986, 108, 1309-1311.

- 70. Kim, D.; Su, Y.O.; Spiro, T.G., Inorg. Chem. 1986, 25, 3988-3993.
- 71. Actually the question of radical ground state for these compounds is not completely clear-cut. Of the ClO₄⁻ complexes used in the correlations, only MgOEP⁺ and ZnOEP⁺ have been firmly assigned a ground electronic state (²A_{1u}) based on EPR studies (ref. 8). Coupling between the paramagnetic metal centers and the porphyrin radical of Co^{II}OEP⁺·ClO₄⁻ and CuOEP⁺ render these complexes EPR silent. Although the uv-visible absorption spectra of Cu, Co^{II} and NiOEP⁺ imply ²A_{2u} character for their ClO₄⁻ complexes, the electronic state of CuOEP⁺·ClO₄⁻ is assigned as ²A_{1u} based on NMR spectra (ref. 10a). To our knowledge, the EPR spectrum of NiOEP⁺·ClO₄⁻ (ref. 29) has never been discussed in terms of ²A_{2u} or ²A_{1u} ground state symmetry.
- 72. Based on RR frequencies, the precurser compound, Co^{III}OEPBr⁻, is predicted to have a contracted core, ~1.957 ± 0.009 Å. We also note that this one-electron oxidized compound displays certain Raman absorption spectroscopic features analogous to a structure known to possess a buckled porphyrin core, namely the μ-nitrido dimer, (FeOEP)₂N. See: (a) Hoffman, J.A.; Bocian, D.F., J. Phys. Chem. 1984, 88, 1472-1479; (b) Scheidt, W.R.; Summerville, D.A.; Cohen, I.A., J. Am. Chem. Soc. 1976, 98, 6623-6628; for spectra and crystal structure of μ-nitrido dimers, respectively. However, it is not yet clear if the geometry of this precurser (not "parent" as defined above) is relevant to the structure of the two-electron oxidized product, Co^{III}OEP**2Br⁻.
- 73. Hanson, L.K.; Chang, C.K.; Davis, M.S.; Fajer, J., J. Am. Chem. Soc. 1981, 103, 663-670.
- 74. Loew, G.H.; Herman, Z.S., J. Am. Chem. Soc. 1980, 102, 6174-6175.
- 75. Fujita, I.; Hanson, L.K.; Walker, F.A.; Fajer, J., J. Am. Chem. Soc. 1983, 105, 3296-3300.
- 76. Fujita, E.; Chang, C.K.; Fajer, J., J. Am. Chem. Soc. 1985, 107, 7665-7669.
- 77. Chang, C.K., Hanson, L.K.; Richardson, P.F.; Young, R.; Fajer, J., Proc. Natl. Acad. Sci. USA 1981, 78, 2652-2656.
- 78. (a) Roberts, J.E.; Hoffman, B.M.; Rutter, R.; Hager, L.P., J. Biol. Chem. 1981, 256, 2118-2121; (b) Rutter, R.; Hager, L.P., J. Biol. Chem. 1982, 257. 7958-7961; (c) Schultz, C.E.; Rutter, R.; Sage, S.T.; Debrunner, P.G.; Hager, L.P., Biochemistry 1964, 23, 4743-4754.
- 79. Sontum, S.F.; Case, D.A., J. Am. Chem. Soc. 1985, 107, 4013-4015.

CHAPTER 5

DETAILS OF PEROXIDASE CATALYSIS SUGGESTED BY RESONANCE RAMAN MEASUREMENTS OF IRON-OXYGEN STRETCHING FREQUENCIES OF HORSERADISH PEROXIDASE INTERMEDIATES

INTRODUCTION

Horseradish Peroxidase (HRP) uses hydrogen peroxide to catalyze the oxidation of indole acetic acid (a growth hormone) in plant roots. The generally accepted reaction pathway, as proposed independently by Chance¹ and George,² occurs in four steps:

- 1. $HRP + H_2O_2 \rightarrow HRP-I + H_2O$
- 2. $HRP-I + AH \rightarrow HRP-II + A^*$
- 3. HRP-II + AH \rightarrow HRP + A' + H₂O
- 4. 2A° → products

Other pathways, however, may have physiological significance.³ The prosthetic group of the enzyme in the native state (HRP) consists of a ferric protoporphyrin IX ligated on the proximal side of the heme plane by histidine nitrogen. In the first intermediate state, compound I (HRP-I), the heme most likely retains the histidine imidazole (Im) ligand and undergoes two-electron oxidation, forming

an oxoferryl protoporphyrin IX π cation radical, O=Fe^{IV}(Im)PP+. The second intermediate, compound II (HRP-II), is formed via the oxidation of the substrate (AH) which leaves the low-spin (S=1) oxoferryl-imidazole linkage intact but reduces the porphyrin macrocyclic back to the neutral state.⁴⁻⁶ The intermediates of the HRP reaction are of interest because of the possible general application by nature of similar structures in the catalysis of not only other peroxidases, but also catalases, oxygenases and oxidases.⁷

The oxoferryl structure of HRP-I and HRP-II is well characterized by a variety of physical techniques. Three unpaired electrons (S = 3/2) are indicated by magnetic susceptibility measurements of HRP-I,8 consistent with a low-spin (S=1) Fe^{IV} ferromagnetically coupled to a S=1/2 radical center. Mössbauer measurements of HRP-I and HRP-II are compatible with similar Fe^{IV} configurations for both intermediates. 9 170 electron nuclear double resonance (ENDOR) spectroscopy of HRP-I prepared with H₂17O₂ demonstrates the incorporation of a single ¹⁷O atom in the first intermediate. ¹⁰ Proton nuclear magnetic resonance (NMR) studies of the second intermediate and its synthetic models provide further evidence for the oxoferryl structure in HRP-II.11 Although somewhat controversial, 12,13 recent evidence from extended X-ray absorption fine structure (EXAFS) spectroscopy presents detailed structures for HRP-I and HRP-II with relatively short (1.65 Å) FeO bond lengths and contracted (1.99 Å) heme center-to-pyrrole nitrogen distances. 14,15 Recent resonance Raman (RR) measurements of the FeO stretching frequency, v(FeO), of HRP-II^{16,17} and model oxoferryl porphyrins¹⁸⁻²¹ confirm the double-bonded character and short bond length of the oxoferryl structure. Furthermore, the frequencies of the porphyrin core vibrational modes are consistent with the 1.99 \mathring{A} core size for HRP-II^{22,23} and for the synthetic oxoferryl complexes. 19,24 We present here RR evidence that these structural features are maintained in HRP-I as well. RR studies of HRP-II also reveal a pH dependency for $\nu(\text{FeO})$ which suggests H-bonding of the oxo ligand to a protonated distal histidine with a pK_a of 8.6. 25,26 We report a $\nu(\text{FeO})$ for the first intermediate at pH 7 which is very similar to that of HRP-II at pH 11 in the absence of H-bonding. This suggests that the oxoferryl of HRP-I is not H-bonded at pH 7. The significance of these structural features to the kinetics and mechanism of peroxidase catalysis is discussed.

RR studies of the first intermediate are complicated by its reactivity and photolability.²⁷ Past studies^{28,29} were interpreted to suggest that cryogenic techniques may be insufficient to stabilize HRP-I to laser irradiation in the region of the Soret absorption (300-450 nm). Because of this we have adopted an alternative approach, using pulsed, near-uv RR excitation of flowing samples of HRP-I generated by rapid mixing. 30 Similar approaches have been applied to reaction intermediates of cytochrome c oxidase, and both pulsed^{31,32} and continuous wave (CW) laser excitation³³ have been used. The high frequency (1200-1700 cm⁻¹) spectrum of HRP-I we obtained earlier with pulsed RR excitation³⁰ has been independently confirmed by Ogura and Kitagawa³⁴ with CW excitation. We have also carried out an extensive RR study of porphyrin cation radicals (P++) and other oxidized forms of Co, Cu and Zn octaethylporphyrin (OEP).35,37 We present here preliminary results from an additional RR study of synthetic ferric porphyrin cation radicals. 38 Based on these recent results from the P++ model compounds and further characterization of the RR scattering from HRP-II presented here, we have reanalyzed the high frequency RR spectrum obtained for HRP-I. We find no vibrational frequencies characteristic of a metalloporphyrin π cation radical (MP⁺). In view of the evidence in favor of the P+ formulation for HRP-I from uv-visible absorption, 39 electron paramagnetic resonance (EPR), 40,41 ENDOR, 42 and NMR 43,44 spectroscopies, we offer possible explanations for the RR results.

EXPERIMENTAL

Materials. Horseradish peroxidase was purchased from Sigma (Type VI) and used without further purification. Sodium phosphate and sodium carbonate buffers (50 mM) were used at pH 7 and 10.8, respectively, for all enzyme and hydrogen peroxide solutions. 30% $\rm H_2^{16}O_2$ was purchased from Mallinkrodt. $\rm H_2^{18}O_2$ was made from $\rm ^{18}O_2$ (98%, Cambridge Isotope Laboratories) using glucose oxidase (SIGMA) according to the procedure of Asada and Badger. HRP and peroxide solutions were quantified photometrically by using extinction coefficients at 403 nm⁴⁶ and 240 nm⁴⁷ of 103 mM⁻¹cm⁻¹ and 43.6 M⁻¹cm⁻¹, respectively.

HRP-I. Flowing HRP-I samples (pH 7) for RR measurements were prepared by rapid mixing of equal volumes of cooled solutions of 0.1 mM HRP and 1 mM hydrogen peroxide. These were loaded in 10.0 ml syringes and driven through two eight-jet tangential mixers in series 48 with a Sage 355 syringe pump. After mixing, the HRP-I sample passed through a 0.5 mm i.d. capillary. Raman scattering from HRP-I was measured both with pulsed excitation at 390 nm and 420 nm, and with CW excitation at 406.7 nm. Enzyme solutions were collected during the measurement and subsequently allowed to relax back to the native state overnight, whereupon they were pre-filtered (0.45 µm pore size, Gelman) and concentrated (the enzyme concentration is halved during the mixing experiment) in a Diaflow ultrafiltration cell (Amicon, PM 10) and used again. HRP-I samples prepared from the recycled solutions had a much longer lifetime owing to the removal of potential substrates present in the preparations.⁴⁹ Initial RR spectra of HRP-I were obtained using 0.65 - 0.85 ml/min flow rates which produced dead times of 3.1 - 2.4 s between mixing and laser excitation. As a spatial beam width of 1.5 mm incident on the 0.5 mm i.d. capillary was used, these flow rates insured that 3.6 - 4.7 scattering

volumes (one scattering volume is 0.2 µl) passed through the capillary between laser pulses. After preliminary characterization of the spectrum under these conditions, we determined that a 0.22 ml/min flow rate (corresponding to a 9.3 s dead time) produced identical results for the recycled preparations. At this slower flow rate, 1.2 scattering volumes passed between pulses, corresponding to the minimum necessary to insure that each pulse was incident on a fresh sample aliquot. This was used to increase accumulation time for the low frequency spectra which suffered from intense background scattering from the capillary walls. Under the conditions described above for our system we estimate that 1.0 mJ pulses at 390 nm provide ~35 photons absorbed/molecule, for those molecules from which Raman scattering is collected, regardless of flow rate. For the CW experiment at 406.7 nm, we estimate 22 and 69 photons/molecule absorbed by the sample at flow rates of 0.70 and 0.22 ml/min, respectively, for a 15 mW laser power, and 0.5 mm beam waist. Thus, for pulsed excitation, photon flux is independent of flow rate above a threshold which insures that each pulse is incident on a fresh sample aliquot. Photon flux then depends directly (and exclusively) on pulse energy if spatial beam width and capillary i.d. (which determine scattering volume) remain constant. On the other hand, for CW excitation, photon flux is inversely proportional to flow rate and directly proportional to laser power for a system in which the laser beam waist and capillary i.d. are equal (i.e. all photons are incident on the sample and all sample molecules are illuminated).

The formation of HRP-I was confirmed for each rapid mixing experiment by visual detection of the flowing green solution in the capillary prior to the onset of the RR measurement. After laser irradiation a sample aliquot was collected and checked by a uv-visible absorption measurement during each run. For the recycled samples these spectra were essentially that of HRP-I. For

the less stable fresh samples these spectra reflected a mixture of HRP-I and HRP-II, confirmed by monitoring the return to the native state. The total time from mixing to the absorption spectrum was typically ~ 3 minutes or longer. The formation of HRP-I prior to the RR measurement was further confirmed by an independent optical absorption experiment in which the rapid mixer with a section of rectangular tubing (0.3 mm path, Vitrodynamics) in place of the capillary was used.

HRP-II. HRP-II samples were prepared in the cooled cylindrical quartz cell which was spun during RR measurements. Addition of stochiometric amounts of p-cresol (Aldrich) and 1.5 x stochiometric quantities of hydrogen peroxide to solutions of native HRP at pH 7 resulted in formation HRP-II. RR spectra of these samples were collected with OMA detection for 2.5 min after which absorption spectra were monitored and the experiment was repeated with a fresh sample. HRP-II samples at pH 10.8 were prepared by adding 1.5 equivalents of peroxide to solutions of the native enzyme. RR spectra of these more stable solutions were collected for 10 min, and absorption spectra were monitored before and after laser irradiation.

Model compounds. Cl⁻Fe^{III}OEP was prepared from OEPH₂ (Porphyrin Products) by standard methods. 50 Cl⁻Fe^{III}OEP+ ClO₄- was prepared by A. Salehi by stirring Fe(ClO₄)₃ in a CH₂Cl₂ solution of Cl⁻Fe^{III}OEP. Sample integrity was monitored by optical absorption before and after RR measurements. CH₂Cl₂ was freshly distilled from CaH₂.

Instrumentation. Laser pulses (5 ns duration, 10 Hz) from 390-435 nm were provided by a DCR-1A based Quanta Ray System by using three laser dyes (Exciton): LD390 (in methanol), DPS (in dimethylformamide) and Stilbene 420 (in methanol). CW emission at 363.8 nm came from a Coherent Innova 90-5 Argon ion laser. Raman scattering from these sources was measured with a

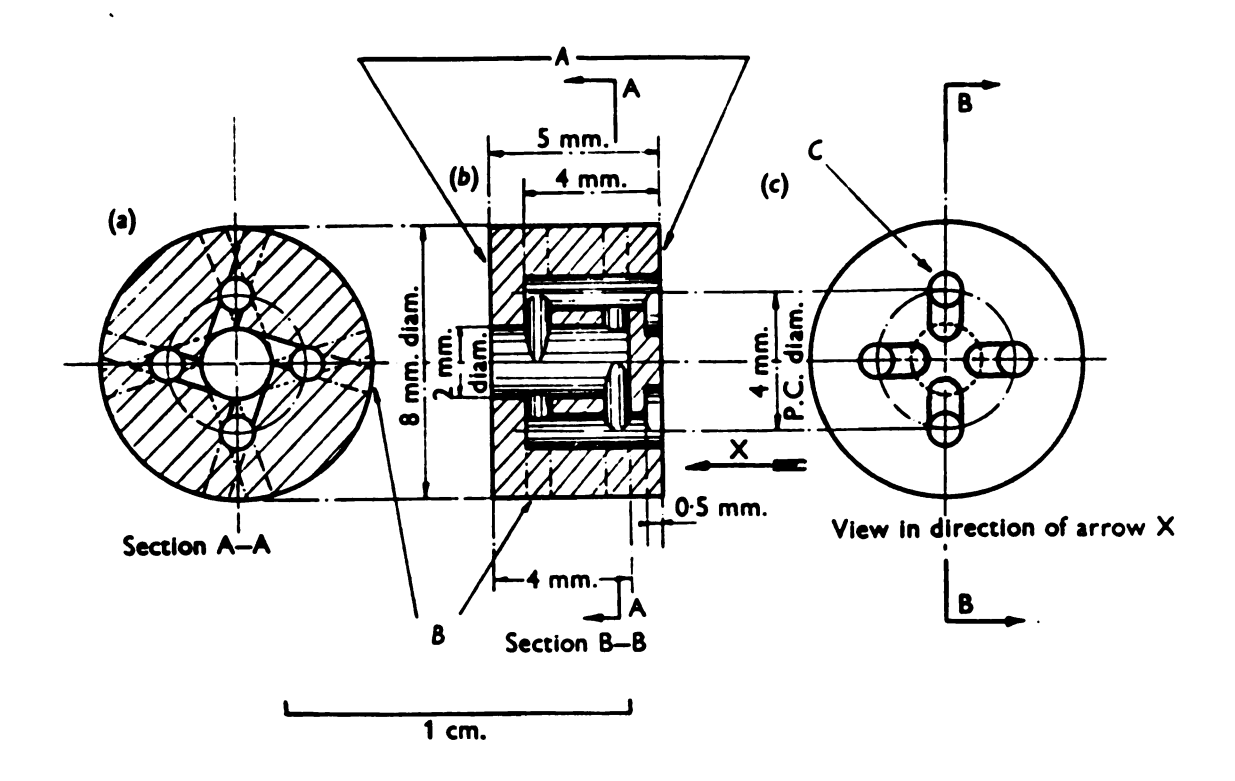
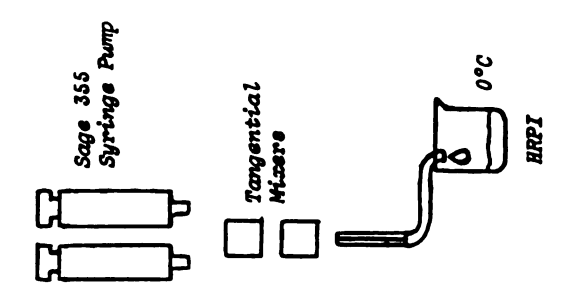
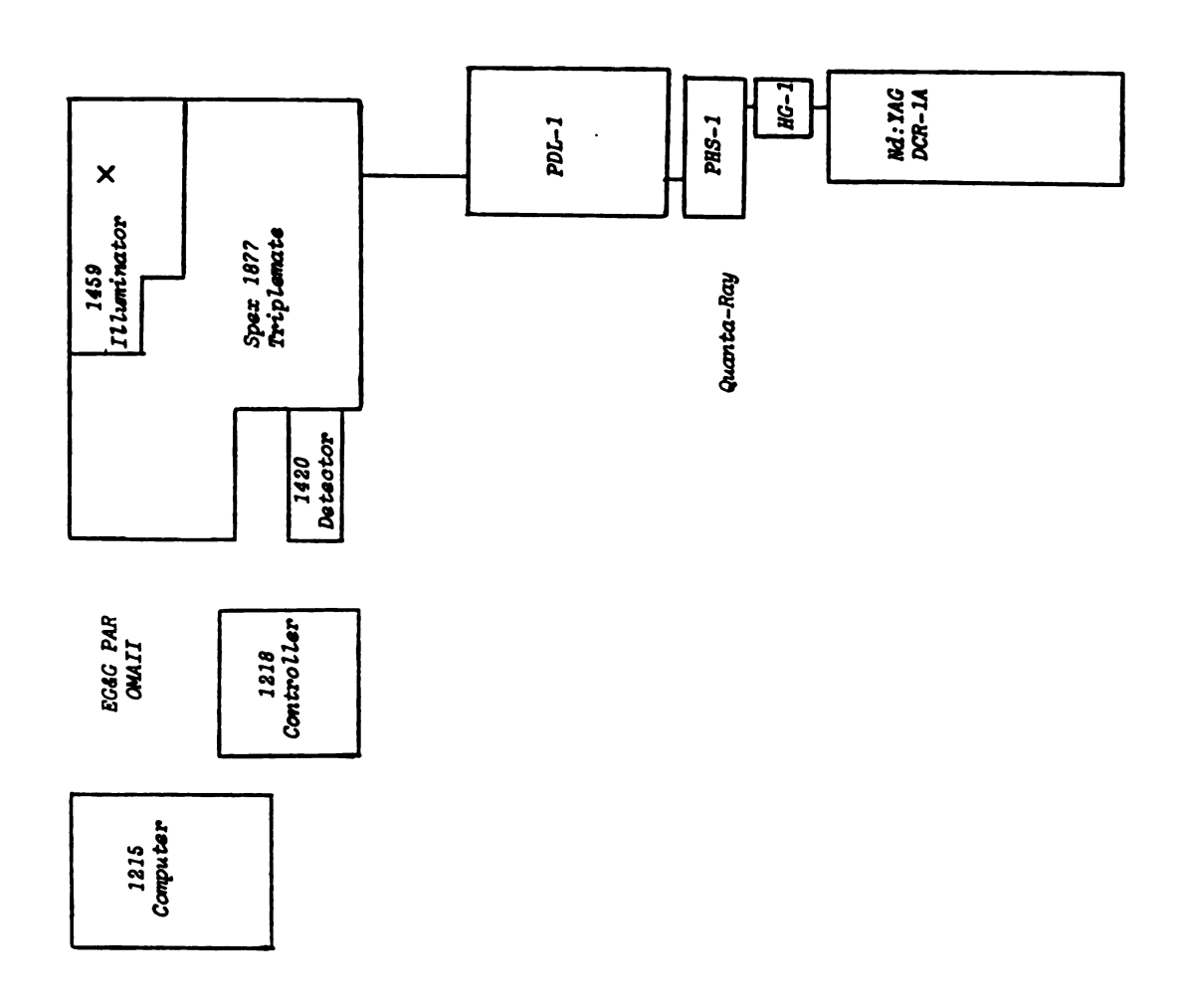


Figure 5-1. End view (a), longitudal section (b) and cross-section (c) of the eight-jet, tangential mixers. Ref. 48.

Figure 5-2.

Instrumental configuration used for pulsed resonance Raman measurements of flowing HRP-I samples prepared by rapid mixing. Laser irradiation at 390 nm (5 ns pulses, 1 mJ/pulse, 10 Hz) was provided by pumping Exciton LD390 laser dye in the Quanta Ray Pulsed Dye Laser (PDL-1) with the third harmonic (355 nm) from the Nd:Yag DCR-1A laser. Raman scattering from the sample (at position X) was collected with a Spex 1459 Illuminator, dispersed in a triple monochromator, and detected and analyzed by using the EG&G PAR 1420 diode array detector and associated OMA II electronics. RR scattering excited at 390-435 nm from HRP-II samples in a cooled (2-5 C) cylindrical quartz spinning cell was also measured using this instrumentation. The 10 Hz rep rate was employed on all occasions.





commercial Spex/EG&G PAR diode array spectrometer described earlier.³⁰ Instrumentation used to measure Raman scattering from the 406.7 nm Krypton ion laser (spectra Physics) emission included a Spex 1401 double-monochromator and is described elsewhere.³⁶ Uv-visible absorption spectra were measured with a Perkin Elmer Lambda 5. Figure 5-1 and 5-2 diagram the experimental apparatus.

RESULTS

High frequency RR scattering from HRP intermediates. Figure 5-3 shows RR spectra obtained with 390 nm excitation of horseradish peroxidase at pH 7. The spectrum of the native enzyme, Figure 5-3a, is typical of a five-coordinate, ferric protoheme complex with a high spin (S=5/2) ion. The high frequency vibrations from 1450 to 1700 cm⁻¹ are inversely proportional to the center-to-pyrrole nitrogen distance, or core size of the porphyrin macrocycle.^{51,52} Thus, these modes are sensitive to the spin state of the central iron as controlled by the ligands normal to the heme plane. The bands in Figure 5-3a at 1498, 1548 and 1573 cm⁻¹ are assigned to the normal modes v_3 , v_{11} and v_2 , respectively, as described by Abe et al.⁵³ The shoulder at 1548 cm⁻¹ possibly contains contributions from v_{38} as well.⁵⁴ The band at 1630 cm⁻¹ may also correspond to a superposition of two vibrations: one is a stretching mode of the peripheral vinyl, ν (C=C), and the other is the ν_{10} mode of the porphyrin macrocycle.^{21,55} The intense band at 1373 cm⁻¹ of the native enzyme is assigned to v_4 , the oxidation state marker. Its frequency is inversely related to the occupancy of the porphyrin $e_g(\pi^*)$ orbitals. Although these are the lowest unoccupied molecular orbitals (LUMO) of the porphyrin, they may be populated by overlap with the iron d_{XZ} and d_{VZ} orbitals. This is reflected by lowered vibrational frequencies of modes with C_8N stretching character such as $v_4.56$

Figure 5-3. High frequency RR spectra of HRP samples at 2-10 C, 1 mJ/pulse. Sample conditions and total accumulation times: (a) spinning cell, 20 min; (b) flowing in the capillary of the rapid mixer at 0.65-0.85 ml/min, 40 min; (c) spinning cell, 22 min.

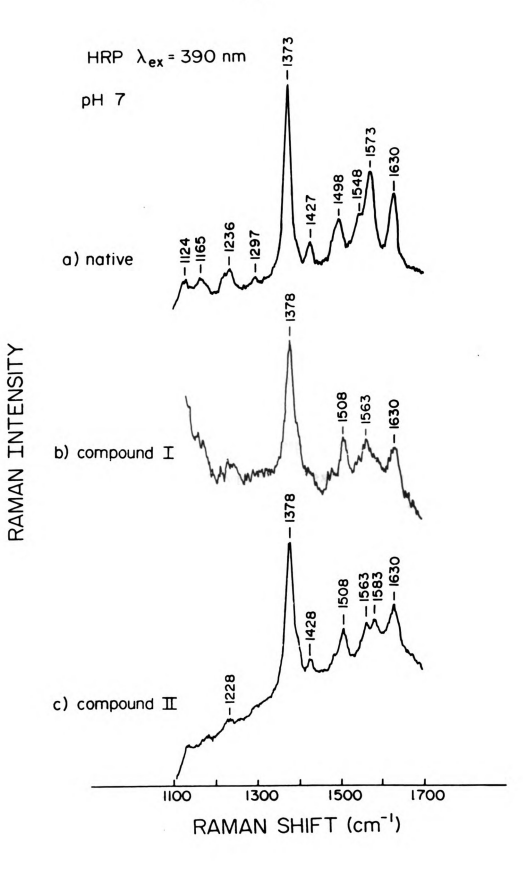


Figure 5-3b and c show the RR spectra of HRP-I and HRP-II, respectively. The similarity of the 390 nm RR spectra of these two intermediates is surprising considering the significant differences displayed in the vibrational frequencies and RR intensities of metalloporphyrin π cation radical (MP⁺) and their neutral metalloporphyrin (MP) parent compounds. 35,36,57 This strong similarity was obscured in our previous analysis of the high frequency RR spectrum of HRP-I³⁰ because we compared it to RR spectra of HRP-II produced with excitation at 514.5 or 457.9 nm from early work. 58,59 Our spectra of HRP-II with excitation from 390-435 nm match the more recent work with 406.7 nm excitation of Terner and coworkers²² as well as Kitagawa and coworkers, ¹⁷ both in vibrational frequencies and relative intensities. Accordingly, a reanalysis of our high frequency RR spectrum of HRP-I is in order. From the RR spectra in Figure 5-3b and c we assign the bands at 1378, 1508, 1563 and 1630 cm⁻¹ to v_4 , v_3 , v_{11} overlapped with v_{38} and v(C=C), respectively, for both HRP-I and HRP-II. (The resonance enhancement of v_{10} at this excitation wavelength is negligible, see below.) Thus, the spectra differ only in the relative intensity of the v2 mode, which appears at 1583 cm⁻¹ in the spectrum of HRP-II (Fig. 5-3c) and is all but absent in the spectrum of HRP-I (Fig. 5-3b).

Model compounds. Figure 5-4 depicts the changes in vibrational frequencies and relative RR intensitites between a ferric octaethylporphyrin π cation radical, Cl⁻Fe^{III}OEP⁺·ClO₄⁻ and its parent compound, Cl⁻Fe^{III}OEP. Studies of analogous tetraphenylporphyrin⁶⁰ complexes suggest that both of these compounds exhibit a five-coordinate, high-spin (S=5/2) configuration for the heme iron and are similar in all aspects except the oxidation state of the macrocycle. In the spectrum of the cation radical (Fig. 5-4a) we recognize the ν_4 , ν_{29} , ν_3 , ν_{11} , ν_2 and ν_{10} modes at 1368, 1388, 1491, 1584, 1600 and 1625 cm⁻¹, respectively. Although the high frequency envelope from 1560-1660 cm⁻¹ is poorly resolved

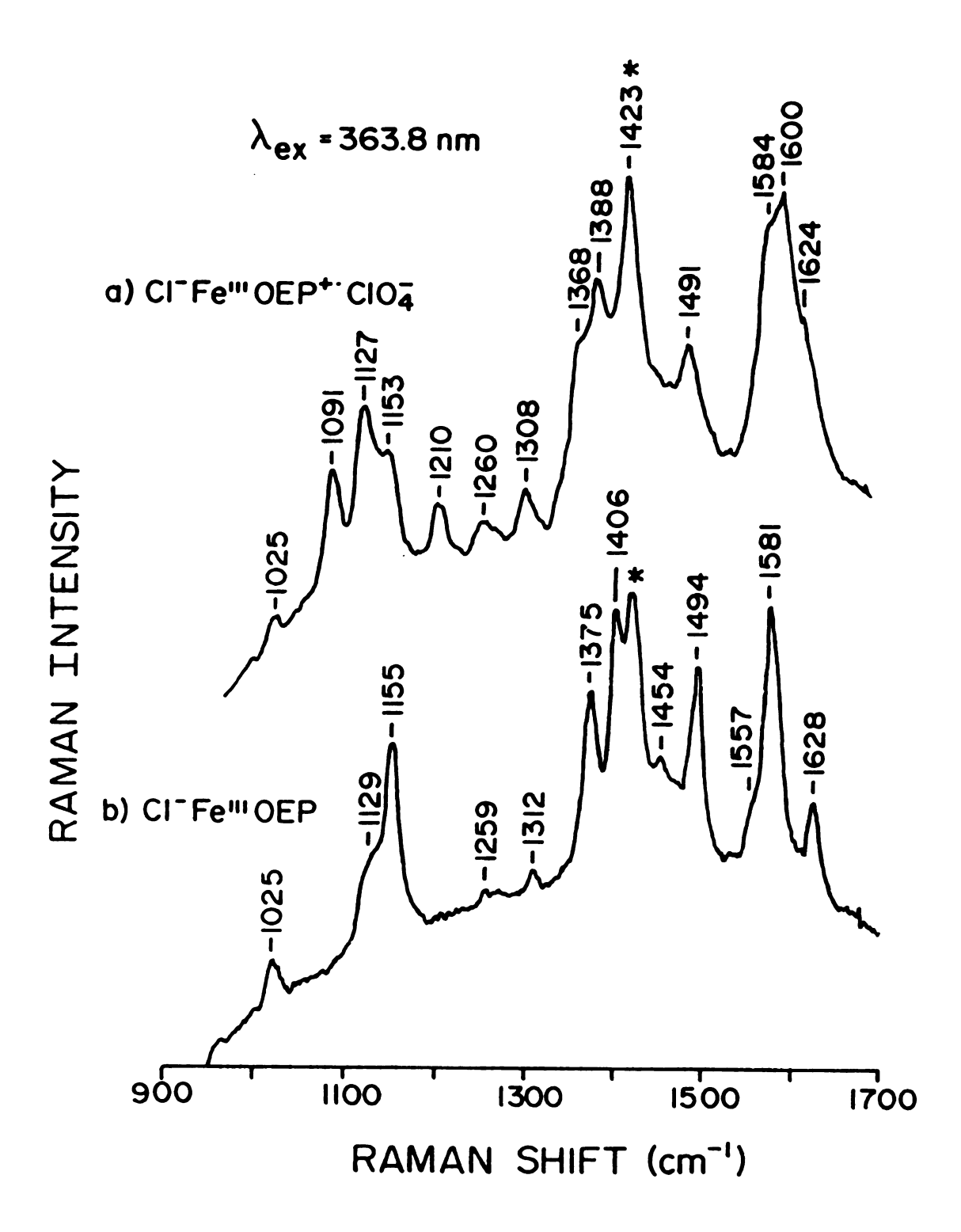


Figure 5-4. RR spectra of model compounds in CH_2Cl_2 . Conditions: 40-50 mW incident on sample in spinning cell at 25 C. Accumulation times: (a) 5.3 min; (b) 10 min.

in Figure 5-4a, three bands with distinct depolarization ratios are evident from polarized scattering (not shown). These vibrational assingments are made by analogy to our previous study of Co, Cu and ZnOEP⁺⁺ complexes.³⁶ The normal mode assignments in the 1450-1700 cm⁻¹ range from that work are based on core size frequency dependencies and depolarization ratios of the Raman bands of these MOEP⁺⁺ species. The assignments of v_4 and v_{29} , however, to the features at 1368 and 1388 cm⁻¹ in Figure 5-4a are tentative because these modes were not included in the previous structural analysis of MOEP spectra.³⁶

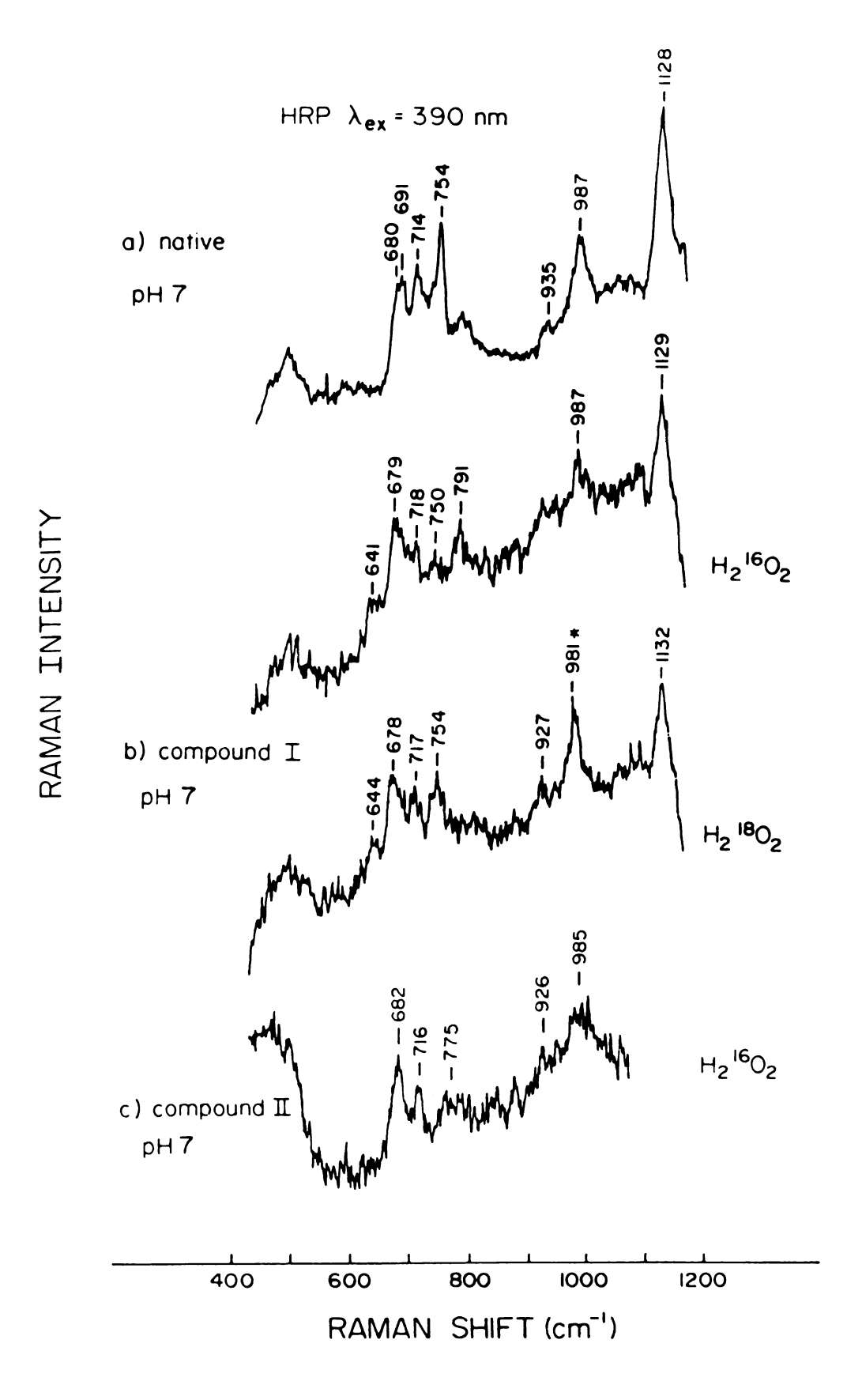
Frequency shifts. The vibrational modes above 1350 cm⁻¹ of the neutral species, Cl-Fe^{III}OEP are straight-forward: v4, v29, v3, v11, v2 and v10 occur at 1375, 1406, 1494, 1557, 1581 and 1629 cm $^{-1}$, respectively (Fig. 5-4b). The RR enhancement of v_{38} observed for protoheme complexes does not occur here owing to the higher symmetry the OEP macrocycle, and of course there are no vinyl substituent vibrations. The changes in the vibrational frequencies which accompany ring oxidation of these ferric compounds agree qualitatively with those observed with other MOEP+ species, 36 but are smaller in magnitude for v_4 , v_3 , and v_{10} . We find that stretching modes with predominantly C_8N character ($\nu_{\,4})$ or $\,C_{a}C_{\,m}\,$ character ($\nu_{\,3}$ and $\,\nu_{\,10})$ decrease in frequency, while those with C_bC_b character (v_{11} and v_2) increase in frequency when the porphyrin ring is oxidized. We see these frequency shifts regardless of whether the electron is abstracted from the $a_{1u}(\pi)$ or $a_{2u}(\pi)$ molecular orbital. Thus, the observed changes in vibrational frequencies are not completely consistent with predictions made based on either the spin density profiles of metalloporphyrin π cation radicals $(MP^{+*})^{28,30,61}$ or the nodal structure of $a_{1u}(\pi)$ and $a_{2u}(\pi)$ orbitals. 56,62,63 These two approaches (which yield predictions inconsistent with one another) fail possibly because they consider only changes in the π bonding of the macrocycle upon oxidation and ignore

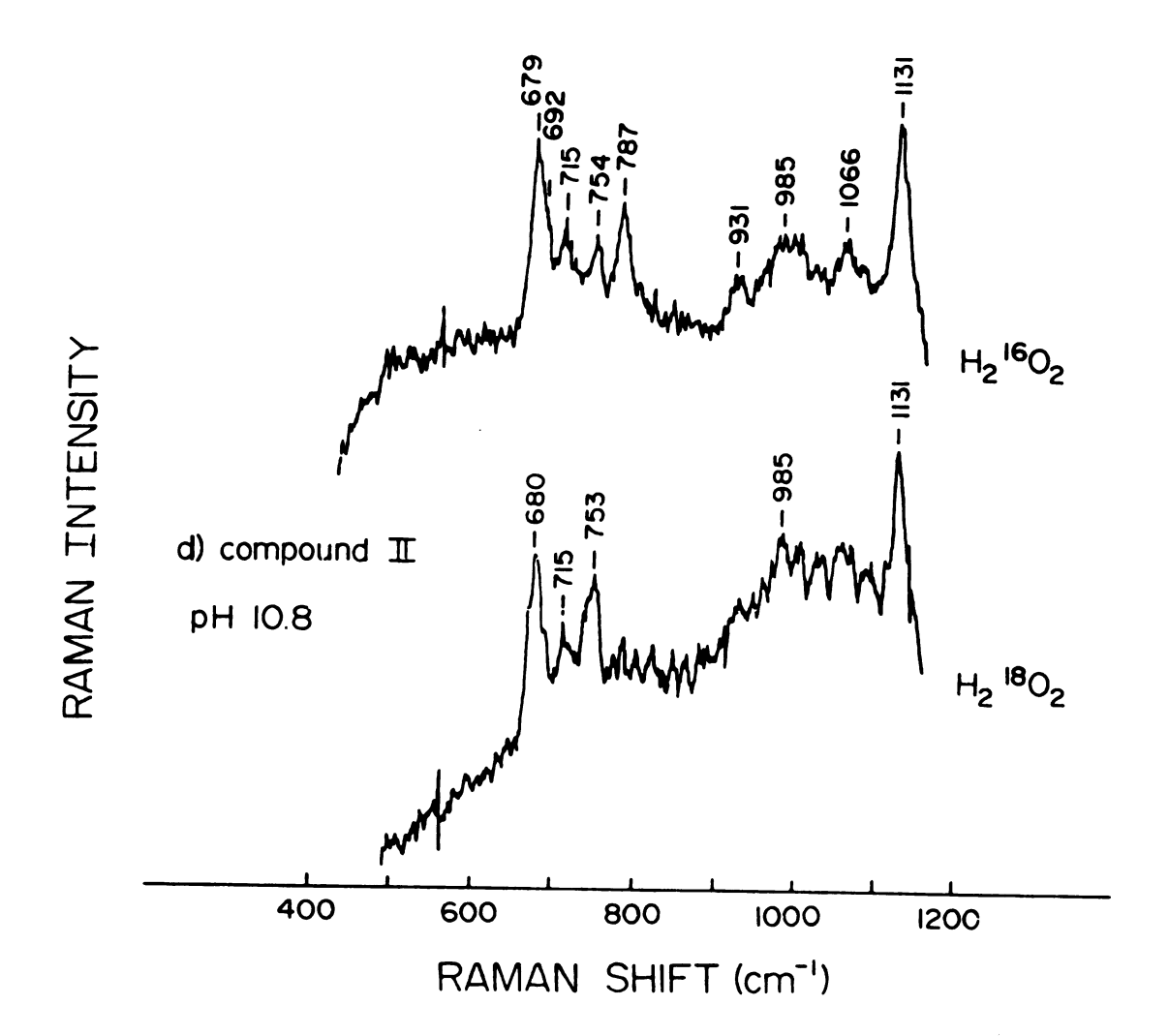
possible changes in the σ framework.⁶⁴ Consideration of both σ and π effects to the force constants may better explain the changes in vibrational frequencies of the porphyrin core upon oxidation.

Low frequency RR scattering from HRP intermediates. Figure 5-5 shows low frequency RR scattering from pulsed, 390 nm excitation of HRP, HRP-I and HRP-II. The spectrum of the native enzyme, Figure 5-5a, is similar to that measured with 406.7 nm excitation reported earlier; 16 however, there are some differences in relative intensities produced by the different excitation frequencies. Spectra of HRP-I at pH 7 prepared with both $\rm H_2^{16}O_2$ and $\rm H_2^{18}O_2$ appear in Figure 5-5b. The feature at 791 cm⁻¹ in the spectrum of the $\rm ^{16}O$ sample is replaced by a band at 754 cm⁻¹ in the $\rm ^{18}O$ sample. This is clearly a mode involving an oxygen atom incorporated from the peroxide. A 35 cm⁻¹ decrease is expected for a Fe-O harmonic oscillator upon substitution of $\rm ^{18}O$ for $\rm ^{16}O$. Thus, this band is assigned to $\rm ^{16}O$, the symmetric stretch of the oxoferryl of HRP-I.

Figure 5-5c and d show spectra of HRP-II at pH 7 and 10.8, respectively. As shown by recent work, 16,25 at pH 7 the oxoferryl stretch of HRP-II appears as a weak feature at 774-779 cm⁻¹ in RR spectra produced with 406.7 nm excitation. This band shifts to 740-743 cm⁻¹ upon substitution of 18 O for 16 O. Our RR spectrum obtained at $\lambda_{\rm ex}$ = 390 nm of the second intermediate at pH 7 is consistent with these findings. At our signal/noise level, the ν (FeO) band is not clearly visible in Figure 5-5c, although its contribution appears at approximately 775 cm⁻¹. On the other hand, for HRP-II at pH 10.8, RR excitation at 390 nm results in strong enchancement of ν (FeO) as shown in Figure 5-5d. Our results at pH 10.8 match those of Hashimoto et al. 17 and Sitter et al. 25 We find the ν (FeO) at 787 cm⁻¹ for HRP-II at high pH, shifting to 753 cm⁻¹ upon 18 O substitution. Thus, the ν (FeO) measured for HRP-I at pH 7 appears

Figure 5-5. Low frequency RR spectra of HRP samples obtained under 390 nm excitation. Total accumulation times: (a) 85 min; (b) 16 O sample: 144 min, 18 O sample: 78 min; (c) 52 min; (d) 16 O sample: 48 min, 18 O sample: 48 min. The feature at 981 cm $^{-1}$ in (b) is due to sulfate ion in the $\mathrm{H_2^{18}O_2}$ preparation.



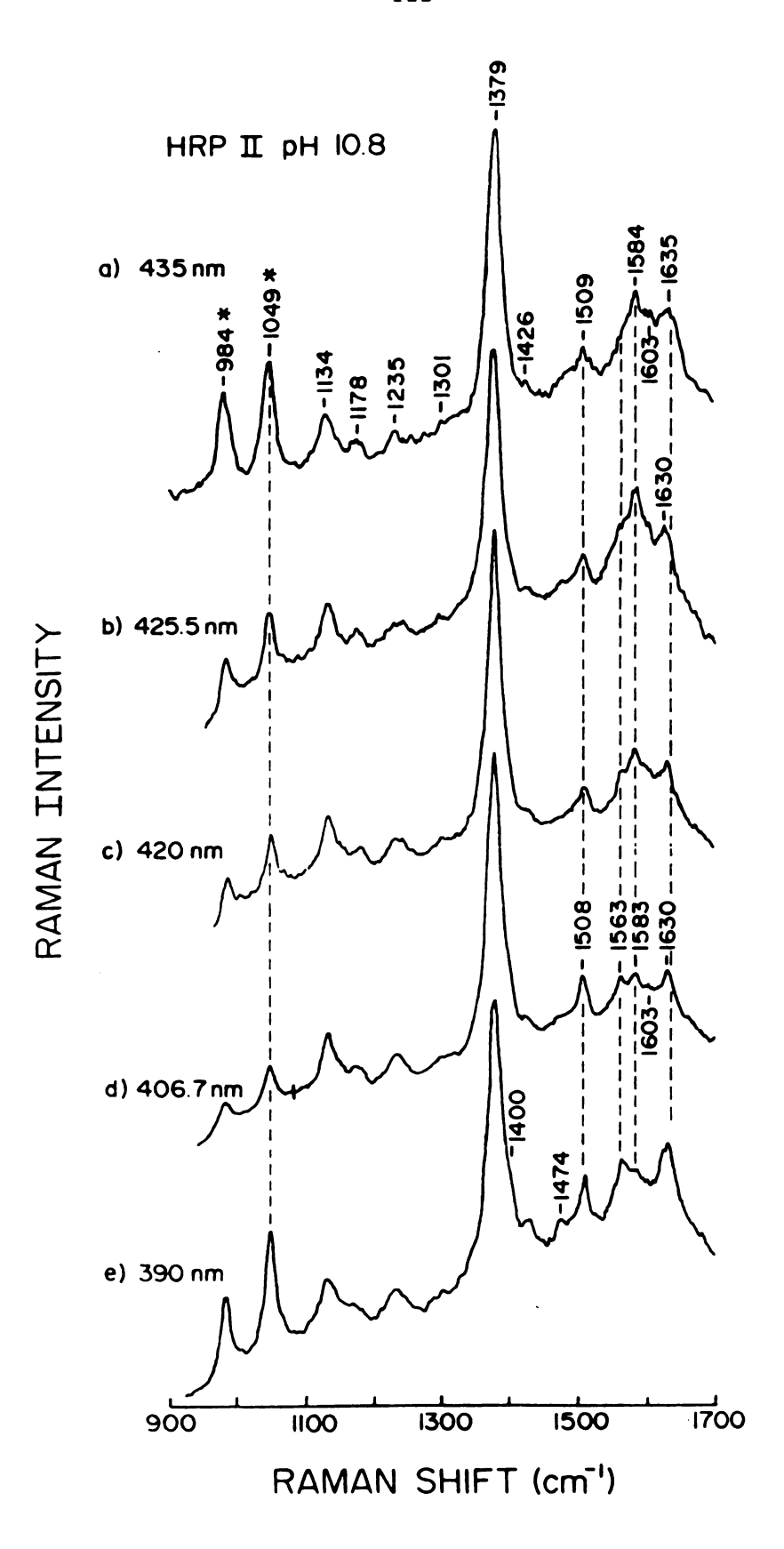


to be almost identical to that of HRP-II at pH 10.8. By analogy to the work of Sitter et al.²⁵ and Hashimoto et al.²⁶ this suggests that the oxo ligand of HRP-I is not H-bonded at pH 7 as is the case for HRP-II. Experiments to confirm this are in progress.

Aside from the similarity of the v(FeO) of HRP-I at pH 7 to HRP-II at pH 10.8, other low frequency features require comment. The spectra of both of these species (Fig. 5-5b and d) exhibit slight frequency decreases in v_7 (\sim 679 cm⁻¹) compared to HRP-II at pH 7 (682 cm⁻¹, Fig. 5-5c). This is consistent with observations by Sitter et al.²⁵ concerning the pH dependence of the RR spectrum of HRP-II. The feature at 641-644 cm⁻¹ in the spectra of HRP-I (Fig. 5-5b), however, does not appear in the high pH HRP-II spectra (Fig. 5-5d). We offer no assignment for this mode at present but we note that an out-of-plane asymmetric vinyl wag is expected in this region.65 Although Terner et al.16 assigned this mode to the poorly resolved band at $\sim 691~\text{cm}^{-1}$ labelled in Figure 5-5a and c, the 641-644 cm⁻¹ value is closer to the expected frequency (630 cm⁻¹). The assignment by Terner and co-workers represents the first possible observation of this mode in a heme complex. Its activation could be caused by the co-planar configuration of the pyrrole I vinyl group with the heme in HRP, which may serve to stabilize the porphyrin cation radical of HRP-I.66 There has been no vinyl-protein interaction unique to HRP-I proposed. Should the 641-644 cm⁻¹ feature arise from the vinyl groups, its unique activation in HRP-I might be an indication of such or else it could be due to electronic factors.

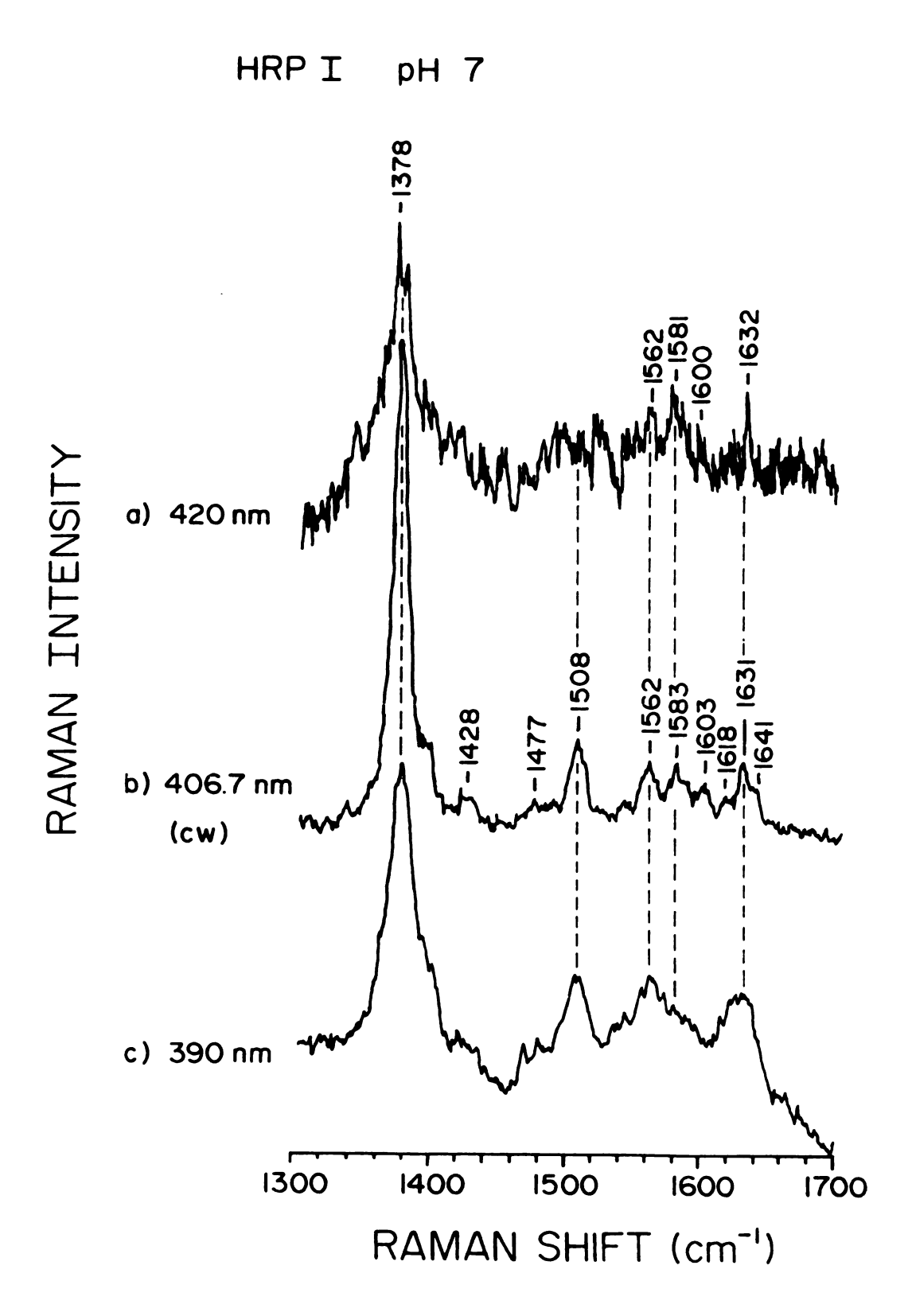
Excitation profiles. The similarity between our RR results for HRP-I at pH 7 and HRP-II at pH 10.8 prompted us to examine the spectrum of both the second intermediate at high pH and the first intermediate at neutral pH as a function of excitation frequency. Figure 5-6 shows the spectrum of HRP-II

Figure 5-6. High frequency RR scattering from HRP-II, pH 10.8. Accumulation time for each spectrum was 10 min using 1 mJ/pulse. Excitation wavelengths were as indicated. The 1049 cm $^{-1}$ peak is from 0.2 M NO $_3$ $^{-}$ used as an internal standard to measure relative intensities. The 984 cm $^{-1}$ feature is from SO $_4$ $^{-}$.



at pH 10.8 at five excitation frequencies between 435 and 390 nm. Because the differences in the high frequency spectra of HRP-I and HRP-II both at pH 7 (Fig. 5-3b and c, respectively) is limited to the relative intensities of the features at 1563 and 1584 cm⁻¹, the behavior of these bands is of principal interest. With 435 nm excitation (Fig. 5-6e) high frequency bands appear at 1509 (v_3), 1584 (v_2), 1603 (v_{37}) and 1635 cm⁻¹ (v_{10}). Figure 5-6b shows that the v_{10} intensity falls off quickly as λ_{ex} moves to the blue and that with 425.5 nm excitation the v(C=C) mode at 1630 cm⁻¹ begins to dominate this region. Also, at this λ_{ex} , a shoulder is apparent at 1563 cm⁻¹. In Figure 5-6c-e this feature becomes more obvious as RR excitation is varied toward higher energy, while the intensity of v_2 (1584 cm⁻¹) decreases. Finally, with 390 nm excitation (Fig. 5-6a), the feature at 1563 cm⁻¹ dominates this region of the spectrum and the 1584 cm⁻¹ mode now appears as a shoulder. Figure 5-7 shows the RR scattering from our flowing HRP-I sample at pH 7 at three excitation frequencies in the Soret region. Although the spectrum excited at 420 nm (Figure 5-7a) is very weak owing to the short accumulation time, the dominant features can be recognized at 1378, 1562, 1581, and 1632 cm⁻¹ and can be assigned to v_4 , v_{11} + v_{38} , v_2 and v (C=C), respectively. The intensity of v_2 (1581 cm⁻¹) is greater relative to the intensity of the band at 1562 cm⁻¹ at this excitation wavelength. The spectrum in Figure 5-7b was obtained under CW excitation at 406.7 nm. Vibrational bands are apparent at 1378 cm⁻¹ (v_4), 1399 cm⁻¹ (v_{29}), 1428 cm⁻¹ (δ_s (=CH₂)), 1477 cm⁻¹ (v_{28}), 1508 cm⁻¹ (v_{3}), 1562 cm⁻¹ ($v_{11} + v_{38}$), 1583 cm⁻¹ (v_{2}), 1603 cm⁻¹ (v_{37}), 1618, 1631 cm⁻¹ (v (C=C)), and 1641 cm⁻¹ (v_{10}). The intensities of the features at 1583 and 1562 cm⁻¹ are roughly equal in Figure 5-7b. Finally, Figure 5-7c juxtaposes the scattering excited at 390 nm with the other HRP-I spectra. Comparison of Figure 5-6c-e with Figure 5-7a-c suggests that the RR excitation profiles Figure 5-7. High frequency RR scattering from HRP-I, pH 7.

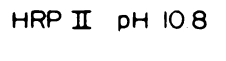
(a) 1.9 mJ/pulse, 4 min; (b) 15 mW, 0.5 s/cm⁻¹; sample flow rate, 0.22 ml/min; similar results were obtained flowing at 0.7 ml/min; (c) 1 mJ/pulse, 40 min.

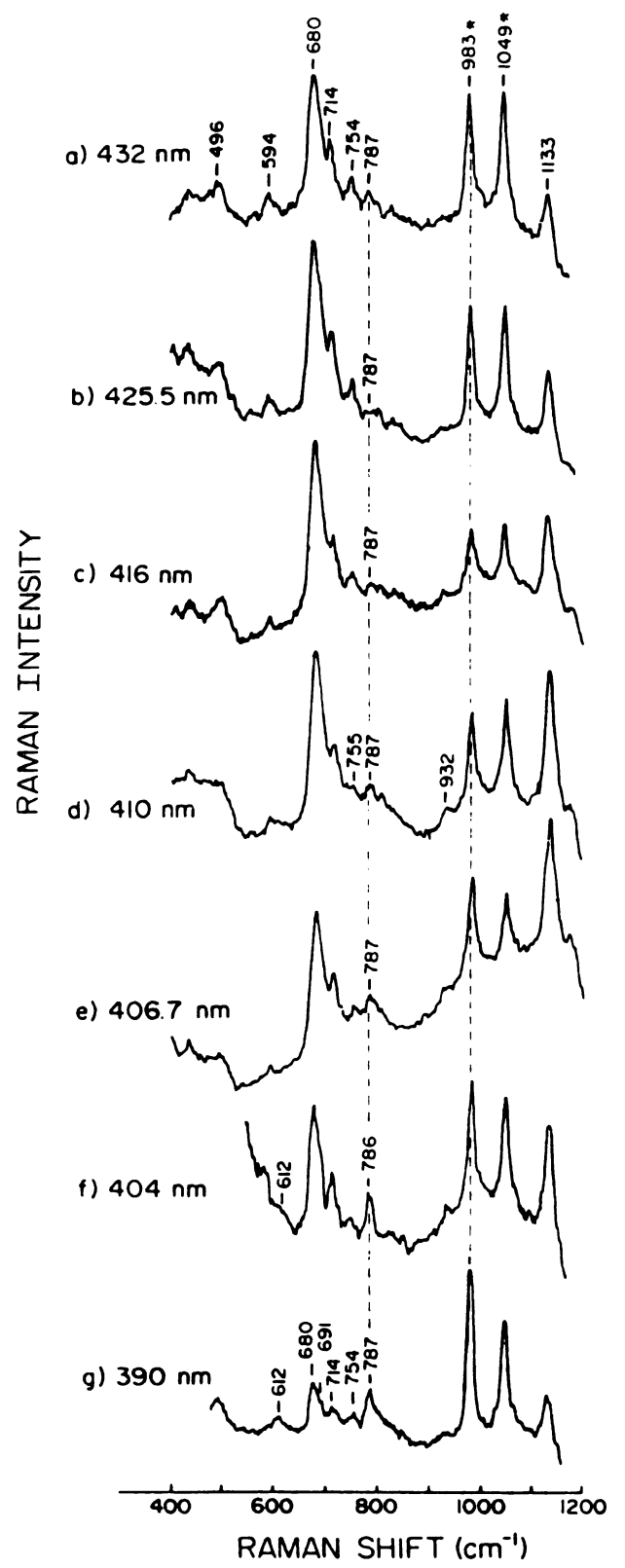


of the vibrational modes of the scattering species in the HRP-II pH 10.8 and HRP-I pH 7 samples are similar. In both cases the v_2 mode at ~ 1583 cm⁻¹ dominates the region from 1550-1600 cm⁻¹ with 420 nm excitation, while a feature at ~ 1563 cm⁻¹ dominates under 390 nm excitation. The intensities of these features are roughly equal with $\lambda_{\rm ex} = 406.7$ nm. The similarity of these excitation profiles suggests that the heme complexes of HRP-II (at pH 10.8) and HRP-I (at pH 7) have similar electronic states.

The large relative intensity of the oxoferryl stretch in the RR spectra excited at 406.7 nm of HRP-II, oxoferryl myglobin²³ and model compounds¹⁸ has been noted to suggest the presence of a charge transfer (CT) electronic transition along the oxoferryl axis. 16,19 Figure 5-8 shows RR spectra of HRP-II (pH 10.8) obtained with seven excitation wavelengths from 432-390 nm. The v (FeO) is obvious only in spectra produced with excitation to the blue of 410 nm, significantly higher energy than the Soret absorption maximum at 419 nm. A crude excitation profile (EP) of the v (FeO) = 787 cm⁻¹ vibration is shown in Figure 5-9. Along with this, the excitation profiles (a plot of relative Raman intensity vs. excitation frequency, λ_{ex}) of the porphyrin core vibrations v_7 = 680 cm⁻¹ and v_4 = 1379 cm⁻¹ are also displayed. The latter two agree well with the excitation profiles for the v₇ and v₄ modes of deoxy myoglobin observed by Bangcharoenpaurpong et al.67 On the other hand, the Fe^{II}-N(histidine) stretching frequency, v (FeNIm), of deoxy myoglobin displays a different excitation profile than the v(FeO) of HRP-II. While the EP of the former vibration of deoxy myoglobin matches the Soret absorption and was judged inconsistent with CT enhancement, 67 the EP of the v(FeO) vibration displayed in Figure 5-9 appears to have a maximum around 400 nm, well to the blue of the Soret absorption maximum. This is consistent with but not proof of the occurrence of a CT transition on the high energy side of the Soret (0-0) transition of HRP-II.

Figure 5-8. Low frequency RR scattering from HRP-II, pH 10.8. Accumulation time was 10 min for (a)-(d), 20 min for (e)-(f), using 1 mJ pulses. The 983 cm⁻¹ peak is from 0.2 M SO₄⁻ used as an internal intensity standard. The 1049 cm⁻¹ feature is from NO₃⁻.





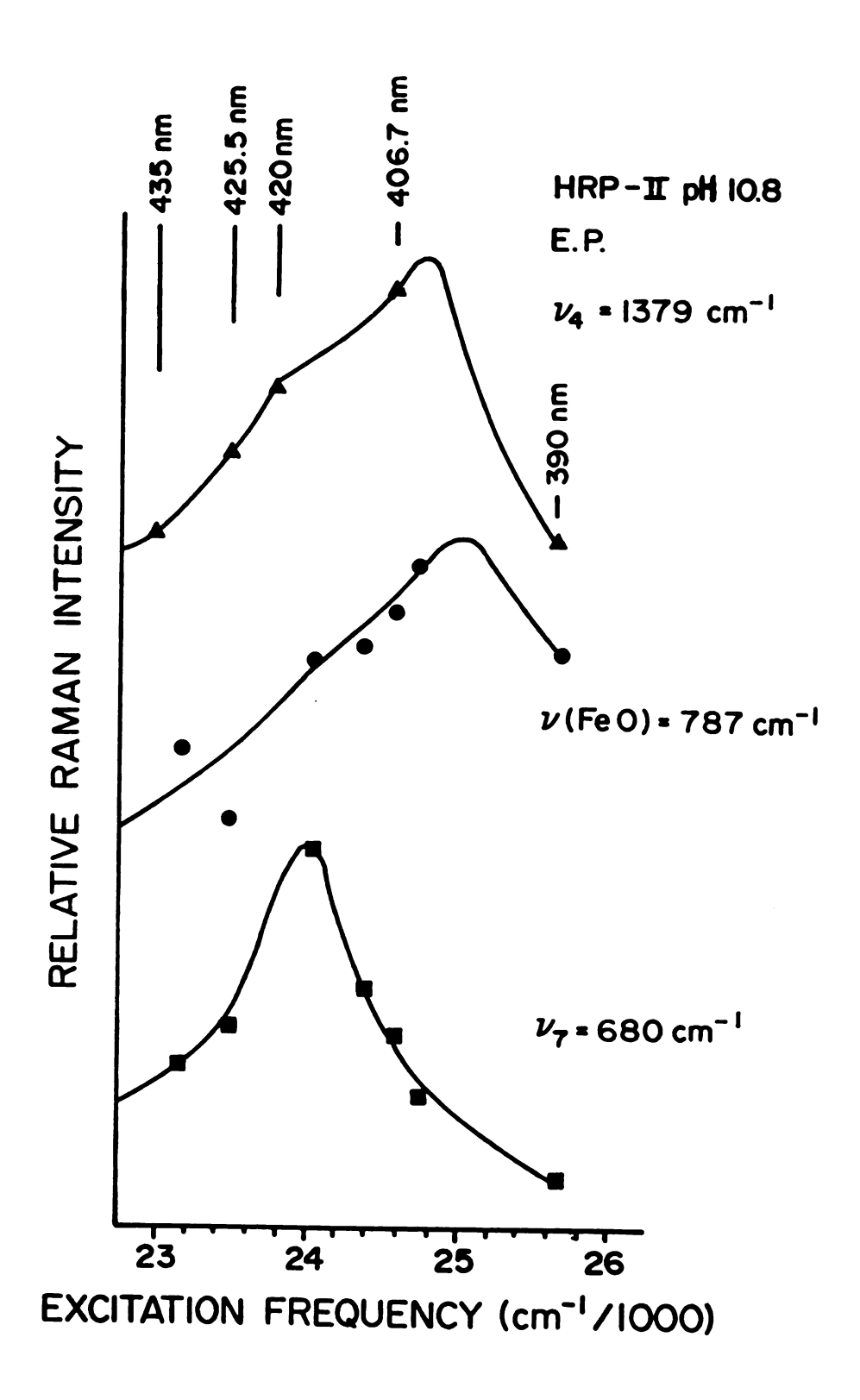


Figure 5-9. Excitation profiles of $v_7 = 680 \text{ cm}^{-1}$, $v(\text{FeO}) = 787 \text{ cm}^{-1}$ and $v_4 = 1379 \text{ cm}^{-1}$.

DISCUSSION

Prediction of HRP-I vibrations from structural correlations. The similarity between the high frequency RR spectra of HRP-I and HRP-II in Figure 5-3b and c is unexpected. The vibrational frequencies between 1450 and 1700 cm⁻¹ are a sensitive probe of the structure of both the neutral metalloporphyrin⁵² and the metalloporphyrin π cation radical. Studies of model compounds suggest that oxidation of the macrocycle does not significantly influence porphyrin core geometry, particularly if the oxidation state and axial ligation of the metal center remain unchanged. 36,68 This is in agreement with EXAFS measurements of HRP-I and HRP-II by Penner-Hahn et al. 15 Thus, we expect the porphyrin core sizes of HRP-I and HRP-II to be similar. Despite the structural similarities between MP and MP+ the electronic states of the cation are clearly distinct netural form and our metallooctaethylporphyrin π cation radicals (MOEP++ where M = Zn, Cu, Co, and Ni) demonstrate that vibrational frequencies and relative intensities in the RR spectra of the MOEP+ species are substantially changed from those of the parent MOEP compounds. 36 Thus we expect significant differences in the RR spectra of HRP-I vs. HRP-II, analogous to those we observed in the MOEP+ vs. MOEP spectra. Based on our recently presented36 structural correlations and assuming a core size of 1.99 Å, we expect v_3 , v_{11} and v_2 to occur at approximately 1501, 1590 and 1606 cm⁻¹, respectively, for HRP-I. Here we have assumed that the frequencies of the $v(C_bC_b)$ modes, v_{11} and v₂, are 10 cm⁻¹ less for PP⁺⁺ compared to OEP⁺⁺ compounds as they are in the ring-neutral complexes.⁶⁹ Thus, the v_3 value of 1508 cm⁻¹ for HRP-I (Fig. 5-3b), unchanged from that of HRP-II (Fig. 5-3c), and the absence of features in the 1590 to 1610 cm⁻¹ range, suggest that the species producing the spectrum in Figure 5-3b is not a porphyrin π cation radical. Since the evidence for a porphyrin radical in HRP-I, particularly from ENDOR results,⁴² is strong, we consider here possible explanations for the RR result.

HRP-II. The trivial explanation is that our HRP-I spectrum is produced by bona-fide HRP-II contaminants in the sample, produced either by photo-reduction or reduction by impurities acting as substrates. However, although similar, the RR spectra of HRP-I and HRP-II at pH 7 are clearly distinct, most notably in terms of the behavior of the oxoferryl stretching mode (Fig. 5-5). Furthermore, optical absorption spectra following each RR measurement of HRP-I solutions (particularly for the recycled samples) were like that of HRP-I. Thus, reduction to HRP-II (which would be irreversible) is not the cause of the similar RR spectra of the two intermediates (Fig. 5-3b and c).

Photochemistry. Both frozen and solution samples of HRP-I are known to undergo photoreaction when exposed to light in the Soret band region.²⁷ The photoproduct, called Y, has an absorption spectrum like that of HRP-II (i.e. characteristic of an oxoferryl, ring-neutral heme), and gives an EPR signal of a free radical located on a protein residue.⁷⁰ Although a different interpretation has been offered,⁷¹ photo-induced electron transfer from a nearby amino acid to the porphyrin cation radical could leave a structure analogous to cytochrome c peroxidase compound I.^{4-6a} This species would have an oxoferryl, ring-neutral heme with a protein free radical and would account to the EPR and absorption spectrum of the photoproduct.⁷¹ If this were the case, the RR spectrum of Y should resemble that of HRP-II. Thus, our spectrum (Fig. 5-3b) might represent scattering from Y despite the measures taken to prevent the photoreaction. Under our typical experimental conditions (1 mJ/laser pulse) we estimate a maximum of 35 photons/molecule was absorbed by the scattering sample. With a quantum yield of 0.003,⁷¹ this would correspond

to less than 11% photoconversion possible per 5 nanosecond laser pulse. Thus, a maximum of 11% impurity could be reflected in the RR spectrum only if Y is formed in less than 5 ns. We estimate that a 17% impurity with an extinction coefficient at 420 nm of $100 \text{ mM}^{-1}\text{cm}^{-1}$ would be required to produce scattering ($\lambda_{\text{ex}} = 390 \text{ nm}$) at intensitites comparable to that of the green cation radical, HRP-I, with an extinction coefficient at 400 nm of $50 \text{ mM}^{-1}\text{cm}^{-1}$. Thus, an 11% photoconversion could feasibly cause artifacts in the HRP-I RR spectrum. The close similarity of the RR excitation profiles of HRP-I at pH 7 and HRP-II at pH 10.8 are consistent with possible photoconversion as they suggest scattering species with similar electronic absorption spectra. On the other hand, similar experiments with CW excitation at 406.7 nm at a wide range of flow rates (from 0.2-20 ml/min) carried out both in our lab (Fig. 5-7b) and elsewhere, 34 as well as pulsed measurements at laser energies ranging from 0.5-2.0 mJ/pulse, all produced similar results. These facts argue against not only artifacts due to photoconversion to Y but also possible scattering from excited states of HRP-I.

Spin delocalization. Using an approach similar to ours, but with CW excitation at 406.7 nm and high flow rates (5-20 ml/min.) Ogura and Kitagawa³⁴ recently obtained a high frequency RR spectrum of HRP-I, although with a very low signal-to-noise ratio. Their result is similar to our high frequency spectrum³⁰ (see also Fig. 5-3b) and is also atypical of a MP+*. As these authors point out, extensive spin delocalization of the porphyrin radical onto the axial oxoferryl-imidazole system might account for the absence of vibrations characteristic of the oxidized porphyrin in the RR spectrum of HRP-I. Delocalization of the porphyrin cation radical spin onto an axial pyridine ligand has been described for PyZnTPP+* (TPP = tetraphenylporphyrin).⁷² Perhaps more significant, the spin systems of the oxoferryl (S=1) and porphyrin cation radical (S=1/2) may interact strongly in compound I structures.^{73,74} While

these factors may well influence vibrational frequency shifts between oxidized and neutral porphyrin complexes, this may not be sufficient to explain the essentially identical RR spectra of HRP-II (pH 10.8) and HRP-I (pH 7) presented in Figures 5-6c-e and 5-7, respectively.

ENDOR measurements clearly show that the unparied electron in the radical site of HRP-I is hyperfine coupled to both ^1H and ^{14}N nuclei. 42 These could come from either the methine and b-carbon substituents and the pyrrole nitrogen of the porphyrin or from the α - and β -protons and imidazole nitrogen of the axial histidine. Although deuterium substitution ENDOR experiments which would demonstrate that the radical site is indeed the porphyrin rather than the histidine are mentioned by Roberts et al. 42 , they are not presented.

HRP-I*. Given the possibility of a product of photo-induced electron transfer within the heme pocket, we must address the relationship of the photoproduct to the green form of HRP-I and to the catalytic sequence. We will call this putative photoproduct HRP-I* to acknowledge the possibility that it may be distinct from the product Y proposed earlier, 70,71 and to emphasize that it is formally equivalent to HRP-I in oxidation state. Figure 5-10 depicts HRP-I* in rapid equilibrium with HRP-I. In the dark, formation of HRP-I* is negligible, but under high illumination HRP-I* is favored, being reached presumably through an excited state of HRP-I. HRP-I* lacks both the prophyrin radical and the H-bonded oxoferryl. Devoid of these two features, HRP-I* is an unreactive structure and must return to the green form, HRP-I, in order for peroxidase catalysis to continue. The heme of HRP-I* is thus identical to that of HRP-II at high pH. This accounts for the similarity of the spectra in Figures 5-6 and 5-7. In this interpretation, HRP-I and HRP-I* have metal centers with identical valences and axial ligands and thus differ only in the porphyrin oxidation state. Our RR studies of (CH₃OH)₂Co^{III}OEPClO₄ and (ClO₄-)₂Co^{III}OEP+ suggest

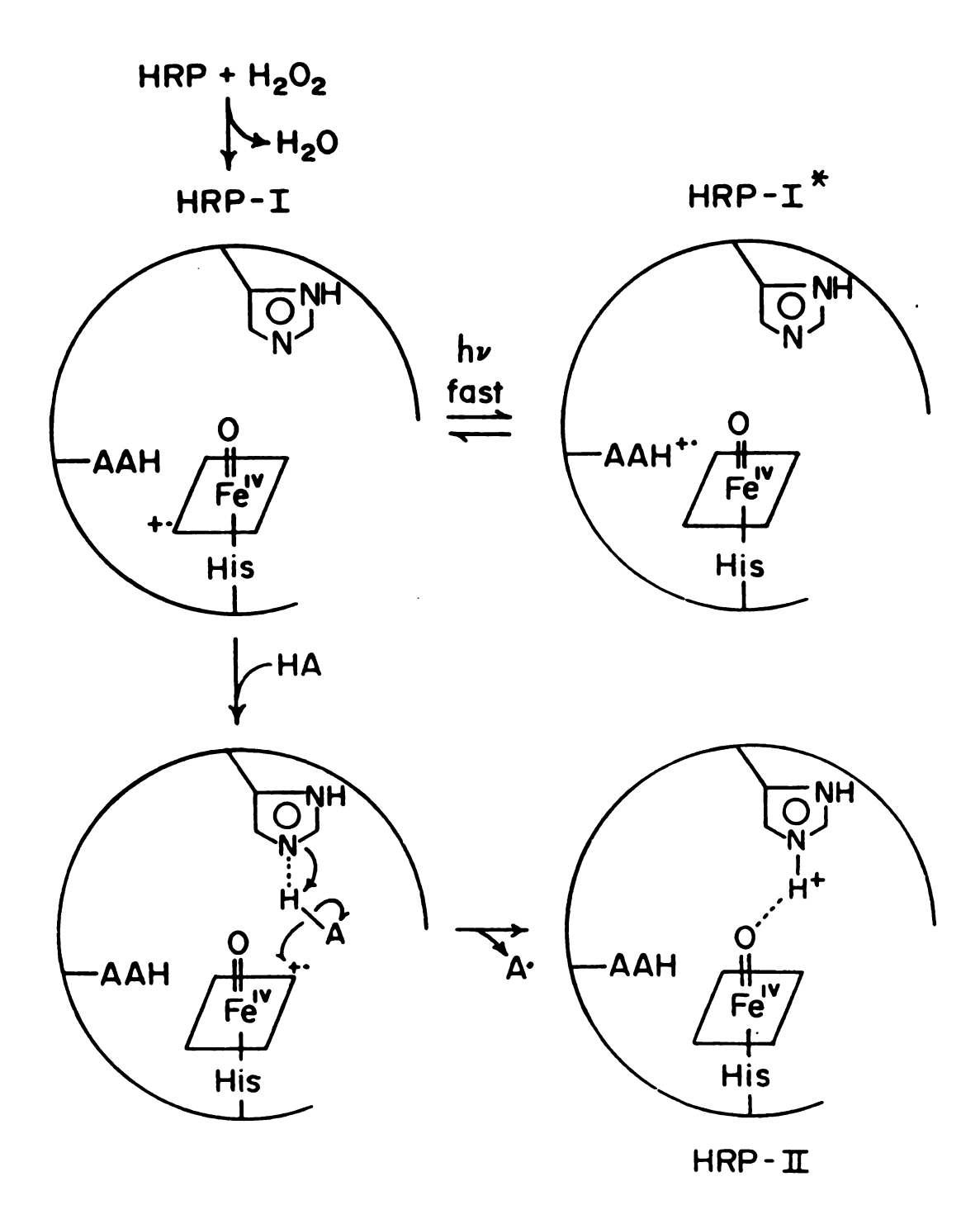


Figure 5-10. Schematic diagram of the active site of HRP catalytic intermediates, showing HRP-I, the postulated photoproduct HRP-I*, the reaction of HRP-I with a phenolic substrate, and HRP-II.

similar six-coordinate cobaltic solution structures with 1.97 Å core sizes for both complexes.³⁶ By analogy to these and other MOEP^{+*}, MOEP pairs, we conclude that HRP-I and HRP-I* possess similar geometries. Thus, should our HRP-I RR result actually be due to an HRP-I* photoproduct, we propose that the structural information contained in the RR spectrum is still valid to the green P⁺ form of HRP-I. Therefore, given either possible explanation (i.e. photochemistry or spin delocalization) for the similarity of the high frequency RR scattering of HRP-I and HRP-II, the results presented in Figures 5-3 and 5-5 suggest that the core sizes of these two species are equal and that, at pH 7, the oxoferryl of HRP-I is not H-bonded as is the oxoferryl of HRP-II. In the absence of the H-bond at high $pH,^{25,26}$ HRP-II is unreactive. The association between this H-bond and the reactivity of HRP-II suggests that the oxoferryl unit requires the H-bond for activation, presumably in order to facilitate the formation of leaving H₂O as depicted in reaction 3, above. Thus, the absence of the H-bond in HRP-I helps explain the initial reduction of the porphyrin radical cation, rather than the ferryl structure, to form the second intermediates.

Kinetics and mechanism of HRP-I reduction. A host of kinetic studies of the reaction of HRP-I with a variety of substrates suggest the involvement of a distal amino acid residue exhibiting a pK_a of 5.1,6 identified possibly as histidine 42 (His-42).6b For the substrates p-cresol and L-tyrosine, the reaction proceeds by a base catalyzed mechanism.6 Figure 5-10 proposes a mechanism for the reaction of p-cresol with HRP-I at pH 7. The substrate is oriented by H-bonding to distal His-42. This is consistent with studies which show that the acid form of p-cresol will bind to the cyanide complex of HRP at a distinct but nearby binding site at pH 7.75 As an electron is transferred from the substrate to the porphyrin cation radical, a proton is transferred along the H-bond to His-42. This homolytic cleavage of the H-A bond (or H-O bond of p-cresol)

results in the formation of the free radical of the substrate 76 along with HRP-II. The oxoferryl of HRP-II is H-bonded to the protonated His-42 residue. 25,26 The reaction of HRP-II with the substrate is influenced by an acid group with pK₈ 8.6.6 Thus, the participating acid group is most likely His-42 in both cases as was speculated earlier. The pK₈ is shifted by the positive charge of the porphyrin cation in HRP-I. This mechanism is consistent with Hammett and Okamoto-Brown plots constructed from rate constants for the reduction of HRP-I by a series of substituted phenols. These were taken to suggest a mechanism wherein the neutral substrate donates an electron to HRP-I and simultaneously loses a proton. 78

CONCLUSIONS

Using RR spectroscopy applied to a flowing sample of HRP-I (pH 7) prepared by rapid mixing, we have characterized a distinct intermediate formed by the reaction of HRP with hydrogen peroxide. This compound is two oxidation equivalents above the native state and decays through a species with an absorption spectrum characteristic of HRP-II. The RR scattering in the 1300-1700 cm⁻¹ range obtained from this intermediate is not characteristic of a metalloporphyrin π cation radical and is suggestive of an oxoferryl heme with the same geometric and electronic structure as that of HRP-II (particularly the high pH form). We have considered two possible explanations for our result: (i) photo-induced electron transfer to the porphyrin radical cation of HRP-I occuring in less than 5 ns and resulting in a new species, HRP-I*, which produces the RR spectrum, or (ii) extensive delocalization of the porphyrin radical of HRP-I onto the axial ligands.

The low frequency RR scattering in the 600-1000 cm $^{-1}$ range from this species reveals a ν (FeO) at 791 cm $^{-1}$, typical of the non-hydrogen bonded form

of HRP-II. This suggests that the oxo ligand of HRP-I is not hydrogen bonded at pH 7. This proposal is consistent with the kinetics of the reaction of HRP-I with p-cresol. Because the oxoferryl structure requires the hydrogen bond for activation, 25,26 this result explains why the porphyrin radical is the site of reduction of HRP-I. We represent a mechanism for HRP-I reduction by p-cresol in which a proton from the substrate binds to His 42 and forms a hydrogen bond to the oxo ligand of HRP-II.

FUTURE WORK

At the present time it is not possible to address conclusively the question of photoconversion vs. radical delocalization to explain the high frequency RR result for HRP-I. In addition to the work presented here, we have utilized cryogenic techniques, both in aqueous (unpublished results) and antifreeze solvents, 30 to obtain RR spectra of HRP-I similar to those we obtained with both pulsed, 390 nm and CW, 406.7 nm excitation. Variations of the rapid mixing approach have included the following: (i) off-resonance CW excitation at 363.8 nm which failed to produce detectable Raman scattering, and (ii) comparative CW measurements at 406.7 nm at different flow rates (we used 0.22 and 0.7 ml/min: Ogura and Kitagawa³⁴ report flow rates of 5-20 ml/min), all of which produced similar results. Felton et al.⁵⁸ also describe results similar to these obtained under 457.9 nm excitation for HRP-I samples at temperatures of 0 to -30 C. In conclusion we must assume that if these results do not represent Raman scattering from the green MP+ form of HRP-I, such scattering is prohibitively difficult to obtain under CW or nanosecond pulsed laser excitation. On the other hand, in collaboration with A. Salehi, RR studies of the model compound O=Fe^{IV}OEP^{+.79} are in progress and will greatly facilitate further analysis. In particular, methods to produce ¹⁸O=Fe^{IV}OEP⁺ are being developed. Time-resolved optical absorption measurements of flowing HRP-I samples illuminated by pulsed laser irradiation are planned. These experiments will be carried out in collaboration with Dr. Dewey Holten and coworkers and will conclusively address the question of the involvement of HRP-I photochemistry in these RR results.

Regardless of these complications, the pH dependence of the ν (FeO) observed for our putative HRP-I species should be determined. Low frequency data should be obtained from samples at pH 4, 5 and 6 in order to estimate the pK₈ of the proposed histidine group involved in the reaction. Also, the experiment should be repeated in D₂O buffer at pH 7 to establish more firmly the absence of hydrogen bonding of the oxo ligand. Finally, RR studies of intermediates involved in the catalysis of other peroxidases (notably myeloperoxidase, lactoperoxidase and heme bromoperoxidase) have already begun. This work will be carried out in the MSU Shared Laser Laboratory with Drs. R. Wever and J. Manthey.

ACKNOWLEDGMENTS

We thank Dr. T. Kitagawa for manuscripts prior to publication and Drs. R. Wever and J. Manthey for discussion and critical reading. T.O. thanks A. Salehi for technical assistance. This work was supported by NIH grant GM-25480.

REFERENCES

- 1. Chance, B., Arch. Biochem. Biophys. 1952, 41, 416-424.
- 2. George, P., Nature 1952, 169, 612-613.
- 3. Smith, A.M.; Morrison, W.L.; Milham, P.J., Biochemistry 1982, 21, 4414-4419.
- 4. Frew, J.E.; Jones, P. in "Advances in Inorganic and Bioinorganic Mechanism"; Academic Press: New York, 1984; Vol. 3, pp. 175-213.
- 5. Hewson, W.D.; Hager, L.P. in "The Porphyrins", Dolphin, D., Ed.; Academic Press: New York, 1979, Vol. 7, pp. 295-332.
- 6. (a) Dunford, H.B.; Stillman, J.S., Coord. Chem. Rev. 1976, 19, 187-251; (b) Dunford, H.B., Adv. Inorg. Biochem. 1982, 4, 41-68.
- 7. Naqui, A.; Chance, B., Ann. Rev. Biochem. 1986, 55, 137-166.
- 8. Theorell, H.; Ehrenberg, A., Arch. Biochem. Biophys. 1952, 41, 442-461.
- 9. Moss, T.H.; Ehrenberg, A.; Bearden, A.J., Biochemistry 1969, 8, 4159-4162.
- 10. Roberts, J.E.; Hoffman, B.M., J. Am. Chem. Soc. 1981, 103, 7654-7656.
- 11. LaMar, G.N.; de Ropp, J.S.; Latos-Grazynski, L.; Balch, A.L.; Johnson, R.B.; Smith, K.M.; Parish, D.W.; Cheng, R.-J., J. Am. Chem. Soc. 1983, 105, 782-787.
- 12. Chance, B.; Powers, L.; Ching, Y.; Poulos, T.; Schonbaum, G.R.; Yamazaki, I.; Paul, K.G., Arch. Biochem. Biophys. 1984, 235, 596-611.
- 13. (a) Chance, M.; Powers, L.; Kumar, C.; Chance, B., Biochemistry 1986, 25, 1259-1265; (b) Chance, M.; Powers, L.; Poulos, T.; Chance, B., Biochemistry 1986, 25, 1266-1270.
- 14. Penner-Hahn, J.E.; McMurry, T.J.; Davis, I.M.; Balch, A.L.; Groves, J.T.; Dawson, J.H.; Hodgson, K.O., J. Biol. Chem. 1983, 258, 12761-12764.

- 15. Penner-Hahn, J.E.; Smith-Eble, K.; McMurry, T.J.; Groves, J.T.; Dawson, J.H.; Hodgson, K.O., J. Am. Chem. Soc. 1987, in press.
- 16. Terner, J.; Sitter, A.J.; Reczek, C.M., Biochim. Biophys. Acta 1985, 828, 73-70.
- 17. Hashimoto, S.; Tatsuno, Y.; Kitagawa, T., Proc. Japan Acad. 1984, <u>60</u>, Ser. B.; 345-348.
- 18. Bajdor, K.; Nakamoto, K., J. Am. Chem. Soc. 1984, 106, 3045-3046.
- 19. Proniewicz, L.M.; Bajdor, K.; Nakamoto, K., J. Phys. Chem. 1986, 90, 1760-1766.
- 20. Chappacher, M.; Chottard, G.; Weiss, R., J. Chem. Soc., Chem. Commun. 1986, 2, 93-94.
- 21. Kean, R.T.; Oertling, W.A.; Babcock, G.T., J. Am. Chem. Soc. 1987, in press.
- 22. Terner, J.; Reed, D.E., Biochim. Biophys. Acta 1984, 789, 80-86.
- 23. Sitter, A.J.; Reczek, C.M.; Terner, J., Biochim. Biophys. Acta 1985, 828, 229-235.
- 24. Kean, R.T.; Babcock, G.T., manuscript in preparation.
- 25. Sitter, A.J.; Reczek, C.M.; Terner, J., J. Biol. Chem. 1985, 260, 7515-7522.
- 26. Hashimoto, S.; Tatsuno, Y.; Kitagawa, T., Proc. Natl. Acad. Sci. USA 1986, 83, 2417-2421.
- 27. Stillman, J.S.; Stillman, M.J.; Dunford, H.B., Biochemistry 1975, 14, 3183-3188.
- 28. Teraoka, J.; Ogura, T.; Kitagawa, T., J. Am. Chem. Soc. 1982, 104, 7354-7356.
- 29. Van Wart, H.E.; Zimmer, J., J. Am. Chem. Soc. 1985, 107, 3379-3381.
- 30. Oertling, W.A.; Babcock, G.T., J. Am. chem. Soc. 1985, 107, 6406-6407.
- 31. Babcock, G.T.; Jean, J.M.; Johnston, L.H.; Palmer, G.; Woodruff, W.H., J. Am. Chem. Soc. 1984, 106, 8305-8306.
- 32. Babcock, G.T.; Jean, J.M.; Johnston, L.H.; Woodruff, W.H.; Palmer, G., J. Inorg. Biochem. 1985, 23, 243-251.
- 33. Ogura, T.; Yoshikawa, S.; Kitagawa, T., Biochim. Biophys. Acta 1985, 832, 220-223.
- 34. Ogura, T.; Kitagawa, T., submitted for publication.
- 35. Salehi, A.; Oertling, W.A.; Babcock, G.T.; Chang, C.K., J. Am. Chem. Soc. 1986, 108, 5630-5631.

- 36. Oertling, W.A.; Salehi, A.; Chung, Y.; Leroi, G.E.; Chang, C.K.; Babcock, G.T., J. Am. Chem. Soc. 1987, submitted for publication.
- 37. Oertling, W.A., Salehi, A.; Chang, C.K.; Babcock, G.T., J. Phys. Chem. 1987, in press.
- 38. Salehi, A.; Oertling, W.A., unpublished results.
- 39. Dolphin, D.; Forman, A.; Borg, D.C.; Fajer, J.; Felton, R.H., Proc. Natl. Acad. Sci. USA 1971, 68, 614-618.
- 40. Aasa, R.; Vanngard, T.; Dunford, H.B., Biochim. Biophys. Acta 1975, 391, 259-264.
- 41. Schulz, C.E.; Devaney, P.W.; Winkler, H.; Debrunner, P.G.; Doan, N.; Chiang, R.; Rutter, R.; Hager, L.P., FEBS Lett. 1979, 103, 102-105.
- 42. Roberts, J.E.; Hoffman, B.M.; Rutter, R.; Hager, L.P., J. Biol. Chem. 1981, 256, 2118-2121.
- 43. La Mar, G.N.; de Ropp, J.S., J. Am. Chem. Soc. 1980, 102, 395-397.
- 44. La Mar, G.N.; de Ropp, J.S.; Smith, K.; Langry, K.C., J. Biol. Chem. 1981, 256, 237-243.
- 45. Asada, K.; Badger, M.R., Plant & Cell Physiol. 1984, 25, 1169-1179.
- 46. Schonbaum, G.R.; Lo, S., J. Biol. Chem. 1972, 247, 3353-3360.
- 47. Worthington Biochemical Corporation, "Worthington Enzyme Manual", 1972, p. 41.
- 48. Gibson, Q.H.; Milnes, L., Biochem. J. 1964, 91, 161-171.
- 49. Chance, B., Arch. Biochem. 1949, 22, 224-252.
- 50. Adler, A.; Kampas, F.; Kim, J., J. Inorg. Nucl. Chem. 1970, 32, 3443-3445.
- 51. Spaulding, L.D.; Chang, C.C.; Yu, N.-T.; Felton, R.H., J. Am. Chem. Soc. 1975, 97, 2517-2525.
- 52. Spiro, T.G. in "Iron Porphyrins", Lever, A.P.B.; Gray, H.B., Eds.; Addison-Wesley: Reading, MA, 1983; Part 2, pp. 89-159.
- 53. Abe, M.; Kitagawa, T.; Kyogoku, Y., J. Chem. Phys. 1978, 69, 4526-4534.
- 54. Choi, S.; Spiro, T.G.; Langry, K.C.; Smith, K.M.; Budd, D.L.; La Mar, G.N., J. Am. Chem. Soc. 1982, 104, 4345-4351.
- 55. Desbois, A.; Mazza, G.; Stetzkowski, F.; Lutz, M., Biochim. Biophys. Acta 1984, 785, 161-176.
- 56. Spiro, T.G.; Strekas, T.C., J. Am. Chem. Soc. 1974, 96, 338-345.

- 57. Yamaguchi, H.; Nakano, M.; Itoh, K., Chem. Lett. Jpn. 1982, 1397-1400.
- 58. Felton, R.H.; Romans, A.Y.; Yu., N.-T.; Schonbaum, G.R., Biochim. Biophys. Acta 1976, 434, 82-89.
- 59. Rakhit, G.; Spiro, T.G., Biochem. Biophys. Res. Comm. 1976, 71, 803-808.
- 60. Boersma, A.D.; Goff, H.M., Inorg. Chem. 1984, 23, 1671-1676.
- 61. Hanson, L.K.; Chang, C.K.; Davis, M.S.; Fauer, J., J. Am. Chem. Soc. 1981, 103, 663-670.
- 62. Kim, D.; Miller, L.A.; Rakhit, G.; Spiro, T.G., J. Phys. Chem. 1986, 90, 3320-3325.
- 63. Maggiora, G.M., J. Am. Chem. Soc. 1973, 95, 6555-6559.
- 64. Kashigawa, H. in "Biomolecules: Electronic Aspects", Nagata et al., Eds.; Elsevier: New York, 1985; pp. 31-50.
- 65. Choi, S.; Spiro, T.G.; Langry, K.C.; Smith, K.M., J. Am. Chem. Soc. 1982, 104, 4337-4344.
- 66. La Mar, G.N.; de Ropp, J.S.; Smith, K.; Langry, K.C., J. Am. Chem. Soc. 1983, 105, 4576-4580.
- 67. Bangcharoenpaurpong, K.T.; Schomacher, K.T., Champion, P.M., J. Am. Chem. Soc. 1984, 106, 5688-5698.
- 68. (a) Spaulding, L.D.; Eller, P.G.; Bertrand, J.A.; Felton, R.H., J. Am. Chem. Soc. 1974, 96, 982-987; (b) Gans, P.; Buisson, G.; Duée, E.; Marchon, J.-C.; Erler, B.S.; Scholz, W.F.; Reed, C.A., J. Am. Chem. Soc. 1986, 108, 1223-1234.
- 69. Callahan, P.M.; Babcock, G.T., Biochemistry 1981, 20, 952-958.
- 70. Chu, M.; Dunford, H.B.; Job, D., Biochem. Biophys. Res. Commun. 1977, 74, 159-164.
- 71. Nadezhdin, A.D.; Dunford, H.B., Photochem. Photobiol., 29, 899-903.
- 72. Fujita, I.; Hanson, L.K.; Walker, F.A.; Fajer, J., J. Am. Chem. Soc. 1983, 105, 3296-3300.
- 73. Sontum, S.F.; Case, D.A., J. Am. Chem. Soc. 1985, 107, 4013-4015.
- 74. Schultz, C.E.; Rutter, R.; Sage, J.T.; Debrunner, P.G.; Hager, L.P., Biochemistry 1984, 23, 4734-4754.
- 75. Critchlow, J.E.; Dunford, H.B., J. Biol. Chem. 1972, 247, 3714-3725.
- 76. Shiga, T.; Imaizumi, K., Arch. Biochem. Biophys. 1975, 167, 469-479.
- 77. Dunford, H.B.; Cotton, M.L., J. Biol. Chem. 1975, 250, 2920-2932.

- 78. Job, D.; Dunford, H.B., Eur. J. Biochem. 1976, 66, 607-614.
- 79. Chang, C.K.; Kou, M.-S., J. Am. Chem. Soc. 1979, 101, 3414-3415.

